A Multiscale Approach to Magnetization Dynamics Simulations

Dissertation
zur Erlagung des Grades
"Doktor der Naturwissenschaften"
am Fachbereich Physik, Mathematik und Informatik
der Johannes Gutenberg-Universität in Mainz

Andrea De Lucia
geboren in Neapel, Italien

Mainz, den 30. März 2017

Andrea De Lucia, *A Multiscale Approach to Magnetization Dynamics Simulations* (2017).

Abstract

Simulations of magnetization dynamics in a multiscale environment enable rapid evaluation of the Landau-Lifshitz-Gilbert equation in a mesoscopic sample with nanoscopic accuracy in areas where such accuracy is required. I have developed a multiscale magnetization dynamics simulation approach that can be applied to large systems with spin structures that vary on small length scales locally. To implement this, the conventional micromagnetic simulation framework was expanded to include a multiscale solving routine. The software selectively simulates different regions of a ferromagnetic sample according to the spin structures located within in order to employ a suitable discretization and use either a micromagnetic or an atomistic model. A tracking algorithm was developed in order to shift the atomistic region within the sample to follow the spin structures which vary on a short length scale.

In the first part of this thesis, the theory necessary for the development and the comprehension of this approach was introduced. This includes: the derivation of the LLG equation, the phenomenological background and the evaluation of the energy contributions in the two models, a review on magnetic structures of fundamental and technological interest, with a focus on some structures which cannot be modeled using micromagnetism only, and an analysis of the computational algorithms used in the multiscale simulation.

The second part of the thesis is focused on describing in detail the implementation of the multiscale approach, as well as demonstrating its necessity and validity. To demonstrate the validity of the approach, we simulate the spin wave transmission across the regions simulated with the two different models and different discretizations. We find that the interface between the regions is fully transparent for spin waves with frequency lower than a certain threshold set by the coarse scale micromagnetic model with no noticeable attenuation due to the interface between the models. One further demonstration consists in the comparison of a multiscale DMI spiral with the analytical theory. To demonstrate the reliability of the tracking algorithm, the motion of a domain wall in a magnetic nanostrip was simulated. The approach was then applied to magnetic Skyrmions to quantify their stability. Skyrmions belong to the most interesting spin structures for the development of future information technology as they have been predicted to be topologically protected. As a demonstration for the necessity of a multiscale approach, we first show how the stability of a Skyrmion is influenced by the refinement of the computational mesh and reveal that conventionally employed traditional

micromagnetic simulations are inadequate for this task. Furthermore, we determine the stability quantitatively using our multiscale approach.

As a key operation for devices and as a first application of the approach, the process of annihilating a Skyrmion by exciting it with a spin polarized current pulse is analyzed, showing that different transformations in the topology of the system can be reliably induced by designing the pulse shape.

Zusammenfassung

Simulationen von Magnetisierungsdynamik in einem multiskalen Umfeld ermöglichen die schnelle Berechnung der Landau-Lifshitz-Gilbert Gleichung mit nanoskopischer Genauigkeit in einem mesoskopicher Probe, in den Gebieten, in denen eine solche Genauigkeit erforderlich ist. Ich habe einen Ansatz zu Magnetisierungdynamiksimulationen entwickelt, die auf große Systeme mit lokal in kleinen Skalenlängen abweichenden Spinstrukturen angewendet werden kann. Für die Implementation wurde die übliche Grundstruktur der micromagnetische Simulation erweitert, um eine multiskalen Lösungroutine zu enthalten. Das Programm simuliert wahlweise verschiedene Gebiete von einer ferromagnetischen Probe. Je nach den Spinstrukturen, die sich in dem Gebiet befinden, benutzt das Programm eine geeignete Diskretisierung und entweder ein micromagnetisches oder ein atomistisches Modell. Um das atomistisches Gebiet innerhalb des Samples umzustellen, wurde ein Verfolgungsalgorithmus entwickelt. Auf diese Weise werden Spinstrukturen, die lokal in kleinen Skalenlängen abweichen, verfolgt.

Im ersten Teil dieser Doktorarbeit enthält die erforderliche Theorie, um diesen Ansatz zu entwickeln und zu verstehen. Dieser Teil enthält: die Herleitung der LLG Gleichung, den phänomenologischen Hintergrund und die Berechnung von den energetischen Beiträgen in beide Modellen, einen Überblick über magnetischen Strukturen von grundsätzlichem und technologischem Interesse mit Schwerpunkt auf Strukturen, die nicht mikromagnetisch modelliert werden können sowie eine Analyse von den Algorithmen, die in Multiskalensimulationen benutzt werden.

Der zweite Teil dieser Doktorarbeit fokussiert sich auf auf die detaillierte Beschreibung der Umsetzung des Multiskalenansatzes, ebenso wie eine Beweisführung dessen Notwendigkeit und Gültigkeit. Um die Gültigkeit des Ansatzes zu beweisen, simulieren wir die Übertragung von Spinwellen durch Gebiete mit 2 unterschiedlichen Modellen und Diskretisierungen. Wir finden heraus, dass die Grenzfläche zwischen den Gebieten (für Spinwelle mit einer niedrigeren Frequenz als einem gewissen Schwellenwert, den die grobe mikromagnetische Diskretisierung bestimmt) vollig durchsichtig ist, deswegen wird keine Dämpfung durch die Grenzfläche verursacht. Eine weitere Betrachtung besteht aus dem Vergleich einer DMI-Spirale zwischen der Multiskalensimulation und analytischen Theorie. Um die Gültigkeit des Verfolgungsalgorithmus zu beweisen, wurde die Bewegung einer Domänenwände in einer magnetischen Nanostrip simuliert. Danach wurde der Ansatz auf magnetische

Skyrmionen angewandt, um ihre Stabilität quantitativ zu bestimmen Skyrmionen gehören zu den interessantesten Spinstrukturen fürs Entwicklung der zukünftigen Informationstechnologie, da es Vorhersagen gibt, dass sie topologisch geschützt sind. Um die Notwendigkeit eines Multiskalenansatzes zu beweisen, zeigen wir zuerst, wie die Stabilität eines Skyrmions durch die Verfeinerung des Berechnungnetz beeinflusst wird, und finden heraus, dass die traditionell üblich angewendeten mikromagnetischen Simulationen, für diese Aufgabe nicht angemessen sind. Außerdem, bestimmen wir quantitativ, mit unserem Multiskalenansatz, die Stabilität. Wir regen einen Skyrmion mit einem spin-polarisiert Strompuls an, um den Vernichtungvorgang zu untersuchen.

Dieser ist ein wesentlicher Bestandteil um Geräte zu konstruiren, und die erste Anwendung unseres Ansatzes. Wir zeigen, dass verschiedene Veränderungen der Topologie des Systems betriebssicher durch die Gestaltung des Pulses eingeleitet werden können.

Contents

Motivation

The interest towards microscopic magnetic structures originated during the 20th century, when experimental techniques and the motivation for research in this field increased dramatically. While research on magnetic patterns was traditionally of fundamental interest, it became strongly technologically oriented in the last decades of the century. Micromagnetic theory [?, ?, ?, ?], developed in the 1960s, constituted the main mathematical model to describe magnetic structures and patterns, from domain walls [?, ?, ?, ?] and vortices [?, ?, ?, ?], until Skyrmions, the latest, and therefore most discussed spin structure within the community [?, ?, ?, ?, ?]. Advancements in data storage technology in magnetic thin films made a further understanding of the dynamics of magnetic structures necessary. The earliest example of magnetic structures employed in data storage technology is constituted by magnetic tapes and discs. These devices exploited domain walls in bubble materials [?, ?, ?, ?] as information units. The technological obstacles of these device had to be overcome in order to achieve currently used technology such as hard drives.

The discovery of the giant magnetoresistance (GMR) effect advanced this field, as, for this fundamental finding P. Grünberg [?, ?] and A. Fert [?] were rewarded with the Nobel Prize in Physics in 2007. The tunnel magnetoresistance effect [?] (TMR), is an analogous magnetotransport effect that allowed for a great reduction both in the price and in the size of magnetic hard drive technology. In both the aforementioned effects, the electric resistance of a multilayer stack consisting of at least two ferromagnetic layers, separated by a non magnetic one, depends strongly on the relative orientation of the magnetization of one magnetic layer with respect to the other one. The main difference between the two effects lies in the non-magnetic material, which is conducting for GMR, insulating for TMR. In devices based on these effect, the exchange bias is used to pin one magnetic layer to an underlying antiferromagnetic layer, while the orientation in the magnetization of the other magnetic layer is free to rotate, a small external magnetic field results in a large change of electrical resistance.

Since such devices are very sensitive, the most obvious room for improvement lies in the information density of hard drives. Due to the current inflation in the demand for higher data storage density, eventually a transition from rotating discs to a novel storage technology could be necessary. Another topic of widespread interest is that of the operating speed of devices, since the increase in the amount of data being stored and retrieved should not be accompanied by a proportional dilation in the time needed to manipulate it.

One device worthy of mention is the racetrack memory proposed by S. Parkin [**?**], where bits encoded in magnetic domains in a ferromagnetic nanowire were used as a shift register with the application of a spin transfer torque [**?**, **?**, **?**, **?**, **?**].

Other suggestions propose the application of topologically stabilized magnetic structures, such as vortices [**?**] and Skyrmions [**?**]. Modelling such structures from a computational point of view, and in particular simulating phenomena involving the overcoming of their topological protection is the central problem that is treated in this thesis.

Chapter 1 constitutes an introduction on magnetization dynamics, showing how the LLG equation is derived and how its solution, the magnetization vector $\mathbf{M}$, is defined.

Chapter 2 presents the two main models currently used in the field, including the derivation of the continuous micromagnetic model from the discrete, atomistic, classical Heisenberg model. The different effective terms, used to describe magnetic materials are derived in detail. A comparison between the two models, describing their limits of validity and application is included.

Chapter 3 describes magnetic structures of technological and fundamental interest, such as domain walls, vortices and Skyrmions. The analytical theory desctibing Bloch points [**?**, **?**] is presented.

Chapter 4 includes a derivation and description of the computational methods used to simulate magnetization dynamics. Namely, algorithms used for the solution of differential equation, the approximation of a function on a discrete grid and its interpolation are presented.

Chapter 5 motivates the development of a multiscale approach, showing how a method which employs both the models presented in chapter 2, is necessary to accurately simulate structures and phenomena of interest. Original work, showing how the annihilation of a Skyrmion is strongly influenced by the choice of the computational parameters is shown.

Chapter 6 describes the implementation of the multiscale approach. The algorithms presented in chapter 4 are used to run in parallel simulations in the two models, describing different regions of the same magnetic system. Devising an accurate strategy to achieve this constitutes the main effort towards the development of the multiscale approach.

Chapter 7 presents a first application of the approach. In this application the multiscale model was used to simulate the annihilation of Skyrmions induced by spin-orbit torque pulses of different size and length. Three different regimes, corresponding to different topological transformations were discovered.

Chapter 1

The Landau-Lifshitz-Gilbert equation

The aim of magnetization dynamics simulations is to numerically solve the equations determining the dynamics of magnetic structures. Some equations are specific for the particular magnetization structures being considered. These can be derived from more general equations. Amongst the most general ones, the Landau-Lifshitz-Gilbert equation predicts the dynamics of the magnetization configuration. The multiscale approach, object of this thesis, proposes to solve this equation in an efficient and robust way, coupling two different models with different advantages and drawbacks according to the peculiarities of the magnetic structures and, in particular, to the spatial resolution required in different regions of the magnetic system. L.D. Landau and E.M. Lifshitz proposed the equation of motion for a spin in a ferromagnetic system in 1935 [**?**]. Here a derivation of their equation based on quantum mechanical arguments is discussed [**?**]. Let $\hat{H}$ be the Hamiltonian operator of the system and $\mathbf{S}$ a general spin, the dynamic time evolution of a component S_j of $\mathbf{S}$ is described by the Heisenberg equation of motion for an observable:

$$\frac{dS_j}{dt} = \frac{i}{\hbar}\left[\hat{H}, S_j\right] = \frac{i}{\hbar}\left(\sum_{k=x,y,z} \frac{\partial \hat{H}}{\partial S_k}\left[S_k, S_j\right] + \mathcal{O}\left(\hbar^2\right)\right) \tag{1.1}$$

where first order Taylor approximation of $\hat{H}$ was applied and $\mathcal{O}\left(\hbar^2\right)$ denotes a vector function of at least quadratic order in $\hbar$. Applying the commutation relations for the angular momentum

$$\left[S_k, S_j\right] = -i\hbar \sum_l \epsilon_{jkl} S_l \tag{1.2}$$

to the spin components, eq.(**??**) reads:

$$\frac{dS_j}{dt} = \sum_{k,l} \frac{\partial \hat{H}}{\partial S_k} \epsilon_{jkl} \, S_l + \mathcal{O}\left(\hbar\right), \tag{1.3}$$

where the symbol ϵ_{jkl} denotes the antisymmetric tensor. Exploiting the relation for the l-th component of the vector $\mathbf{a} \times \mathbf{b}$:

$$\left(\mathbf{a} \times \mathbf{b}\right)_l = \sum_{j=1}^{3} \sum_{k=1}^{3} \epsilon_{jkl} a_j b_k \tag{1.4}$$

eq.(**??**) can be written in terms of the vector product:

$$\frac{d\mathbf{S}}{dt} = \frac{\partial \hat{H}}{\partial \mathbf{S}} \times \mathbf{S} + \mathcal{O}\left(\hbar\right) \tag{1.5}$$

where the notation $\frac{\partial}{\partial \mathbf{S}} \equiv \left(\frac{\partial}{\partial \mathbf{S_x}}, \frac{\partial}{\partial \mathbf{S_y}}, \frac{\partial}{\partial \mathbf{S_z}}\right)$ was used. A quantum-mechanical, discrete theory can be approximated to a semi-classical, continuous one, by taking the limit $\hbar \to 0$, and transforming analogously its observables. In this spirit we can assume an arbitrary volume of ferromagnetic material of size $\Delta\tau$ to contain ΔN classical spins $\mathbf{S}$ with magnetic moment $\boldsymbol{\mu} = -\frac{g\mu_B}{\hbar}\mathbf{S}$. The direction of the magnetic moment is opposite to the spin due to the electrons having negative charge. It is then possible [**?**] to define the magnetization vector $\mathbf{M}$ at the position corresponding to the volume element $\Delta\tau$:

$$\mathbf{M} \equiv \lim_{\Delta\tau \to 0} \frac{1}{\Delta\tau} \sum_{i}^{\Delta N} \boldsymbol{\mu}_i = \lim_{\Delta\tau \to 0} \frac{\Delta N}{\Delta\tau} \left\langle \boldsymbol{\mu} \right\rangle \tag{1.6}$$

where the limit of $\Delta\tau$ approaching zero is to be intended in macroscopic terms, in order for it to be large enough to contain a statistically significant number of spins to evaluate the average magnetic moment $\langle\boldsymbol{\mu}\rangle$. For practical applications on cubic lattices we will assume $\lim_{\Delta\tau\to 0} \frac{\Delta N}{\Delta\tau} = \frac{c_s}{a^3}$ with c_s the number of spins per lattice site and a the lattice constant. In such an approximation eq.(**??**) can be written as:

$$\frac{d\mathbf{M}}{dt} = -\gamma \mathbf{M} \times \mathbf{H}_{eff} \tag{1.7}$$

where the gyromagnetic ratio $\gamma = \frac{g\mu_0\mu_B}{\hbar}$ contains fundamental constants of quantum origin such as the Bohr magneton μ_B, the magnetic permeability of vacuum μ_0, and the g-factor. The effective field $\mathbf{H}_{eff}$ is defined as:

$$\mathbf{H}_{eff} \equiv \frac{1}{\gamma} \left\langle \frac{\partial \hat{H}}{\partial \mathbf{S}} \right\rangle = -\frac{1}{\mu_0} \frac{dE}{d\boldsymbol{\mu}}, \tag{1.8}$$

where the average of the quantum operator $\hat{H}$ was replaced with the classical observable E. Equation (**??**) describes the precession of the magnetization around the effective field. In the continuum limit the effective field is defined as $-\frac{1}{\mu_0}\frac{\delta E}{\delta \mathbf{M}}$ with the δ symbol indicating the variational derivative:

$$\frac{\delta E\left[\mathbf{M}\left(\mathbf{r}\right)\right]}{\delta \mathbf{M}\left(\mathbf{r}_0\right)} \equiv \lim_{\epsilon\to 0}\frac{1}{\epsilon}\begin{pmatrix} E\left[\mathbf{M}\left(\mathbf{r}\right)+\epsilon\mathbf{e}_x\delta^3\left(\mathbf{r}-\mathbf{r}_0\right)\right]-E\left[\mathbf{M}\left(\mathbf{r}\right)\right] \\ E\left[\mathbf{M}\left(\mathbf{r}\right)+\epsilon\mathbf{e}_y\delta^3\left(\mathbf{r}-\mathbf{r}_0\right)\right]-E\left[\mathbf{M}\left(\mathbf{r}\right)\right] \\ E\left[\mathbf{M}\left(\mathbf{r}\right)+\epsilon\mathbf{e}_z\delta^3\left(\mathbf{r}-\mathbf{r}_0\right)\right]-E\left[\mathbf{M}\left(\mathbf{r}\right)\right] \end{pmatrix}, \tag{1.9}$$

where ε has the dimensions of the magnetization $\left(\frac{\mathrm{A}}{\mathrm{m}}\right)$. It can be shown that for a system where the dynamics is described by the equation of motion (**??**), the energy is conserved:

$$\frac{dE}{dt} = \int dV\,\frac{\delta E}{\delta \mathbf{M}}\cdot\frac{d\mathbf{M}}{dt} = \int dV\,\left(-\mu_0\mathbf{H}_{eff}\right)\cdot\left(-\gamma\mathbf{M}\times\mathbf{H}_{eff}\right) = 0. \tag{1.10}$$

In order to account for some dissipative effects, occurring at a macroscopic level, T.L. Gilbert proposed [**?**] to add to eq.(**??**) a phenomenological damping term. The effect of the damping term is to align the magnetization to the effective field and it is therefore perpendicular to the precession term; the Landau-Lifshitz-Gilbert equation yields:

$$\frac{d\mathbf{M}}{dt} = -\gamma\mathbf{M}\times\mathbf{H}_{eff} + \frac{\alpha}{M_s}\mathbf{M}\times\frac{d\mathbf{M}}{dt} \tag{1.11}$$

with the saturation magnetization $M_s \equiv |\mathbf{M}|$ and the damping parameter α. Since the terms on the right hand side of eq.(**??**) are perpendicular to $\mathbf{M}$, its module M_s is conserved. This can be demonstrated as follows:

$$\frac{d}{dt}M_s^2 = \frac{d}{dt}|\mathbf{M}|^2 = 2\mathbf{M}\cdot\frac{d\mathbf{M}}{dt} = 2\mathbf{M}\cdot\left(-\gamma\mathbf{M}\times\mathbf{H}_{eff} + \frac{\alpha}{M_s}\mathbf{M}\times\frac{d\mathbf{M}}{dt}\right) = 0. \tag{1.12}$$

Computational application requires eq.(**??**) to be made explicit in $\frac{d\mathbf{M}}{dt}$, this can be accomplished by taking the vector product with $\mathbf{M}$ on both sides in order to evaluate $\mathbf{M}\times\frac{d\mathbf{M}}{dt}$:

$$\mathbf{M}\times\frac{d\mathbf{M}}{dt} = \mathbf{M}\times\left(-\gamma\mathbf{M}\times\mathbf{H}_{eff}\right) + \mathbf{M}\times\left(\frac{\alpha}{M_s}\mathbf{M}\times\frac{d\mathbf{M}}{dt}\right). \tag{1.13}$$

The Grassmann identity $\mathbf{a}\times\left(\mathbf{b}\times\mathbf{c}\right) = \left(\mathbf{a}\cdot\mathbf{c}\right)\mathbf{b} - \left(\mathbf{a}\cdot\mathbf{b}\right)\mathbf{c}$ can be applied to the damping term, and yields:

$$\mathbf{M}\times\frac{d\mathbf{M}}{dt} = -\gamma\mathbf{M}\times\left(\mathbf{M}\times\mathbf{H}_{eff}\right) + \frac{\alpha}{M_s}\left[\left(\mathbf{M}\cdot\frac{d\mathbf{M}}{dt}\right)\mathbf{M} - M_s^2\frac{d\mathbf{M}}{dt}\right]. \tag{1.14}$$

Since

$$\mathbf{M} \cdot \frac{d\mathbf{M}}{dt} = \frac{1}{2}\frac{dM_s^2}{dt} = 0, \tag{1.15}$$

eq.(**??**) can be written as:

$$\mathbf{M} \times \frac{d\mathbf{M}}{dt} = -\gamma \mathbf{M} \times (\mathbf{M} \times \mathbf{H}_{eff}) - \alpha M_s \frac{d\mathbf{M}}{dt}. \tag{1.16}$$

Inserting eq.(**??**) into the damping term in eq.(**??**) yields:

$$\begin{aligned} \frac{d\mathbf{M}}{dt} &= -\gamma \mathbf{M} \times \mathbf{H}_{eff} + \frac{\alpha}{M_s}\left[-\gamma \mathbf{M} \times (\mathbf{M} \times \mathbf{H}_{eff}) - \alpha M_s \frac{d\mathbf{M}}{dt}\right] \\ &= -\gamma' \left[\mathbf{M} \times \mathbf{H}_{eff} - \frac{\alpha}{M_s}\mathbf{M} \times (\mathbf{M} \times \mathbf{H}_{eff})\right] \end{aligned} \tag{1.17}$$

with $\gamma' \equiv \frac{\gamma}{1+\alpha^2}$.

1.1 Magnetization dynamics in a constant effective field

In order to fully understand eq.(**??**) it is interesting to solve it analytically for a constant effective field, this can be easily achieved using a spherical coordinates system. In this system the magnetization vector and its time derivative read:

$$\mathbf{M} = \begin{pmatrix} M_s \sin\varphi \cos\theta \\ M_s \sin\varphi \sin\theta \\ M_s \cos\varphi \end{pmatrix}, \tag{1.18}$$

$$\frac{d\mathbf{M}}{dt} = \frac{\partial \mathbf{M}}{\partial M_s}\dot{M}_s + \frac{\partial \mathbf{M}}{\partial \theta}\dot{\theta} + \frac{\partial \mathbf{M}}{\partial \varphi}\dot{\varphi} \tag{1.19}$$

where θ and φ denote respectively the polar and azimuthal angle. The partial derivative terms can be easily evaluated as:

$$\frac{\partial \mathbf{M}}{\partial M_s} = \begin{pmatrix} \sin\varphi\cos\theta \\ \sin\varphi\sin\theta \\ \cos\varphi \end{pmatrix} \quad \frac{\partial \mathbf{M}}{\partial \theta} = \begin{pmatrix} -M_s\sin\varphi\sin\theta \\ M_s\sin\varphi\cos\theta \\ 0 \end{pmatrix} \quad \frac{\partial \mathbf{M}}{\partial \varphi} = \begin{pmatrix} M_s\cos\varphi\cos\theta \\ M_s\cos\varphi\sin\theta \\ -M_s\sin\varphi \end{pmatrix}. \tag{1.20}$$

It can be easily noticed that in eq.(**??**) the time derivative appears as the linear combination of three perpendicular vectors. We can assume without loss of generality that H_{eff} is aligned along the positive z direction, so that

$H_{eff} = H\mathbf{e}_z$. The two terms on the right-hand side of the LLG equation as written in eq.(**??**) read in the chosen coordinate system:

$$\begin{aligned} \mathbf{M} \times \mathbf{H}_{eff} &= -H\frac{\partial \mathbf{M}}{\partial \theta} \\ \mathbf{M} \times \mathbf{M} \times \mathbf{H}_{eff} &= -M_s H \sin\varphi \frac{\partial \mathbf{M}}{\partial \varphi} \end{aligned} \tag{1.21}$$

so that the whole equation can be solved as a system of three independent differential equations:

$$\begin{cases} \dot{M}_s = 0 \\ \dot{\theta} = \gamma' H \\ \dot{\varphi} = -\gamma' H \alpha \sin\varphi \end{cases} \tag{1.22}$$

While the first equation recovers the result of constant M_s, the second equation determines the counterclockwise precession of the magnetization around the direction set by H_{eff} with constant angular velocity $\dot{\theta} = g\mu_0\mu_B H/\hbar$ also known as Larmor frequency. The third equation is nonlinear, an approximation is needed in order to solve it analytically, this can be achieved expanding $\sin\varphi$ to the first order in Taylor series:

$$\dot{\varphi} = -\gamma' H \alpha \varphi + \mathcal{O}\left(\varphi^3\right). \tag{1.23}$$

Eq.(**??**) can be solved analytically and it results in the exponential decay of φ which corresponds to the alignment of $\mathbf{M}$ in the direction of H_{eff}. The

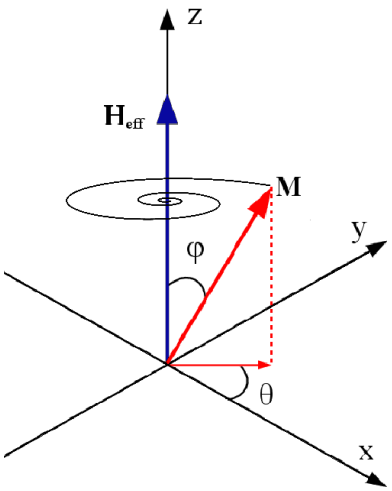

Figure 1.1: Effect of the two terms in the LLG equation on $\mathbf{M}$: a conservative precession motion in the plane perpendicular to H_{eff} induced by the field term, and the alignment induced by the damping term.

solution of the LLG equation for a constant effective field, can therefore be summarized as the linear combination of two perpendicular terms: the gyrotropic motion around the effective field, and the alignment along the effective field proportional to the α parameter.

Chapter 2

From the Heisenberg model to micromagnetism

Several theories have been developed in order to describe magnetism, according to the different length scales on which magnetic problems can be studied, from the atomic to the cosmic one. On the atomic scale ab-initio calculations are commonly used to obtain properties and parameters of materials as a result of their electronic structure. Since the computational complexity of such problems scales with the number of considered electrons (therefore atoms), the size of the systems that can be treated by this method is very restricted. These calculations are usually executed on very powerful clusters or supercomputers, usually exploiting symmetrical properties to reduce the computational time such as periodic boundary conditions.

If the focus of the problem is the orientation of magnetic moments, rather than the electronic structure, a suitable approximation is to use Heisenberg models. In these models interacting spins are located at discrete positions within the atomic lattice. In this work we will restrict our focus on the classical Heisenberg model, which treats each spin as a classical magnetic moment $\boldsymbol{\mu}_i$ located on the lattice site i. Spins can rotate continuously in three dimensions and the exchange interaction between neighboring spins is treated as a simple coupling between their moments. This model neglects quantum effects while still considering some parameters, of quantum origin such as the lattice constant, the exchange coupling, or the number of Bohr magnetons per lattice site which can be calculated ab-initio or measured experimentally.

Magnetic structures of technological and fundamental interest [?, ?, ?, ?, ?, ?, ?, ?, ?, ?, ?, ?, ?, ?], such as domain walls, vortices, and Skyrmions, come about in ferromagnets on larger length scales than those which can be efficiently simulated in the Heisenberg model. The most suitable tool to describe

such structures is the micromagnetic theory, which can be considered a large scale approximation of the Heisenberg model. In the micromagnetic theory, magnetization ($\mathbf{M}$) is considered as a continuous vector field with a constant module (M_s).

Unlike the atomistic model, where the correct lattice constant must be used in order to obtain realistic results, the micromagnetic model becomes more and more accurate by refining the computational mesh used to approximate the continuous function $\mathbf{M}$ [see **??**]. Ideally, in the infinitely fine mesh limit the analytical theory is recovered. Nevertheless even in the analytical theory, predictions made by the micromagnetic model can be in disagreement with the experimental evidence. These intrinsic limitations are derived from the micromagnetic model neglecting of the length scales comparable to the lattice constant. The magnetization vector itself, which is the fundamental quantity that the model investigates, is proportional to the local average of the atomic magnetic moments, according to the definition of the magnetization vector given in chapter **??**:

$$M = \lim_{\tau \to 0} \frac{1}{\tau} \sum_{i}^{N} \boldsymbol{\mu}_i = \lim_{\tau \to 0} \frac{N}{\tau} \langle \boldsymbol{\mu} \rangle \qquad (??)$$

where τ indicates a volume element containing N magnetic moments $\boldsymbol{\mu}$, with the limit $\tau \to 0$ restricted to the volume of elements which are small compared to the full magnetic system but large enough to contain a statistically significant number of magnetic moments. One basic example is the excitation of spin waves with a wavelength smaller than the lattice constant, a phenomenon that does indeed arise in a continuum model despite being forbidden in experiments and in realistic atomistic simulations. This thus shows that only a multiscale simulation can reproduce the dynamics realistically.

There are very few cases of magnetic structures varying on the scale of the atomic lattice, the most prominent of which is the Bloch point. Such structures constitute a fundamental limit of the theory and cannot be accurately treated within it, in accord with the condition on eq.(**??**) for $\mathbf{M}$ to be proportional to the average of a statistically meaningful number of magnetic moments. The aim of this chapter is to show how the micromagnetic theory is derived as a continuum approximation of the classical Heisenberg model by approximating different phenomenological effects which contribute to the energy of the system and to the effective field. Furthermore, the limitations in the spatial resolution of the micromagnetic theory are analyzed quantitatively.

2.1 Exchange Energy

Exchange interaction is a purely quantum-mechanical phenomenon arising from the Pauli exclusion principle of fermions. Since it depends on the electronic structure of the individual ferromagnetic material, the most suitable technique to evaluate the exchange interaction parameters consists in ab-initio calculations. In this framework the scale of this effect is evaluated as the overlap integral between two localized electronic orbitals. For the classical Heisenberg model, the result of such an integral, the exchange constant J, is treated as a simple coupling energy between magnetic moments. The focus of this section will be restricted to nearest neighbor interactions, the phenomenon known as Dzyaloshinskii-Moriya Interaction (DMI) which can be considered as a case of anisotropic exchange interaction is treated in **??**.

In the classical Heisenberg model the exchange energy of two neigboring spins $\mathbf{S}$ is defined as:

$$E_{xc} = -J \sum_{\langle i,j \rangle} \mathbf{S}_i \cdot \mathbf{S}_j \tag{2.1}$$

where the sum is intended to run on every couple of first neighboring spins in the system. This can be rewritten as:

$$E_{xc} = -J \sum_i \sum_{nn} \mathbf{S}_i \cdot \mathbf{S}_{nn} = -JS^2 \sum_i \sum_{nn} \cos \phi_{i,nn} \tag{2.2}$$

with $\phi_{i,nn}$ the angle between the two spins, the subscript nn indicates the nearest neighbors of the spin labeled with i.

We assume that in the exact position of the lattice site where a spin is localized, the continuous magnetization function $\mathbf{M}(\mathbf{r})$ introduced in eq. (**??**), is proportional to $\mathbf{S}$ according to

$$\mathbf{M}(\mathbf{r}_i) = -\frac{c_s}{a^3} \frac{g\mu_B}{\hbar} \mathbf{S}_i = -\frac{M_s}{S} \mathbf{S}_i,$$

the term $\cos \phi_{i,nn}$ can be calculated as :

$$\left[\mathbf{M}(\mathbf{r}_i + \mathbf{r}_{nn}) - \mathbf{M}(\mathbf{r}_i)\right]^2 = 2M_s^2 - 2M_s^2 \cos \phi_{i,nn} \tag{2.3}$$

in order to write eq.(**??**) as

$$E_{xc} = \frac{JS^2}{2M_s^2} \sum_i \sum_{nn} \left[\mathbf{M}(\mathbf{r}_i + \mathbf{r}_{nn}) - \mathbf{M}(\mathbf{r}_i)\right]^2 \tag{2.4}$$

where the constant term in eq.(**??**) was neglected. Applying first order Taylor approximation, thus implying that this theory is restricted to structures with

magnetization varying slowly in space, eq.(**??**) reads:

$$E_{xc} = \frac{JS^2}{2M_s^2} \sum_i \sum_{nn} \left[\left(\mathbf{r}_{nn} \cdot \nabla \right) \mathbf{M} \left(\mathbf{r}_i \right) \right]^2 . \tag{2.5}$$

which in the case of a cubic lattice with lattice constant a, yields:

$$E_{xc} = \frac{JS^2 a^2}{M_s^2} \sum_i \left[\left(\frac{\partial \mathbf{M}}{\partial x} \right)^2 + \left(\frac{\partial \mathbf{M}}{\partial y} \right)^2 + \left(\frac{\partial \mathbf{M}}{\partial z} \right)^2 \right]. \tag{2.6}$$

Introducing the density of spins per unit cells $\frac{c_s}{a^3}$:

$$E_{xc} = \frac{JS^2 a^2}{M_s^2} \int_V d\mathbf{r} \, \frac{c_s}{a^3} \left[\left(\frac{\partial \mathbf{M}}{\partial x} \right)^2 + \left(\frac{\partial \mathbf{M}}{\partial y} \right)^2 + \left(\frac{\partial \mathbf{M}}{\partial z} \right)^2 \right] \tag{2.7}$$

which is commonly written as:

$$E_{xc} = \frac{A}{M_s^2} \int_V d\mathbf{r} \, \left[\left(\frac{\partial \mathbf{M}}{\partial x} \right)^2 + \left(\frac{\partial \mathbf{M}}{\partial y} \right)^2 + \left(\frac{\partial \mathbf{M}}{\partial z} \right)^2 \right] = \frac{A}{M_s^2} \int_V d\mathbf{r} \, \left| \nabla \mathbf{M} \right|^2 \tag{2.8}$$

with $A \equiv \frac{JS^2 c_s}{a}$ the exchange constant in the micromagnetic model. Using eq.(**??**) it is possible to evaluate the exchange contribution to the effective field as:

$$\begin{aligned} \mathbf{H}_{xc} \left(\mathbf{r} \right) &\equiv -\frac{1}{\mu_0} \frac{\delta E_{xc}}{\delta \mathbf{M} \left(\mathbf{r} \right)} = -\frac{2A}{\mu_0 M_s^2} \sum_{\xi = x,y,z} \left[\int_V d\mathbf{r}' \, \frac{\partial \mathbf{M} \left(\mathbf{r}' \right)}{\partial \xi'} \frac{\partial \delta^3 \left(\mathbf{r}' - \mathbf{r} \right)}{\partial \xi'} \right] = \\ &= -\frac{2A}{\mu_0 M_s^2} \sum_{\xi = x,y,z} \left[\frac{\partial \mathbf{M} \left(\mathbf{r}' \right)}{\partial \xi'} \delta^3 \left(\mathbf{r}' - \mathbf{r} \right) \Big|_{\mathbf{r}' \in \partial V} - \int_V d\mathbf{r}' \, \frac{\partial^2 \mathbf{M} \left(\mathbf{r}' \right)}{\partial \xi'^2} \delta^3 \left(\mathbf{r}' - \mathbf{r} \right) \right] = \\ &= \frac{2A}{\mu_0 M_s^2} \left[\frac{\partial^2 \mathbf{M} \left(\mathbf{r} \right)}{\partial x^2} + \frac{\partial^2 \mathbf{M} \left(\mathbf{r} \right)}{\partial y^2} + \frac{\partial^2 \mathbf{M} \left(\mathbf{r} \right)}{\partial z^2} \right] = \frac{2A}{\mu_0 M_s^2} \nabla^2 \mathbf{M} \left(\mathbf{r} \right) \end{aligned} \tag{2.9}$$

where ∂V refers to the boundary of the system where the δ function vanishes. It is intuitive that uniform magnetization constitutes the lowest exchange energy configuration.

2.1.1 Accuracy of the micromagnetic description at atomic length scales

The aim of this subsection is to quantitatively show how much the micromagnetic theory deviates from the classical Heisenberg model [**?**]. Since the description of the exchange interaction exposed in this section is isotropic we can consider without loss of generality a one-dimensional spin spiral [see Fig. **??**] with wavelength λ, described by the formulas:

$$\mathbf{S}_i = \begin{pmatrix} S\sin\pi\frac{x_i}{\lambda} \\ S\cos\pi\frac{x_i}{\lambda} \\ 0 \end{pmatrix} \qquad \mathbf{M}(x) = \begin{pmatrix} M_s\sin\pi\frac{x}{\lambda} \\ M_s\cos\pi\frac{x}{\lambda} \\ 0 \end{pmatrix} \tag{2.10}$$

in the Heisenberg model and in micromagnetic theory respectively. The respective exchange energy density for the two models can be extrapolated by eqs.(**??**, **??**):

$$e_H(\lambda) = -\frac{c_s}{a^3}JS^2\sum_{nn}\cos\phi_{nn} = -2\frac{c_s}{a^3}JS^2\cos\left(\frac{\pi a}{\lambda}\right) \tag{2.11}$$

$$e_{MM}(\lambda) = \frac{A}{M_s^2}\left(\frac{\partial\mathbf{M}}{\partial x}\right)^2 = A\frac{\pi^2}{\lambda^2}\begin{pmatrix}\cos\frac{\pi x}{\lambda} \\ -\sin\frac{\pi x}{\lambda}\end{pmatrix}^2 = A\frac{\pi^2}{\lambda^2} = \frac{c_s}{a^3}JS^2\left(\frac{\pi a}{\lambda}\right)^2. \tag{2.12}$$

In order to compare the energy levels in the two models, their asymptotic limit for λ can be exploited:

$$\begin{aligned} &\lim_{\lambda\to\infty} e_{MM}(\lambda) = 0 \\ &\lim_{\lambda\to\infty} e_H(\lambda) = -2\frac{c_s}{a^3}JS^2 = e_{offs} \end{aligned} \tag{2.13}$$

so that the constant term e_{offs} must be subtracted from e_H. As can be easily demonstrated using Taylor expansion:

$$\begin{aligned} &e_H(\lambda) - e_{offs} = -2\frac{c_s}{a^3}JS^2\left[\cos\left(\frac{\pi a}{\lambda}\right) - 1\right] = \\ &= \frac{c_s}{a^3}JS^2\left(\frac{\pi a}{\lambda}\right)^2 + \mathcal{O}\left(\frac{a^4}{\lambda^4}\right) = e_{MM}(\lambda) + \mathcal{O}\left(\frac{a^4}{\lambda^4}\right). \end{aligned} \tag{2.14}$$

The ratio between the two expressions can then be written as:

$$\frac{e_H}{e_{MM}} = \frac{2\left[1-\cos\left(\frac{\pi a}{\lambda}\right)\right]}{\left(\frac{\pi a}{\lambda}\right)^2}, \tag{2.15}$$

a plot of this function (Fig. **??**) shows how the energy density diverges in the micromagnetic model for λ in the same order of magnitude as a.

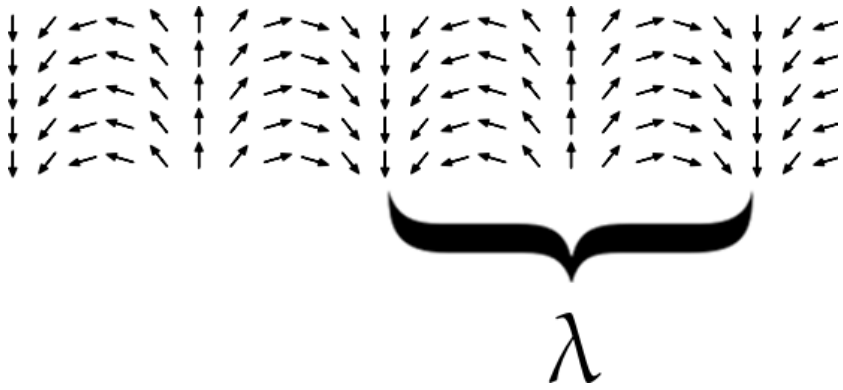

Figure 2.1: The magnetization structure described in Eq. **??**.

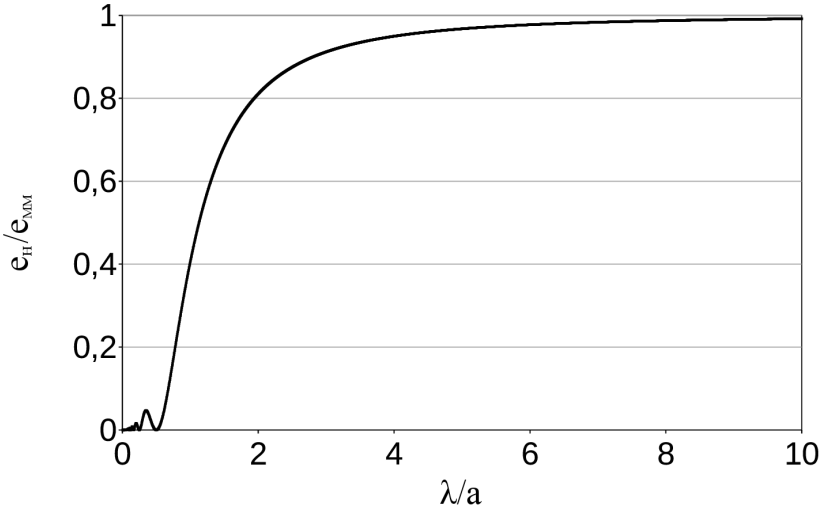

Figure 2.2: The ratio between the exchange energy density in the Heisenberg and micromagnetic model for a spin spiral as a function of λ/a shows how the micromagnetic model fails to accurately predict the effect of exchange interaction for magnetization structures varying on a length scale comparable to that of the atomic lattice.

2.2 Zeeman Energy

The energy of an external magnetic field $\mathbf{H}_{ext}$ acting on a ferromagnetic system can be written in the Heisenberg model as:

$$E_{Zee} = -\mu_0 \sum_i \boldsymbol{\mu}_i \cdot \mathbf{H}_{ext}, \tag{2.16}$$

since this is a local effect, namely affecting individually each magnetic moment, it can be easily generalized to micromagnetic theory:

$$E_{Zee} = -\mu_0 \int_V d\mathbf{r}\, \mathbf{M} \cdot \mathbf{H}_{ext}. \tag{2.17}$$

It can be immediately noticed that the Zeeman energy has a minimum if all the magnetic moments are aligned in the direction set by the external field.

2.3 Anisotropy Energy

The energy of a ferromagnetic system depends on the orientation of its magnetic moments, with respect to the structural axes of its crystal lattice. Anisotropies in the electronic orbitals remove degeneracies in the spin-orbit interaction making some particular orientations energetically favorable. This phenomenon can be intrinsic of the crystal lattice, or can arise as a surface effect. In any case, it is a local effect, therefore its treatment in the Heisenberg model does not differ from the micromagnetic one, with the obvious exception of treating individual magnetic moments rather than the continuous magnetization field. Here only low order terms of the anisotropy energy are given, since higher orders are usually averaged out by thermal agitation [**?**].

2.3.1 Uniaxial Anisotropy

In crystals with tetragonal or hexagonal structure, the magnetization tends to align according to the direction of a particular axis depending on the symmetry of the lattice. This is the case for materials such as gadolinium, cobalt, or dysprosium. This effect can also be induced in a multilayer system, in this case the axis will be perpendicular to the interface between layers of different materials. The energy for this effect can be written as:

$$E_{uni} = \int_V d\mathbf{r} \left[-\frac{K_1}{M_s^2} \left(\mathbf{M} \cdot \mathbf{e}_U\right)^2 - \frac{K_2}{M_s^4} \left(\mathbf{M} \cdot \mathbf{e}_U\right)^4 + \mathcal{O}\left(\mathbf{M} \cdot \mathbf{e}_U\right)^6 \right]. \tag{2.18}$$

It is noteworthy, that the even powers of the scalar product ensure the presence of an easy axis rather than an easy direction. In the case of $K_2 = 0$, if $K_1 > 0$, the axis $\mathbf{e}_U$ is the easy axis of the system, while for $K_1 < 0$ the magnetization tends to align in the plane perpendicular to $\mathbf{e}_U$ which is then a hard axis.

Choosing for simplicity $\mathbf{e}_U = \mathbf{e}_z$, the effective field for uniaxial anisotropy, can be written as:

$$\mathbf{H}_{uni} = -\frac{1}{\mu_0}\frac{\delta E_{uni}}{d\mathbf{M}} = \frac{2K_1}{\mu_0 M_s^2}\begin{pmatrix}0\\0\\M_z\end{pmatrix} + \frac{4K_2}{\mu_0 M_s^4}\begin{pmatrix}0\\0\\M_z^3\end{pmatrix}. \tag{2.19}$$

2.3.2 Cubic Anisotropy

In ferromagnetic materials with a cubic lattice, such as iron or nickel, the anisotropy energy contribution can be deduced from the symmetry of the system. The energy depends on the three components of the magnetization, chosen for the sake of simplicity parallel to the axes of the crystal, therefore it can be written as a series expansion of powers of the three components. Due to inversion symmetry, only even power terms are considered, while invariance for 90-degrees rotation ensures that this contribution is conserved under the permutation of any two components. This means that the quadratic term is proportional to M_s^2, and therefore constant. The expressions for the cubic anisotropy energy up to the sixth power, and the resulting effective field read:

$$E_{cub} = \int_V d\mathbf{r}\left[\frac{K_1}{M_s^4}\left(M_x^2M_y^2 + M_y^2M_z^2 + M_z^2M_x^2\right) + \frac{K_2}{M_s^6}\left(M_x^2M_y^2M_z^2\right)\right] \tag{2.20}$$

$$\mathbf{H}_{cub} = -\frac{1}{\mu_0}\frac{\delta E_{cub}}{d\mathbf{M}} = -\frac{2K_1}{\mu_0 M_s^4}\begin{pmatrix}M_xM_y^2 + M_xM_z^2\\M_yM_z^2 + M_yM_x^2\\M_zM_x^2 + M_zM_y^2\end{pmatrix} - \frac{2K_2}{\mu_0 M_s^6}\begin{pmatrix}M_xM_y^2M_z^2\\M_x^2M_yM_z^2\\M_x^2M_y^2M_z\end{pmatrix}. \tag{2.21}$$

2.4 Demagnetization Energy

The demagnetization field accounts for the interaction between one magnetic moment and the magnetic induction field generated by all the other magnetic moments in the system. In order to derive an analytical expression for this term, one can refer to the Coulomb experiment [**?**], where the force that two magnetic charges p_1 and p_2, at a distance r, exert on each other was measured

as:

$$\mathbf{F} = k\frac{p_1 p_2}{r^2}\mathbf{e}_r = p_1\mathbf{H} \tag{2.22}$$

with $k = 1/4\pi\mu_0$, the potential energy of an hypothetical magnetic monopole, in its own field can be therefore written as:

$$U = k\frac{p}{r}. \tag{2.23}$$

Since isolated magnetic monopoles are forbidden by the Maxwell equations, we will consider two poles, of equal magnitude p and opposite sign, at a relative position $\mathbf{l}$, forming the magnetic dipole:

$$\boldsymbol{\mu} = \frac{p}{\mu_0}\mathbf{l}, \tag{2.24}$$

inducing the potential energy:

$$U_{dip} = U^+ + U^- = kp\left(\frac{1}{|\mathbf{r} - \mathbf{l}\,|} - \frac{1}{r}\right) \tag{2.25}$$

that can be approximated to the first order in Taylor expansion as:

$$U_{dip} = -kp\,\mathbf{l}\cdot\nabla\left(\frac{1}{r}\right) = -kp\,\frac{\mathbf{l}\cdot\mathbf{r}}{r^3} \tag{2.26}$$

which recalling eq.(**??**) can be written as:

$$U_{dip} = -\frac{1}{4\pi}\,\frac{\boldsymbol{\mu}\cdot\mathbf{r}}{r^3} \tag{2.27}$$

and the related dipole field:

$$\mathbf{H}_{dip} = \frac{\partial U_{dip}}{\partial \mathbf{r}} = -\frac{1}{4\pi}\left(\frac{\boldsymbol{\mu}}{r^3} - 3\frac{\boldsymbol{\mu}\cdot\mathbf{r}}{r^5}\mathbf{r}\right). \tag{2.28}$$

The demagnetization field generated by a system of dipoles can therefore be written as:

$$\mathbf{H}_D = -\frac{1}{4\pi}\sum_i\left[\frac{\boldsymbol{\mu}}{|\mathbf{r} - \mathbf{r}_i|^3} - 3\frac{\boldsymbol{\mu}\cdot(\mathbf{r} - \mathbf{r}_i)}{|\mathbf{r} - \mathbf{r}_i|^5}(\mathbf{r} - \mathbf{r}_i)\right] \tag{2.29}$$

and the corresponding energy term:

$$E_D = \frac{\mu_0}{8\pi}\sum_j \boldsymbol{\mu}_j \cdot \sum_{i\neq j}\left[\frac{\boldsymbol{\mu}_i}{|\mathbf{r}_j - \mathbf{r}_i|^3} - 3\frac{\boldsymbol{\mu}_i\cdot(\mathbf{r}_j - \mathbf{r}_i)}{|\mathbf{r}_j - \mathbf{r}_i|^5}(\mathbf{r}_j - \mathbf{r}_i)\right]. \tag{2.30}$$

To derive the same contribution in the micromagnetic model, the theory of Maxwell equations in magnetic media can be used, in the absence of currents or electric fields Ampere's law yields:

$$\nabla \times \mathbf{H} = 0 \tag{2.31}$$

the magnetic field is therefore conservative and can be written as the gradient of a scalar potential:

$$\mathbf{H} = -\nabla U_D. \tag{2.32}$$

From the Gauss's law for magnetism

$$\nabla \cdot \mathbf{B} = 0 \tag{2.33}$$

and the relation

$$\mathbf{B} = \mu_0 \left(\mathbf{H} + \mathbf{M}\right) \tag{2.34}$$

follows:

$$\nabla \cdot \mathbf{H} = -\nabla \cdot \mathbf{M}, \tag{2.35}$$

therefore the scalar potential fulfills the Poisson equation:

$$\nabla^2 U_D = \nabla \cdot \mathbf{M} \tag{2.36}$$

for which the general solution is:

$$U_D\left(\mathbf{r}\right) = \frac{1}{4\pi}\left[\int_V d\mathbf{r}' \, \frac{-\nabla' \cdot \mathbf{M}\left(\mathbf{r}'\right)}{\left|\mathbf{r} - \mathbf{r}'\right|} + \oint_{\partial V} d\mathbf{r}' \, \frac{\mathbf{M}\left(\mathbf{r}'\right) \cdot \mathbf{e}_n\left(\mathbf{r}'\right)}{\left|\mathbf{r} - \mathbf{r}'\right|}\right] \tag{2.37}$$

with $\mathbf{e}_n\left(\mathbf{r}\right)$ perpendicular to the surface ∂V at position $\mathbf{r}$ and pointing outwards. Applying eq.(**??**):

$$\mathbf{H}_D\left(\mathbf{r}\right) = -\frac{\nabla}{4\pi}\left[\int_V d\mathbf{r}' \, \frac{-\nabla' \cdot \mathbf{M}\left(\mathbf{r}'\right)}{\left|\mathbf{r} - \mathbf{r}'\right|} + \oint_{\partial V} d\mathbf{r}' \, \frac{\mathbf{M}\left(\mathbf{r}'\right) \cdot \mathbf{e}_n\left(\mathbf{r}'\right)}{\left|\mathbf{r} - \mathbf{r}'\right|}\right]. \tag{2.38}$$

The demagnetization energy then yields:

$$
\begin{aligned}
E_D &= -\frac{\mu_0}{2}\int_V d\mathbf{r}\,\mathbf{M}(\mathbf{r})\cdot\mathbf{H}_D(\mathbf{r}) = \\
&= \frac{\mu_0}{8\pi}\int_V d\mathbf{r}\,\mathbf{M}(\mathbf{r})\cdot\nabla\left[\int_V d\mathbf{r}'\,\frac{-\nabla'\cdot\mathbf{M}(\mathbf{r}')}{|\mathbf{r}-\mathbf{r}'|}+\oint_{\partial V} d\mathbf{r}'\,\frac{\mathbf{M}(\mathbf{r}')\cdot\mathbf{e}_n(\mathbf{r}')}{|\mathbf{r}-\mathbf{r}'|}\right] = \\
&= \frac{\mu_0}{8\pi}\left[\oint_{\partial V} d\mathbf{r}'\,\mathbf{M}(\mathbf{r}')\cdot\mathbf{e}_n(\mathbf{r}') - \int_V d\mathbf{r}'\,\nabla'\cdot\mathbf{M}(\mathbf{r}')\right]\int_V d\mathbf{r}\,\mathbf{M}(\mathbf{r})\cdot\nabla\frac{1}{|\mathbf{r}-\mathbf{r}'|}.
\end{aligned}
\tag{2.39}
$$

Using the divergence theorem:

$$
\begin{aligned}
&\oint_{\partial V} d\mathbf{r}\,\frac{\mathbf{M}(\mathbf{r})\cdot\mathbf{e}_n(\mathbf{r})}{|\mathbf{r}'-\mathbf{r}|} = \int_V d\mathbf{r}\,\nabla\cdot\frac{\mathbf{M}(\mathbf{r})}{|\mathbf{r}'-\mathbf{r}|} = \\
&= \int_V d\mathbf{r}\,\left[\frac{\nabla\cdot\mathbf{M}(\mathbf{r})}{|\mathbf{r}'-\mathbf{r}|}+\mathbf{M}(\mathbf{r})\cdot\nabla\frac{1}{|\mathbf{r}'-\mathbf{r}|}\right]
\end{aligned}
\tag{2.40}
$$

one finds:

$$
\begin{aligned}
&\int_V d\mathbf{r}\,\mathbf{M}(\mathbf{r})\cdot\nabla\frac{1}{|\mathbf{r}'-\mathbf{r}|} = \\
&= \oint_{\partial V} d\mathbf{r}\,\frac{\mathbf{M}(\mathbf{r})\cdot\mathbf{e}_n(\mathbf{r})}{|\mathbf{r}'-\mathbf{r}|} - \int_V d\mathbf{r}\,\frac{\nabla\cdot\mathbf{M}(\mathbf{r})}{|\mathbf{r}'-\mathbf{r}|}
\end{aligned}
\tag{2.41}
$$

so that eq.(**??**) can be rewritten as:

$$
\begin{aligned}
&E_D = \\
&= \frac{\mu_0}{8\pi}\left(\oint_{\partial V} d\mathbf{r}'\,\mathbf{M}\cdot\mathbf{e}_n - \int_V d\mathbf{r}'\,\nabla'\cdot\mathbf{M}\right)\left(\oint_{\partial V} d\mathbf{r}\,\mathbf{M}\cdot\mathbf{e}_n - \int_V d\mathbf{r}\,\nabla\cdot\mathbf{M}\right)\frac{1}{|\mathbf{r}-\mathbf{r}'|} = \\
&= \frac{\mu_0}{8\pi}\left[\oint_{\partial V} d\mathbf{r}'\,\sigma(\mathbf{r}') + \int_V d\mathbf{r}'\,\rho(\mathbf{r}')\right]\left[\oint_{\partial V} d\mathbf{r}\,\sigma(\mathbf{r}) + \int_V d\mathbf{r}\,\rho(\mathbf{r})\right]\frac{1}{|\mathbf{r}-\mathbf{r}'|}
\end{aligned}
\tag{2.42}
$$

where the volume charge density $\rho \equiv -\nabla \cdot \mathbf{M}$ and the surface charge density $\sigma \equiv \mathbf{M} \cdot \mathbf{e}_n$ are used. It can be immediately noticed that these quantities are minimized for a closed flux magnetization pattern, which corresponds to a magnetization field that does not have any source or drain. Alternatively eq.(**??**) can be written in a form similar to eq.(**??**) by explicitly evaluating the derivatives and using the divergence theorem in the form expressed in eq.(**??**) as:

$$\begin{aligned} E_D &= \frac{\mu_0}{8\pi} \int_V d\mathbf{r}' \int_V d\mathbf{r}\, \mathbf{M}(\mathbf{r}') \cdot \nabla' \left[\mathbf{M}(\mathbf{r}) \cdot \nabla \frac{1}{|\mathbf{r}-\mathbf{r}'|} \right] \\ &= \frac{\mu_0}{8\pi} \int_V d\mathbf{r}' \int_V d\mathbf{r}\, \mathbf{M}(\mathbf{r}') \cdot \nabla' \left[\frac{\mathbf{M}(\mathbf{r}) \cdot (\mathbf{r}-\mathbf{r}')}{|\mathbf{r}-\mathbf{r}'|^3} \right] \\ &= \frac{\mu_0}{8\pi} \int_V d\mathbf{r}' \int_V d\mathbf{r} \left\{ \frac{\mathbf{M}(\mathbf{r}) \cdot \mathbf{M}(\mathbf{r}')}{|\mathbf{r}-\mathbf{r}'|^3} - 3\frac{[\mathbf{M}(\mathbf{r}) \cdot (\mathbf{r}-\mathbf{r}')]\,[\mathbf{M}(\mathbf{r}') \cdot (\mathbf{r}-\mathbf{r}')]}{|\mathbf{r}-\mathbf{r}'|^5} \right\}. \end{aligned} \tag{2.43}$$

2.4.1 Reciprocity theorem for magnetism

It can be easily shown that the energy of two ferromagnets, interacting with each other through the demagnetizing field is equally distributed between the two bodies: let $\mathbf{B}_i$ be the magnetic induction field generated by the ferromagnetic body τ_i and $\mathbf{H}_i$ the related magnetic field. From Maxwell's equations

$$\nabla \cdot \mathbf{B} = 0 \qquad \nabla \times \mathbf{H} = 0$$

follows that $\mathbf{B}_i$ is solenoidal and $\mathbf{H}_i$ is irrotational, therefore:

$$\int_{\mathbb{R}^3} d\mathbf{r}\, \mathbf{B}_i \cdot \mathbf{H}_j = 0 \tag{2.44}$$

for $i, j = 1, 2$. Using the constitutive relation

$$\mathbf{B}_i = \mu_0 (\mathbf{H}_i + \mathbf{M}_i)$$

where $\mathbf{M}_i$ is the magnetization in the body τ_i, it is possible to write the demagnetization energy for τ_j in the field generated by τ_i as:

$$\begin{aligned} E_D^{ji} &= \int_{\mathbb{R}^3} d\mathbf{r}\, \mathbf{H}_i \cdot \mathbf{M}_j = \int_{\mathbb{R}^3} d\mathbf{r}\, \mathbf{H}_i \cdot \left(\frac{1}{\mu_0} \mathbf{B}_j - \mathbf{H}_j \right) = - \int_{\mathbb{R}^3} d\mathbf{r}\, \mathbf{H}_i \cdot \mathbf{H}_j \\ &= \int_{\mathbb{R}^3} d\mathbf{r}\, \left(\frac{1}{\mu_0} \mathbf{B}_i - \mathbf{H}_i \right) \cdot \mathbf{H}_j = \int_{\mathbb{R}^3} d\mathbf{r}\, \mathbf{H}_j \cdot \mathbf{M}_i = E_D^{ij} \end{aligned} \tag{2.45}$$

where the integral on the whole three dimensional space $\mathbb{R}^3$ can be restricted to the volume occupied by the ferromagnetic systems without loss of generality.

2.4.2 Demagnetization tensor

The demagnetizing field generated by a uniformly magnetized system can be written as [**?**]

$$\mathbf{H} = -\underline{N} \cdot \mathbf{M} \tag{2.46}$$

where $\underline{N}$ denotes the demagnetization tensor. Since $\underline{N}$ depends only on the shape of the ferromagnetic system, the demagnetization tensor needs to be calculated only once, at the beginning of the simulation, thereby decreasing dramatically the computational complexity of evaluating this effective field term. In order to carry out the evaluation of the tensor, the system is assumed to be composed of several uniformly magnetized domains, this abstraction is mirrored in numerical approaches based on the finite difference method due to the necessity for any continuous system to be discretized for computational application. Eq.(**??**) can be written, with the aid of eq.(**??**) as:

$$U_D(\mathbf{r}) = \frac{1}{4\pi} \int_{\tau'} d\mathbf{r}'\, \mathbf{M}(\mathbf{r}') \cdot \nabla' \left(\frac{1}{|\mathbf{r} - \mathbf{r}'|} \right) = \frac{\mathbf{M}'}{4\pi} \cdot \int_{\tau'} d\mathbf{r}'\, \nabla' \left(\frac{1}{|\mathbf{r} - \mathbf{r}'|} \right) \tag{2.47}$$

where τ' is a volume element with uniform magnetization $\mathbf{M}'$. The average field generated in the volume element τ by the magnetization in τ' is therefore:

$$\langle \mathbf{H}' \rangle_\tau = -\frac{1}{\tau} \int_\tau d\mathbf{r}\, \nabla U_D(\mathbf{r}) = -\frac{\mathbf{M}'}{4\pi\tau} \cdot \int_\tau d\mathbf{r} \int_{\tau'} d\mathbf{r}'\, \nabla \otimes \nabla' \left(\frac{1}{|\mathbf{r} - \mathbf{r}'|} \right) = -\mathbf{M}' \cdot \underline{N} \tag{2.48}$$

where the symbol $\otimes$ denotes the tensor product

$$\nabla \otimes \nabla' = \begin{pmatrix} \frac{\partial^2}{\partial x \partial x'} & \frac{\partial^2}{\partial y \partial x'} & \frac{\partial^2}{\partial z \partial x'} \\ \frac{\partial^2}{\partial x \partial y'} & \frac{\partial^2}{\partial y \partial y'} & \frac{\partial^2}{\partial z \partial y'} \\ \frac{\partial^2}{\partial x \partial z'} & \frac{\partial^2}{\partial y \partial z'} & \frac{\partial^2}{\partial x \partial z'} \end{pmatrix}. \tag{2.49}$$

Following the operative definition from eq.(**??**) used in eq.(**??**) the demagnetization tensor can be written as:

$$\begin{aligned} \underline{N} &= \frac{1}{4\pi\tau} \int_{\tau} d\mathbf{r} \int_{\tau'} d\mathbf{r}' \, \nabla \otimes \nabla' \left(\frac{1}{|\mathbf{r} - \mathbf{r}'|} \right) = \\ &= -\frac{1}{4\pi\tau} \int_{\tau} d\mathbf{r} \int_{\tau'} d\mathbf{r}' \, \nabla' \otimes \nabla' \left(\frac{1}{|\mathbf{r} - \mathbf{r}'|} \right) \end{aligned} \tag{2.50}$$

since $\nabla \left(\frac{1}{|\mathbf{r}-\mathbf{r}'|} \right) = -\nabla' \left(\frac{1}{|\mathbf{r}-\mathbf{r}'|} \right)$. The demagnetization energy induced in the body τ with uniform magnetization $\mathbf{M}$ by the body τ' reads:

$$E_D = -\frac{\tau \mu_0}{2} \, \mathbf{M} \cdot \underline{N} \cdot \mathbf{M}'. \tag{2.51}$$

The properties of $\underline{N}$ can be easily derived. It is clearly symmetric, due to the Schwarz theorem. By choosing reference coordinates $\mathbf{r}_0$ in τ, and $\mathbf{r}'_\mathbf{0}$ in τ', the tensor is a function of $\mathbf{R} \equiv \mathbf{r}_0 - \mathbf{r}'_\mathbf{0}$. Applying the reciprocity theorem, and exploiting the symmetry of $\underline{N}$:

$$M \cdot \underline{N}\,(\mathbf{R}) \cdot M' = M' \cdot \underline{N}\,(-\mathbf{R}) \cdot M = M \cdot \underline{N}\,(-\mathbf{R}) \cdot M' \tag{2.52}$$

therefore: $\underline{N}\,(\mathbf{R}) = \underline{N}\,(-\mathbf{R})$. The trace of $\underline{N}$ satisfies:

$$Tr\,(\underline{N}) = -\frac{1}{4\pi\tau} \int_{\tau} d\mathbf{r} \int_{\tau'} d\mathbf{r}' \, \nabla'^2 \left(\frac{1}{|\mathbf{r} - \mathbf{r}'|} \right) = \frac{1}{\tau} \int_{\tau} d\mathbf{r} \int_{\tau'} d\mathbf{r}' \, \delta^3 (\mathbf{r} - \mathbf{r}') \tag{2.53}$$

this integral is equal to the fraction of τ which overlaps τ', if the two volume elements coincide, $Tr\,(\underline{N}) = 1$, if they do not overlap $Tr\,(\underline{N}) = 0$. Using the Gauss theorem, the integrals in eq.(**??**) can be reduced to surface integrals:

$$\begin{aligned} \underline{N} &\equiv \frac{1}{4\pi\tau} \int_{\tau} d\mathbf{r} \int_{\tau'} d\mathbf{r}' \, \nabla \otimes \nabla' \left(\frac{1}{|\mathbf{r} - \mathbf{r}'|} \right) = \\ &= \frac{1}{4\pi\tau} \int_{\partial\tau} d\mathbf{r} \int_{\partial\tau'} d\mathbf{r}' \, \frac{\mathbf{e}_n (\mathbf{r}) \otimes \mathbf{e}_n (\mathbf{r}')}{|\mathbf{r} - \mathbf{r}'|}. \end{aligned} \tag{2.54}$$

This formula is particularly convenient when evaluating the demagnetization tensor for an array of rectangular blocks, such as in the case of a system simulated numerically in the finite difference method. This allows one to reduce the interaction between two blocks to the interaction between each face of one block with each face of the other. These contributions were calculated by A.J. Newell in Ref. [**?**]. In the Heisenberg model, an expression for the demagnetization tensor, to be applied to magnetic moments can be recovered from eq.(**??**):

$$\underline{N} = \frac{1}{4\pi}\left[\frac{\underline{\mathbb{1}}}{|\mathbf{r}-\mathbf{r}'|^3} - 3\frac{(\mathbf{r}-\mathbf{r}')\otimes(\mathbf{r}-\mathbf{r}')}{|\mathbf{r}-\mathbf{r}'|^5}\right], \tag{2.55}$$

the demagnetization energy of two magnetic moments can be written as:

$$E_D^{i,j} = \boldsymbol{\mu}_i\, \underline{N}\, \boldsymbol{\mu}_j = \frac{1}{4\pi}\, \boldsymbol{\mu}_i \left[\frac{\underline{\mathbb{1}}}{|\mathbf{r}_i-\mathbf{r}_j|^3} - 3\frac{(\mathbf{r}_i-\mathbf{r}_j)\otimes(\mathbf{r}_i-\mathbf{r}_j)}{|\mathbf{r}_i-\mathbf{r}_j|^5}\right] \boldsymbol{\mu}_j.$$

2.5 Anisotropic Exchange

The exchange energy expressed in eq.(**??**) constitutes not only the simplest case of exchange interaction, but also the predominant one, in terms of magnitude, for most ferromagnets. The exchange interaction, can be written in a general form with the aid of the exchange tensor $\underline{J}$.

$$E_{xc} = -\frac{1}{2}\sum_{i\neq j} \mathbf{S}_i\, \underline{J}_{ij}\, \mathbf{S}_j$$

where $\underline{J}_{ij} = \left\{J_{ij}^{\alpha\beta}\right\}$ for $\alpha, \beta = x, y, z$, is a 3×3 matrix. The decomposition of this matrix,

$$\underline{J}_{ij} = J_{ij}\underline{\mathbb{1}} + \underline{J}_{ij}^s + \underline{J}_{ij}^a$$

in a diagonal, a symmetrical, and an antisymmetric matrix; is akin to studying the exchange interaction as three separated phenomena. The diagonal term, with

$$J_{ij} \equiv \frac{1}{3}\, Tr\left(\underline{J}_{ij}\right)$$

constitutes the isotropic exchange exposed in section **??**, it is interesting to notice that J_{ij} is defined as the average value of the diagonal terms of $\underline{J}_{ij}$. The symmetric term is defined as

$$\underline{J}_{ij}^s \equiv \frac{1}{2}\left(\underline{J}_{ij} + \underline{J}_{ij}^T\right) - J_{ij}\underline{\mathbb{1}}$$

where the superscript T denotes the transposed matrix, so that

$$\left(J_{ij}^{T}\right)^{\alpha\beta} = J_{ij}^{\beta\alpha}.$$

Since it usually constitutes a small correction to the isotropic exchange, it is frequently neglected [**?**]. The trace of $\underline{J}_{ij}^{s}$ is evidently zero, due to the properties of the average:

$$Tr\left(\underline{J}_{ij}^{s}\right) = \sum_{\alpha=x,y,z}\left(J_{ij}^{\alpha\alpha} - J_{ij}\right) = \sum_{\alpha=x,y,z}\left(J_{ij}^{\alpha\alpha} - \left\langle J_{ij}^{\xi\xi}\right\rangle\right) = 0$$

where $J_{ij}^{\xi\xi}$ denotes the general diagonal element of $\underline{J}_{ij}$. The energy contribution related to the antisymmetric term

$$\underline{J}_{ij}^{a} \equiv \frac{1}{2}\left(\underline{J}_{ij} - \underline{J}_{ij}^{T}\right)$$

can be written in the form

$$E_{xc}^{a} = -\frac{1}{2}\sum_{i\neq j}\mathbf{S}_i\,\underline{J}_{ij}^{a}\,\mathbf{S}_j = -\frac{1}{2}\sum_{i\neq j}\mathbf{D}_{ij}\cdot\left(\mathbf{S}_i\times\mathbf{S}_j\right) \tag{2.56}$$

and is known as Dzyaloshinsky-Moriya [**?**, **?**] interaction (DMI).

2.5.1 Dzyaloshinskii-Moriya Interaction

Asymmetric exchange interaction occurs naturally in bulk materials which exhibit broken inversion symmetry. It can also be induced, in properly engineered structures, at the asymmetric interface of thin magnetic layers. Due to the innovative features of this phenomenon, materials or devices, exhibiting such behavior, are being investigated for the production of next generation information technology [**?**, **?**, **?**]. The components of $\mathbf{D}_{ij}$ can be derived, as follows, from eq.(**??**):

$$\begin{aligned}
\mathbf{S}_i\,\underline{J}_{ij}^{a}\,\mathbf{S}_j &= \mathbf{S}_i\cdot\left(\underline{J}_{ij}^{a}\,\mathbf{S}_j\right) = \mathbf{S}_i\cdot\sum_{\alpha=x,y,z}\left(\sum_{\beta=x,y,z}J_{ij}^{a,\alpha\beta}S_j^{\beta}\right)\hat{\alpha} = \\
&= \sum_{\alpha,\beta=x,y,z}S_i^{\alpha}J_{ij}^{a,\alpha\beta}S_j^{\beta} = \sum_{\alpha<\beta}S_i^{\alpha}J_{ij}^{a,\alpha\beta}S_j^{\beta} - S_i^{\beta}J_{ij}^{a,\beta\alpha}S_j^{\alpha} = \\
&= \sum_{\alpha<\beta}J_{ij}^{a,\alpha\beta}\left(S_i^{\alpha}S_j^{\beta} - S_i^{\beta}S_j^{\alpha}\right) = \sum_{\gamma=x,y,z}D_{ij}^{\gamma}\epsilon_{\alpha\beta\gamma}\left(S_i^{\alpha}S_j^{\beta} - S_i^{\beta}S_j^{\alpha}\right) = \\
&= \mathbf{D}_{ij}\cdot\left(\mathbf{S}_i\times\mathbf{S}_j\right)
\end{aligned} \tag{2.57}$$

with

$$\mathbf{D}_{ij} = \left(\frac{J_{ij}^{a,yz} - J_{ij}^{a,zy}}{2}, \quad \frac{J_{ij}^{a,zx} - J_{ij}^{a,xz}}{2}, \quad \frac{J_{ij}^{a,xy} - J_{ij}^{a,yx}}{2} \right)$$

In order to obtain a micromagnetic formulation for the DMI, a similar approach as the one for the isotropic exchange can be used, exploiting

$$\mathbf{M}(\mathbf{r}_i) = -\frac{M_s}{S}\mathbf{S_i}$$

and applying a first order Taylor approximation:

$$\begin{aligned} E_{DMI} &= -\frac{1}{2}\sum_{i\neq j} \mathbf{D}_{ij} \cdot (\mathbf{S}_i \times \mathbf{S}_j) = -\frac{S^2}{2M_s^2}\sum_{i\neq j} \mathbf{D}_{ij} \cdot [\mathbf{M}(\mathbf{r}_i) \times \mathbf{M}(\mathbf{r}_j)] = \\ &= -\frac{S^2}{2M_s^2}\sum_{i\neq j} \mathbf{D}_{ij} \cdot \left[\mathbf{M}(\mathbf{r}_i) \times ((\mathbf{r}_j - \mathbf{r}_i)\cdot\nabla)\,\mathbf{M}(\mathbf{r}_i) + \mathcal{O}(\mathbf{r}_j - \mathbf{r}_i)^2\right] \end{aligned} \tag{2.58}$$

neglecting higher orders in the Taylor series, applying the cyclical invariance property for the parallelepiped product, and the fact that the cross product is antisymmetric:

$$\begin{aligned} E_{DMI} &= -\frac{S^2}{2M_s^2}\sum_{i\neq j} \mathbf{D}_{ij} \cdot [\mathbf{M}(\mathbf{r}_i) \times ((\mathbf{r}_j - \mathbf{r}_i)\cdot\nabla)\,\mathbf{M}(\mathbf{r}_i)] = \\ &= \frac{S^2}{2M_s^2}\sum_{i\neq j} \mathbf{M}(\mathbf{r}_i) \cdot [\mathbf{D}_{ij} \times ((\mathbf{r}_j - \mathbf{r}_i)\cdot\nabla)\,\mathbf{M}(\mathbf{r}_i)] = \\ &= \frac{S^2}{2M_s^2}\sum_{i\neq j} \mathbf{M}(\mathbf{r}_i) \cdot [\mathbf{D}_{ij}((\mathbf{r}_j - \mathbf{r}_i)\cdot\nabla) \times \mathbf{M}(\mathbf{r}_i)] \end{aligned} \tag{2.59}$$

where in the last term the fact that $(\mathbf{r}_j - \mathbf{r}_i)\cdot\nabla$ is a scalar was exploited. Defining $\mathbf{r} \equiv \mathbf{r}_j - \mathbf{r}_i$ and D_ξ the generic component of $\mathbf{D}_{ij}$, the first term in the cross product can be rewritten further:

$$\mathbf{D}_{ij}(\mathbf{r}\cdot\nabla) = \begin{bmatrix} D_x r_x \frac{\partial}{\partial x} + D_x r_y \frac{\partial}{\partial y} + D_x r_z \frac{\partial}{\partial z} \\ D_y r_x \frac{\partial}{\partial x} + D_y r_y \frac{\partial}{\partial y} + D_y r_z \frac{\partial}{\partial z} \\ D_z r_x \frac{\partial}{\partial x} + D_z r_y \frac{\partial}{\partial y} + D_z r_z \frac{\partial}{\partial z} \end{bmatrix} = (\mathbf{D}_{ij} \otimes \mathbf{r}_{ij})\,\nabla \tag{2.60}$$

so that:

$$\begin{aligned} E_{DMI} &= \frac{S^2}{2M_s^2}\sum_{i\neq j} \mathbf{M}(\mathbf{r}_i) \cdot [((\mathbf{D}_{ij} \otimes \mathbf{r}_{ij})\,\nabla) \times \mathbf{M}(\mathbf{r}_i)] = \\ &= \frac{S^2}{2M_s^2}\sum_{i} \mathbf{M}(\mathbf{r}_i) \cdot [(\underline{D}_i\nabla) \times \mathbf{M}(\mathbf{r}_i)] \end{aligned} \tag{2.61}$$

where the tensor $\underline{D}_i$ was defined as:

$$\underline{D}_i \equiv \sum_{j \neq i} \mathbf{D}_{ij} \otimes \mathbf{r}_{ij}.$$

The DMI effective field can then be written in the micromagnetic theory as:

$$\mathbf{H}_{DMI}(\mathbf{r}_i) = \frac{S^2}{\mu_0 M_s^2} \left[(\underline{D}_i \nabla) \times \mathbf{M}(\mathbf{r}_i) \right]. \tag{2.62}$$

2.6 Current Induced Spin Torques

The magnetization in a ferromagnet can be influenced by the injection of current, producing effects that cannot be achieved using magnetic fields. The magnetic interaction between injected and localized electrons generates current induced spin torques. While it is not possible to unambiguously distinguish conduction electrons from localized ones, this effect is explained, in good agreement with the experimental evidence, within the sd-model [**?**,**?**, **?**,**?**,**?**], where the interaction between an itinerant spin and a localized one in 3d transition metal ferromagnets such as Iron, Cobalt, and Nickel is described by an energy term analogous to the one used for exchange interaction [see Eq. **??**]: $E_{sd} = -J_{sd} \mathbf{S_s} \cdot \mathbf{S_d}$.

2.6.1 Spin currents

In order for the collective effect of the itinerant electrons on the magnetization to be finite, their average spin must be non-zero, for this reason it is important to distinguish between charge current and spin current. While the charge current density, defined as

$$\mathbf{j}_e = e \left(\mathbf{v}_+ n_+ + \mathbf{v}_- n_- \right)$$

with $n_\pm$ the electron density for each spin state and $\mathbf{v}_\pm$ the respective velocity, describes the total electric charge flowing in the system, the spin current density

$$\mathbf{j}_s = \frac{\hbar}{2} \left(\mathbf{v}_+ n_+ - \mathbf{v}_- n_- \right)$$

describes the flow of spin, therefore of magnetic moment. It can be easily noticed that for $\mathbf{v}_+ n_+ = -\mathbf{v}_- n_-$ a vanishing charge current leads to a finite spin current $\mathbf{j}_s = 2\mathbf{v}_+ n_+$, this is the case of a pure spin current. If $\mathbf{v}_+$ and $\mathbf{v}_-$ are collinear, the polarization defined as $P = |\mathbf{v}_+ n_+ - \mathbf{v}_- n_-| \,/\, |\mathbf{v}_+ n_+ + \mathbf{v}_- n_-|$ relates the two currents:

$$\mathbf{j}_s = \frac{\hbar P}{2e} \mathbf{j}_e. \tag{2.63}$$

2.6.2 Spin transfer torque

The earliest attempts [?, ?, ?] to generate such torques were based on the injection of current from a non-magnetic metal into a conducting ferromagnet. Multilayer systems, such as spin valves, were employed to polarize the current travelling in the direction perpendicular to the layers. Such a device is based on a pinned layer which polarizes the current and a free layer whose magnetization can be manipulated by the torque. An analytical expression for the torque can be derived from the continuity equation for the unit magnetic moment of the itinerant spin $\mathbf{m}$ [?, ?]:

$$\frac{d\mathbf{m}}{dt} + 2\frac{\mu_B}{\hbar}\nabla \cdot \mathbf{j}_s = -\frac{J_{sd}}{\hbar M_s}\left(\mathbf{m} \times \mathbf{M}\right) - \Gamma_{sf}\left(\mathbf{m}\right) \tag{2.64}$$

where the first term on the right-hand side is derived from the Heisenberg equation of motion [see Eq. **??**] and describes the precession of the itinerant magnetization $\mathbf{m}$ around the localized one $\mathbf{M}$, while the second term contains phenomenological effects related to scattering which cause itinerant electrons to flip their spin.

Introducing the characteristic times $\tau_{sd} = \hbar/J_{sd}$ and τ_{sf} Eq. **??** can be rewritten as:

$$\frac{d\mathbf{m}}{dt} + 2\frac{\mu_B}{\hbar}\nabla \cdot \mathbf{j}_s = -\frac{\mathbf{m} \times \mathbf{M}}{\tau_{sd} M_s} - \frac{\delta\mathbf{m}}{\tau_{sf}} \tag{2.65}$$

where the relation $\mathbf{m} = m_0\mathbf{M}/M_s + \delta\mathbf{m}$ was used to separate the equilibrium component of $\mathbf{m}$, parallel to $\mathbf{M}$, from the perpendicular one $\delta\mathbf{m}$.

Assuming a linear response and neglecting the derivatives of order higher than the second in $\delta\mathbf{m}$, Eq. **??** leads to

$$\frac{m_0}{M_s}\frac{d\mathbf{M}}{dt} - \frac{\mu_B P}{eM_s}\left(\mathbf{j}_e \cdot \nabla\right)\mathbf{M} = -\frac{\delta\mathbf{m} \times \mathbf{M}}{\tau_{sd} M_s} - \frac{\delta\mathbf{m}}{\tau_{sf}} \tag{2.66}$$

where Eq. **??** was used.

Eq. **??** is an implicit equation in $\delta\mathbf{m}$ which can be made explicit, as shown in chapter **??**, taking the vector product on both terms. The explicit formulation of Eq. **??** reads:

$$\delta\mathbf{m} = \frac{\mu_B P \tau_{sd}}{eM_s\left(1+\xi^2\right)}\left[\xi\left(\mathbf{j}_e \cdot \nabla\right)\mathbf{M} + \frac{1}{M_s}\mathbf{M} \times \left(\mathbf{j}_e \cdot \nabla\right)\mathbf{M}\right] \tag{2.67}$$

where terms proportional to m_0/M_s were neglected and $\xi = \tau_{sd}/\tau_{sf}$ was defined.

The torque acting on the local magnetization reads then:

$$T = -\frac{\mathbf{M} \times \delta\mathbf{m}}{\tau_{sd} M_s} = -\frac{b_J}{M_s}\left[\xi\mathbf{M} \times \left(\mathbf{j}_e \cdot \nabla\right)\mathbf{M} + \frac{1}{M_s}\mathbf{M} \times \left[\mathbf{M} \times \left(\mathbf{j}_e \cdot \nabla\right)\mathbf{M}\right]\right] \tag{2.68}$$

with $b_J = \mu_B P / e M_s \, (1 + \xi^2)$.

In a similar fashion to the two terms of Eq. **??**, analysed in section **??**, the two terms in the brackets are perpendicular to each other and cause, respectively, a precession of the magnetization around the direction of $(\mathbf{j}_e \cdot \nabla)\,\mathbf{M}$ and alignment towards it. In particular since the latter is not conservative and could in principle compete with the damping term [**?**] in Eq. **??** it is often referred to as non adiabatic or anti-damping torque. Notably, it was suggested as a mechanism to switch the magnetization of domains in data storage devices [**?**]. It can be easily noticed that if spin flip is neglected, which is the limiting case of $\tau_{sf} \to \infty$ or $\xi \to 0$, the adiabatic torque in Eq. **??** vanishes, therefore it can be considered to be a direct consequence of the spin flip phenomena.

The right side of Eq. **??** can be inserted in the LLG equation in order to predict the magnetization dynamics in the presence of a current.

2.6.3 Spin orbit torque

Multilayered systems with broken inversion symmetry, and in particular those composed of a thin ferromagnetic layer between a heavy metal and an oxide, have shown a response to currents which is not compatible with the effects of the spin transfer torque [**?**,**?**,**?**] described in the previous subsection. In particular domain walls moving against the direction of the electron flow and at higher speeds than those predicted by the theory of the spin transfer torque were measured [**?**,**?**,**?**]. These effect could be ascribed to spin polarized currents, generated via the spin Hall effect [**?**,**?**,**?**,**?**].

The spin Hall effect generates a polarized current, perpendicular to the original injected current that allows for faster manipulation of magnetic domains and the possibility to apply torques to a wider range of geometries [**?**,**?**,**?**,**?**]. The LLG equation, can be written including the spin Hall torque [**?**] as:

$$\frac{d\mathbf{M}}{dt} = -\gamma \mathbf{M} \times \left[\mathbf{H}_{eff} + \frac{a_j}{M_s^2} \left(\mathbf{M} \times \mathbf{u}_P \right) + \frac{b_j}{M_s} \mathbf{u}_P \right] + \frac{\alpha}{M_s} \mathbf{M} \times \frac{d\mathbf{M}}{dt} \quad (2.69)$$

where $\mathbf{u}_P$ is the polarization of the spin current while a_J and b_J are constants dependent on the applied current intensity. The term proportional to a_J aligns the magnetization along $\mathbf{u}_P$, while the one proportional to b_J generates a gyrotropic motion around it. For this reason the two terms are usually termed damping-like and field-like. Like the original LLG equation (Eq. **??**), the version including torques can be brought to an explicit form

for computational application:

$$\mathbf{M}\times\frac{d\mathbf{M}}{dt}=-\gamma\mathbf{M}\times\mathbf{M}\times\left[\mathbf{H}_{eff}+\frac{a_j}{M_s^2}\left(\mathbf{M}\times\mathbf{u}_P\right)+\frac{b_j}{M_s}\mathbf{u}_P\right]+\frac{\alpha}{M_s}\mathbf{M}\times\mathbf{M}\times\frac{d\mathbf{M}}{dt} \tag{2.70}$$

since:

$$\mathbf{M}\times\mathbf{M}\times\frac{d\mathbf{M}}{dt}=-M_s^2\frac{d\mathbf{M}}{dt}, \tag{2.71}$$

as shown in Eq. **??**, Eq. **??** can be written as:

$$\mathbf{M}\times\frac{d\mathbf{M}}{dt}=-\gamma\mathbf{M}\times\mathbf{M}\times\left[\mathbf{H}_{eff}+\frac{a_j}{M_s^2}\left(\mathbf{M}\times\mathbf{u}_P\right)+\frac{b_j}{M_s}\mathbf{u}_P\right]-\alpha M_s\frac{d\mathbf{M}}{dt}. \tag{2.72}$$

Plugging this expression for $\mathbf{M}\times\frac{d\mathbf{M}}{dt}$ into Eq. **??** an explicit equation for the magnetization is recovered:

$$\begin{aligned}\frac{d\mathbf{M}}{dt}\left(1+\alpha^2\right)=&-\gamma\mathbf{M}\times\left[\mathbf{H}_{eff}+\frac{a_j}{M_s^2}\left(\mathbf{M}\times\mathbf{u}_P\right)+\frac{b_j}{M_s}\mathbf{u}_P\right]-\\&-\gamma\frac{\alpha}{M_s}\left\{\mathbf{M}\times\mathbf{M}\times\left[\mathbf{H}_{eff}+\frac{a_j}{M_s^2}\left(\mathbf{M}\times\mathbf{u}_P\right)+\frac{b_j}{M_s}\mathbf{u}_P\right]\right\},\end{aligned} \tag{2.73}$$

this expression can be simplified employing the definition $\gamma'=\frac{\gamma}{1+\alpha^2}$ and applying the parallelepiped product:

$$\mathbf{M}\times\mathbf{M}\times\left(\mathbf{M}\times\mathbf{u}_P\right)=\left[\mathbf{M}\cdot\left(\mathbf{M}\times\mathbf{u}_P\right)\right]\mathbf{M}-M_s^2\left(\mathbf{M}\times\mathbf{u}_P\right)=-M_s^2\left(\mathbf{M}\times\mathbf{u}_P\right). \tag{2.74}$$

The LLG equation, inclusive of spin orbit torques can then be written as:

$$\begin{aligned}\frac{d\mathbf{M}}{dt}=&-\gamma'\mathbf{M}\times\left[\mathbf{H}_{eff}+\frac{\alpha}{M_s}\mathbf{M}\times\mathbf{H}_{eff}\right]-\\&-\frac{\gamma'}{M_s^2}\left(a_J+\alpha b_J\right)\mathbf{M}\times\left(\mathbf{M}\times\mathbf{u}_P\right)-\frac{\gamma'}{M_s}\left(b_J-\alpha a_J\right)\left(\mathbf{M}\times\mathbf{u}_P\right)\end{aligned}. \tag{2.75}$$

Defining $\xi\equiv\frac{b_J}{a_J}$ as the ratio between field-like and damping-like torque:

$$\begin{aligned}\frac{d\mathbf{M}}{dt}=&-\gamma'\left[\mathbf{M}\times\mathbf{H}_{eff}+\frac{\alpha}{M_s}\left(\mathbf{M}\times\mathbf{M}\times\mathbf{H}_{eff}\right)\right]-\\&-\frac{\gamma' a_J}{M_s}\left[\left(\xi-\alpha\right)\left(\mathbf{M}\times\mathbf{u}_P\right)+\frac{1+\alpha\xi}{M_s}\left(\mathbf{M}\times\mathbf{M}\times\mathbf{u}_P\right)\right]\end{aligned}. \tag{2.76}$$

2.7 Previous efforts towards a multiscale approach

In continuum mechanics [?, ?], multiscale approaches are commonly applied to the investigation of mechanical properties of materials, such as their response to deformations and fractures. While in magnetization dynamics, adaptive mesh refinement techniques [?, ?] have been used, none of these employed different models for different scales. One related approach has been proposed, addressing the problem of interfaces between layers of different magnetic materials [?, ?, ?]. However, the chosen interface conditions, in particular the choice of applying a coarse scaled exchange field on the magnetic moments along the interface in the fine scale region, restricts the validity of this approach to the systems with uniform magnetization across the interface. While this shortcoming has been later resolved in Refs. [?, ?], these approaches were devised to evaluate equilibrium configurations rather than simulating the dynamics of the systems.

One further related approach [?] employed the finite elements method. It should be noted however that while in this case the atomic lattice in the Heisenberg model can be rendered more accurately, the computational time cannot be dramatically reduced as shown for our finite differences approach in [?], making this approach considerably slower. One further multiscale approach [?], devised for a different scale combination than the presented one, proposed to use the micromagnetic model as the fine scale model and the Maxwell equations as the coarse scale model, this is however restricted to systems with slowly varying magnetization. Another work [?] uses special relativity to evaluate a corrective term to the Landau-Lifshitz-Gilbert equation in the case of domain wall motion.

Chapter 3

Magnetic Structures

In principle the magnetization configuration or the solution of the LLG equation, is a three-dimensional vector field defined on a domain in the three-dimensional space. Nevertheless some patterns (magnetic structures) can be easily recognized and therefore used to easily characterize the state of a ferromagnetic system. Following this treatment, analytical approaches can be applied to a smaller number of variables. The aim of this chapter is to outline some elementary structures which can be easily recognized and employed both in fundamental and technological applications.

3.1 Domain Walls

Room temperature ferromagnets tend to form domains of uniform magnetization in order to minimize exchange energy. Nevertheless, multiple domains can occur as a consequence of the interplay between the exchange interaction and the other contributions, such as the demagnetization which tends to favour closed flux structures. The region separating two adjacent domains is called a domain wall (DW). The simplest examples of DWs are 180° Bloch [**?**] or Néel [**?**] domain walls, which separate domains of opposite magnetization. In a Bloch DW the magnetization rotates in the plane defined by the direction of the domains and the wall itself, while in a Néel DW the magnetization rotates out of the plane [see fig **??**]. In other words, the magnetization in the center of a symmetric Bloch DW is parallel to the direction defined by the wall, while in a Néel DW it is perpendicular.

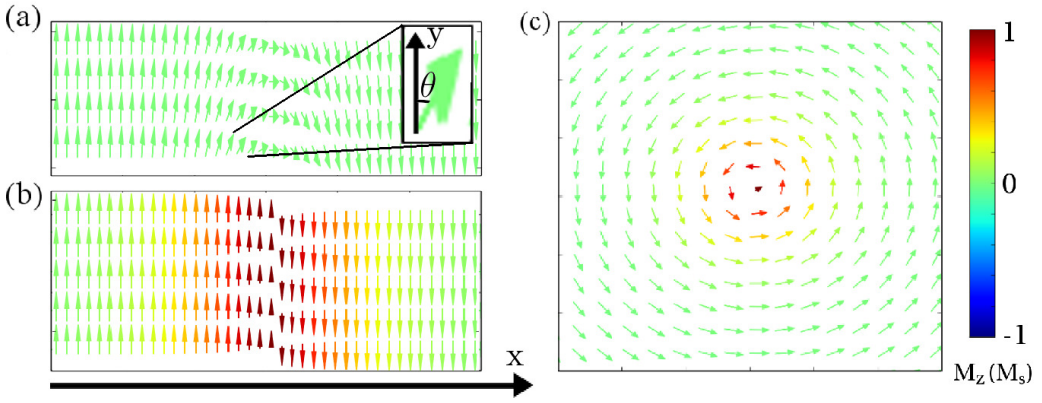

Figure 3.1: The magnetization structure in a Néel DW (a), a Bloch DW (b), and a vortex (c).

The energy of a Bloch or Néel DW can be written as [**?**]:

$$E_{BN} = \int_V dV \left[A \left(\frac{\partial \theta}{\partial x} \right)^2 + A \sin^2 \theta \left(\frac{\partial \phi}{\partial x} \right)^2 + K \sin^2 \theta + K_\perp \sin^2 \theta \sin^2 \phi \right], \tag{3.1}$$

where x is the coordinate perpendicular to the wall, θ is the angle between the magnetization and the easy axis, ϕ is the angle around the easy axis. The terms proportional to A are the exchange energy contributions. The terms proportional to K and $K_\perp$ depend on the crystalline and on the shape anisotropy.

It can be immediately noticed that for a uniform value of ϕ the second term in the DW energy is minimized, furthermore, the fourth term is minimized for $\phi = 0$, the magnetization in a DW will then tend to rotate in a well-defined plane. The two remaining terms:

$$e_{BN} = A \left(\frac{\partial \theta}{\partial x} \right)^2 + K \sin^2 \theta \tag{3.2}$$

can be minimized analytically. The solution for the variational equation

$$\frac{\delta E_{BN}}{\delta \theta} = 2A \frac{\partial^2 \theta}{\partial x^2} + 2K \sin \theta \cos \theta \tag{3.3}$$

is given by the angle:

$$\theta(x) = 2 \arctan \left(e^{\pm \frac{x - X}{\lambda}} \right) \tag{3.4}$$

with X the position of the DW and $\lambda = \sqrt{\frac{A}{K}}$ its width. It can be readily noticed that both types of DW are fourfold degenerate since there are two

possible orientation of the magnetization in the domains, which allow one to distinguish between head-to-head and tail-to-tail DW, and two possible orientation of the magnetization in the domain wall [see fig **??**].

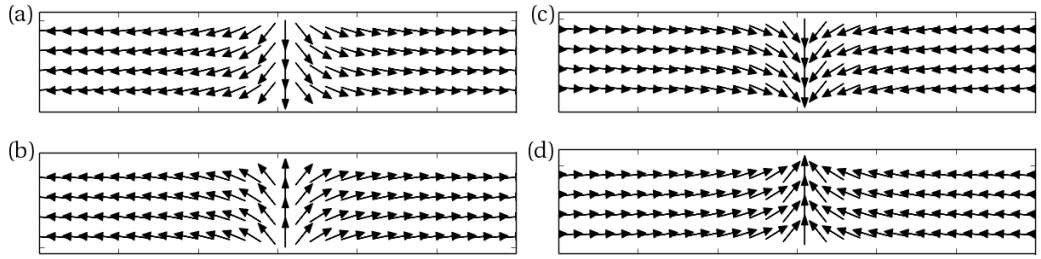

Figure 3.2: Degenerate orientations in a tail-to-tail (a,b) and head-to-head (c,d) tranverse DW [**?**] in the xy plane.

3.2 Vortices

In nanostructured ferromagnetic thin films the magnetization tends to curl around a central core if the lateral size of the system is included within a certain range [**?**, **?**, **?**, **?**, **?**]. In particular, this occurs if the linear dimensions of the systems are large enough to favor a flux closure structure, which minimizes the demagnetization energy contribution, over a single domain state. In a flux closure state, the magnetization aligns along the edges of the system. To prevent singularities in the exchange energy density, the magnetization of the core points out of the film plane. The in-plane component of such structures can be described analytically as [see Fig. **??**]

$$\Theta = N\theta + \frac{c\pi}{2} \tag{3.5}$$

where Θ denotes the angle that the magnetization forms with the x axis, θ the polar component of the two dimensional position vector $\mathbf{r}$ centered on the vortex core, and c the chirality. While the vorticity N could assume any integer value, this chapter will be focused on $N = \pm 1$ which is the case of vortices and antivortices respectively.

The vorticity, can be evaluated as:

$$N = \frac{1}{2\pi} \oint_{\ell} \phi\,(\theta)\, d\ell \tag{3.6}$$

where ℓ is any closed loop encircling the vortex core [**?**, **?**]. This number can be related to the topological charge Q by the formula $Q = Np/2$, where

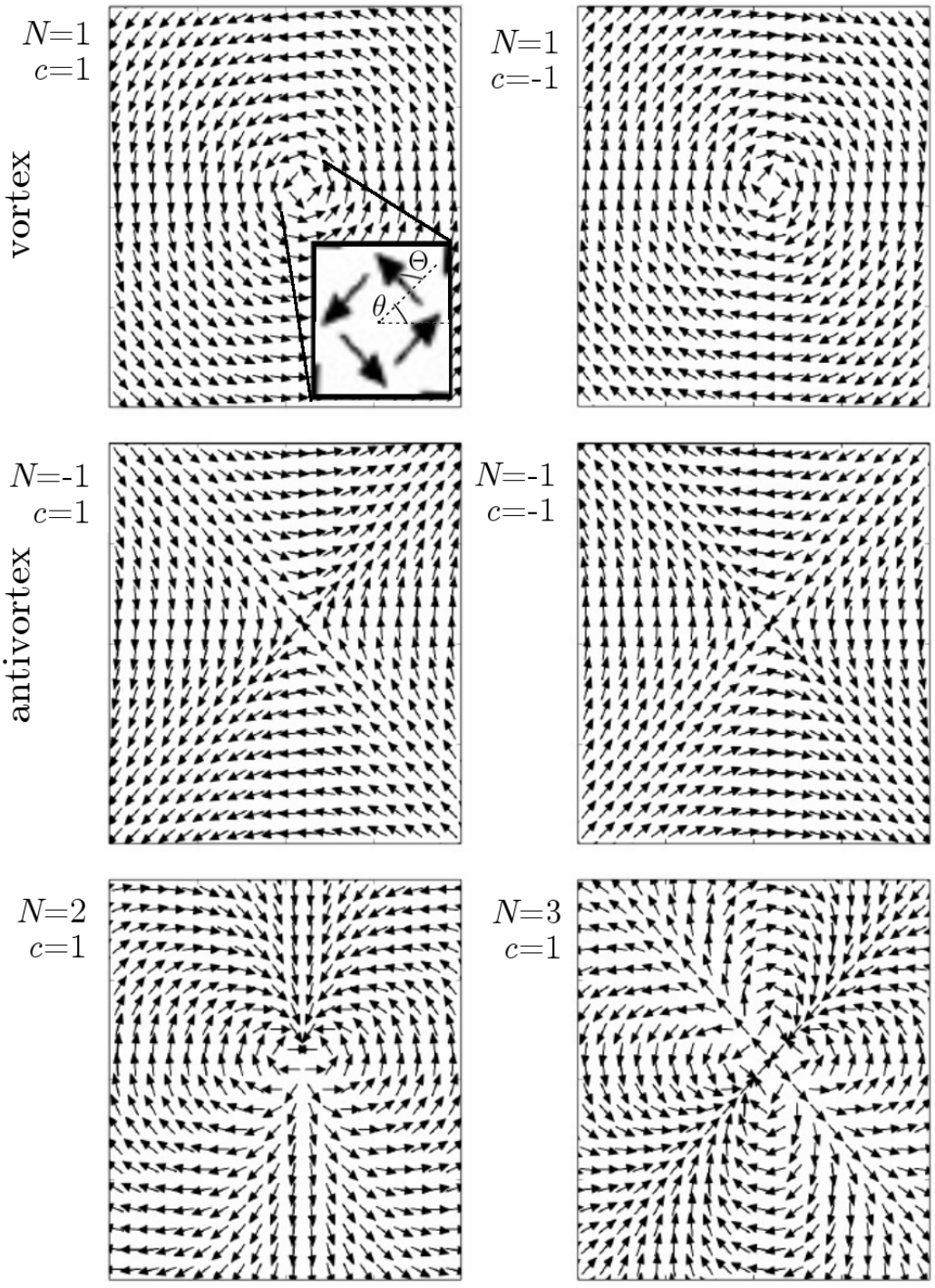

Figure 3.3: Structures generated by the function in Eq. **??** for different values of N and c in the xy plane.

the polarization $p = \pm 1$ is the direction of the magnetization in the vortex core [?].

In continuous models the vorticity, as well as the topological charge, is a conserved quantity [?, ?, ?], while in experiments and in discrete models it is possible to change it once a potential barrier is overcome [?].

Since in the absence of an external field structures with opposite polarization are degenerate, it is possible to switch the system between the two stable states. Due to this feature magnetic vortices have been considered for the realization of data storage devices [?, ?]. During the vortex core reversal process, a vortex-antivortex pair, with polarization opposite to the one of the original vortex, is generated in the system. Since a vortex and an antivortex have opposite N this process conserves the topological charge. Once the vortex-antivortex pair is generated, the original vortex and the antivortex annihilate, leaving in the system only the new vortex with opposite polarization. It should be noticed that the annihilation of the vortex antivortex couple involves a change in Q, therefore it cannot be described by a continuous model.

3.3 Skyrmions

In field theory Skyrmions are defined as fields that can be mapped on a sphere [?]. Magnetic Skyrmions are structures consisting of a domain pointing in the out of plane direction, within a system magnetized in the opposite direction, while the magnetization in the DW separating the two uniformly magnetized regions points in all the directions in the plane. Skyrmions tend to arise in the spin pattern of ferromagnetic systems with broken inversion symmetry, such as chiral crystals [?, ?, ?] or thin magnetic films with different top and bottom interfaces [?, ?, ?, ?, ?, ?]. Skyrmions lattices [?, ?, ?, ?] constitute the ground state in some systems, while isolated Skyrmions can appear as metastable states in magnetic nanostructures [?]. Isolated Skyrmions [see Fig. ??] have been recently considered [?, ?, ?] as the building blocks for ultradense magnetic storage devices [?].

Skyrmions carry a topological charge $Q = \pm 1$ defined as [?]:

$$Q = \frac{1}{4\pi} \int_S \mathbf{m} \cdot \left(\frac{\partial \mathbf{m}}{\partial x} \times \frac{\partial \mathbf{m}}{\partial y} \right) dxdy, \tag{3.7}$$

where S is the area of the system and $\mathbf{m}$ the unit magnetization vector. Since transitions that change Q are forbidden [?] in a continuous description of $\mathbf{m}$, such structures are topologically protected. Nevertheless, in a real system composed of discrete magnetic moments localized on the atomic lattice sites,

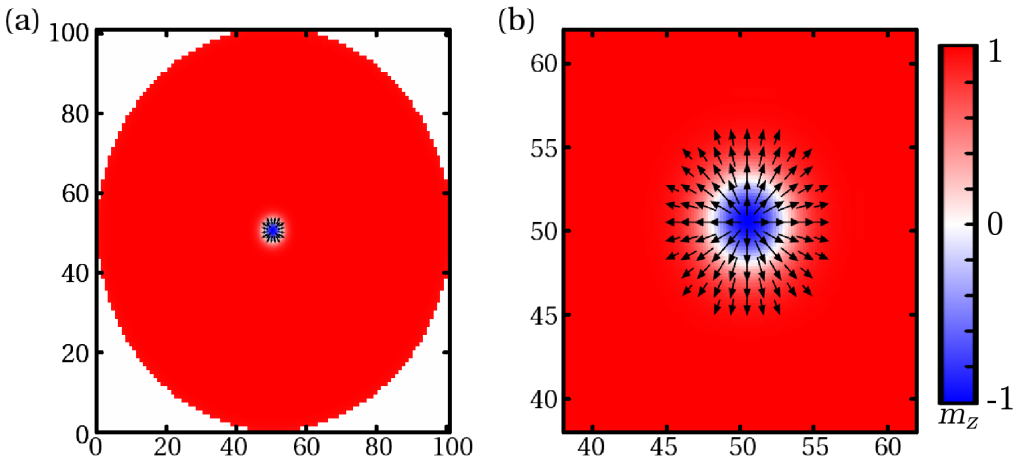

Figure 3.4: (a) A magnetic nanodisk hosting an isolated magnetic Skyrmion. (b) Detail of the Skyrmion core and domain wall. Only moments with an in plane magnetization larger than 10% M_s are marked with an arrow.

no strict topological protection exists [?]. Thus it is necessary to overcome a finite energy barrier to induce transformations that change Q, such as the annihilation of a Bloch line (BL) [see ??] and Refs. [?, ?, ?, ?, ?, ?, ?]. The stability against external fields is indeed a key feature of Skyrmions, making them a good candidate as information carriers in next generation storage devices [?, ?]. Ascertaining the stability of Skyrmions, as well as reliably annihilating them, are the fundamental prerequisites for applications. The computational treatment of processes involving annihilating Skyrmions is very delicate. In analytical micromagnetic theory, singularities in the exchange field arise during topological transformations, making numerical simulations very susceptible to the mesh being used [?] and therefore often inaccurate. The necessity for a computational model, capable of performing quantitatively accurate simulations is therefore obvious and a key prerequisite. While more accurate atomistic simulations would overcome this problem, the computational power required to run such simulations for a sample of realistic experimental size makes this possibility infeasible. The multiscale approach developed in this thesis proposes to overcome this issue.

3.4 Singularities

As it was mentioned in the previous section, topological transformations that occur in nature cannot be predicted in a continuous model. Such processes involve the sudden motion of a small number of magnetic moments, or discon-

tinuous distributions in the spin pattern. Both cases cannot be included in the fundamental approximation of micromagnetism (Eq. **??**), which defines the vector field **M** as the local average of the discrete spin distribution.

The existence of point singularities in magnetic materials was first suggested by E. Feldtkeller [**?**] where angles in the magnetization are large [see Fig. **??**]. In particular, on any closed surface around a Bloch point **M** maps every direction on a sphere. As a consequence of this condition, the analytical prolongations of the magnetization provide different results when they are evaluated on lines crossing the singularity from different directions [**?**]. Since the presence of a Bloch point constitutes a discontinuity in **M** as well as a point where the saturation magnetization vanishes, such structures disobey the constraints of the micromagnetic model. Bloch points are rotationally symmetric around an axis, therefore they can be categorized by parameters similar to the ones used for vortices [see Sec. **??**]. Without loss of generality the symmetry axis of a Bloch point was be chosen in this section as the z axis. In the case of the Bloch point, the polarization $p = \pm 1$ defines whether the magnetization along the z axis points respectively outwards or inwards the singularity, while the vorticity defines the direction of **M** in the $z = 0$ plane according to the examples shown in Fig. **??**. The remaining degree of freedom is constituted by the angle γ that **M** forms with the radial direction in the $z = 0$ plane.

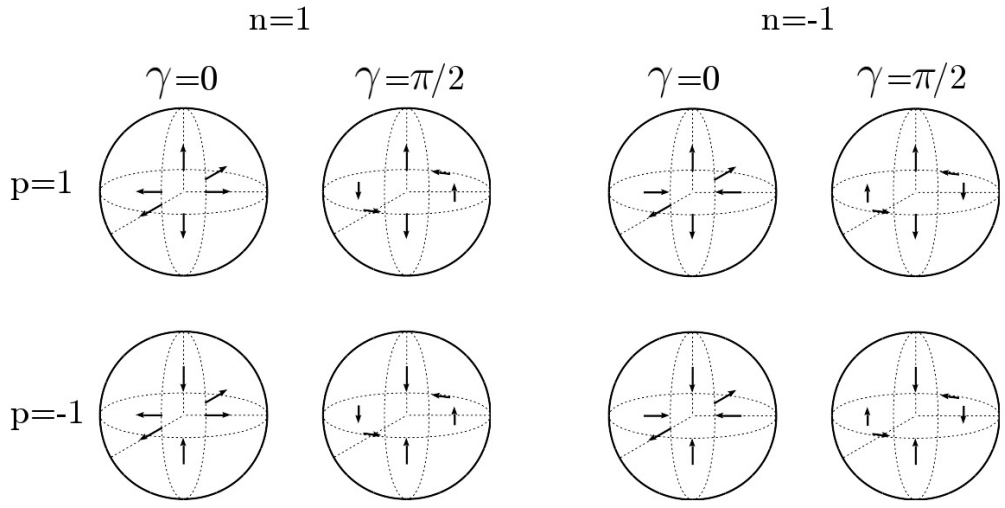

Figure 3.5: Magnetic configurations on a sphere containing Bloch points for different parameters combination.

Another case of a magnetic singularity occurs during the annihilation of a Bloch line. Bloch lines are winding structures [see Fig. **??**], therefore

they carry a topological charge. During their annihilation large angles in **M** are formed, thus breaking the continuity of the magnetization and the conservation of the topological charge which are key characteristics of the micromagnetic model. One noteworthy phenomenon which includes the annihilation of a Bloch line is the annihilation of a vortex-antivortex couple with opposite polarization.

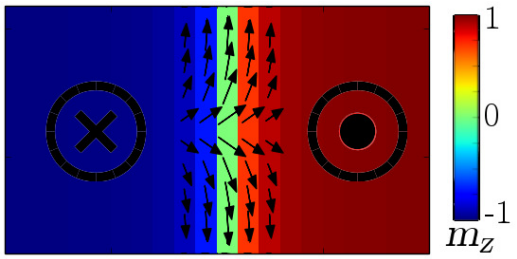

Figure 3.6: Example of a Bloch line as a winding Bloch domain wall.

3.4.1 Analytical treatment of Bloch points

While impossible to model micromagnetically, Bloch points can still occur in experiments and atomistic simulations. It is therefore interesting to study the magnetization pattern in the vicinity of a Bloch point from an analytical point of view. In this chapter the approach suggested by W. Döring [**?**] was followed to evaluate the most stable configuration for the angle γ in the micromagnetic model. In order not to break the validity of the model, the singularity itself was neglected, rather, the approach studied a small sphere around the Bloch point. For this purpose the polar coordinates presented in section **??**, are used to describe the position vector **r** and the unit magnetization **m** according to the following definitions:

$$\mathbf{r} = \begin{pmatrix} r\sin\varphi\cos\theta \\ r\sin\varphi\sin\theta \\ r\cos\varphi \end{pmatrix} \qquad \mathbf{m} = \begin{pmatrix} \sin\Phi\cos\Theta \\ \sin\Phi\sin\Theta \\ \cos\Phi \end{pmatrix}. \tag{3.8}$$

The exchange energy density, written according to Eq. **??** as:

$$e_{xc} = A \sum_{j=x,y,z} \left(\frac{\partial \mathbf{m}}{\partial x_j} \right)^2, \tag{3.9}$$

diverges for $r \to 0$ proportional to $1/r^2$. Its surface integral on a sphere V, with radius $r = R$ arbitrarily small, is finite and assumes a minimum value

at the equilibrium configuration of the Bloch point:

$$\begin{aligned} E_{xc} &= AR^2 \int_{\partial V} \sum_{j=x,y,z} \left(\frac{\partial \mathbf{m}}{\partial x_j}\right)^2 d\Omega = \\ &= AR^2 \iint \left[\left(\frac{\partial \mathbf{m}}{\partial \theta}\cdot\nabla\theta\right)^2 + \left(\frac{\partial \mathbf{m}}{\partial \varphi}\cdot\nabla\varphi\right)^2\right] d\varphi d\theta = \\ &= A \iint \left[\left(\frac{1}{\sin\varphi}\frac{\partial \mathbf{m}}{\partial \theta}\right)^2 + \left(\frac{\partial \mathbf{m}}{\partial \varphi}\right)^2\right] \sin\varphi \, d\varphi d\theta, \end{aligned} \tag{3.10}$$

where the integral runs on the whole sphere.

It is convenient to introduce the set of variables defined as:

$$z = \xi + i\eta = \tan\left(\frac{\varphi}{2}\right)\exp i\theta$$

which runs over the whole complex plane since φ and θ span the whole sphere, the same transformation can be written for $\mathbf{m}$ as:

$$w = u + iv = \tan\left(\frac{\Phi}{2}\right)\exp i\Theta = \frac{m_x + im_y}{1 + m_z}.$$

The integral in Eq. **??** reads in the current coordinates system:

$$E_{xc} = 4A \iint_{-\infty}^{\infty} \frac{\left(\frac{\partial u}{\partial \xi}\right)^2 + \left(\frac{\partial u}{\partial \eta}\right)^2 + \left(\frac{\partial v}{\partial \xi}\right)^2 + \left(\frac{\partial v}{\partial \eta}\right)^2}{\left(1 + u^2 + v^2\right)^2} d\xi d\eta. \tag{3.11}$$

The minimization of the expression in Eq. **??** leads to two nonlinear coupled differential equations of the second order in u and b. While the general solution of these equation is quite complicated [**?**], it is possible to find simple solutions for an arbitrary analytical function f, such that $w = f(z)$.

Under this hypothesis Eq. **??** reads:

$$E_{xc} = 4A \int_{\mathbb{C}} \frac{2\left|\frac{df}{dz}\right|^2}{\left(1 + f^2\right)^2} dz \tag{3.12}$$

where $\mathbb{C}$ is the complex plane. For f the quotient of two polynomial functions with highest degree N such that

$$w = u + iv = f(z) = \frac{\sum_{i=0}^{M} a_i z^i}{\sum_{j=0}^{L} b_j z^j}$$

with $\max(M, L) = N$, the integral in Eq. **??** reads:

$$E_{xc} = 8NA \iint_{-\infty}^{\infty} \frac{du\, dv}{(1 + u^2 + v^2)^2} = 8\pi NA. \tag{3.13}$$

Eq. **??** shows that the solutions that minimizes the exchange energy are those with $N = 1$, thus those where each possible orientation of $\mathbf{m}$ occurs exactly once, therefore $n = \pm 1$. Nevertheless, all the solutions with the same value of N are degenerate in the exchange energy. It is thus necessary to consider the second strongest energy term, the demagnetization energy.

Recalling the theory from section **??**, the demagnetization field can be written in terms of a scalar potential field U_D (Eq. **??**). The potential field depends on the magnetization as shown in Eq. **??**:

$$U_D(\mathbf{r}) = \frac{1}{4\pi} \left[\int_V d\mathbf{r}' \, \frac{-\nabla' \cdot \mathbf{M}(\mathbf{r}')}{|\mathbf{r} - \mathbf{r}'|} + \oint_{\partial V} d\mathbf{r}' \, \frac{\mathbf{M}(\mathbf{r}') \cdot \mathbf{e}_n(\mathbf{r}')}{|\mathbf{r} - \mathbf{r}'|} \right]. \tag{??}$$

Applying the divergence theorem as in Eq. **??** U_D reads:

$$\begin{aligned} U_D(\mathbf{r}) =& \frac{1}{4\pi} \left[\oint_{\partial V} d\mathbf{r}' \, \frac{\sigma(\mathbf{r}')}{|\mathbf{r} - \mathbf{r}'|} + \int_V d\mathbf{r}' \, \frac{\rho(\mathbf{r}')}{|\mathbf{r} - \mathbf{r}'|} \right] = \\ =& \frac{1}{4\pi} \int_V d\mathbf{r}' \, \mathbf{M}(\mathbf{r}') \cdot \nabla' \frac{1}{|\mathbf{r}' - \mathbf{r}|}. \end{aligned} \tag{3.14}$$

The function $|\mathbf{r}' - \mathbf{r}|^{-1}$ can be written in polar coordinates as a series of spherical harmonics:

$$\frac{1}{|\mathbf{r}' - \mathbf{r}|} = \frac{1}{r_>} \sum_{l=0}^{\infty} \sum_{m=-l}^{l} \frac{4\pi}{2l+1} \left(\frac{r_<}{r_>} \right)^l Y_{l,m}(\theta, \varphi)\, Y_{l,-m}(\theta', \varphi') \tag{3.15}$$

where the definitions $r_> = \max(r, r')$ and $r_< = \min(r, r')$ were used.

We consider the following magnetization distribution in polar coordinates [see eq. **??**]:

$$\Theta(\theta) = n\theta + \gamma; \qquad \Phi(\varphi) = p\varphi + \pi(1-p)\,2$$

with $n = \pm 1$ as recovered in the exchange energy calculation, and $p = \pm 1$. Introducing this expression for $\mathbf{M}$ into the last term in Eq. **??** yields for a spherical sample with radius R [**?**, **?**]:

$$U_D(r) = -\frac{M_s}{24}\left[3r\left(p - \cos\gamma\right)\cos 2\varphi + p\left(9r - 8R\right) + \left(16r - 15R\right)\cos\gamma\right]. \tag{3.16}$$

Using the expression in Eq. **??** it is possible to evaluate the demagnetization field as $\mathbf{H}_{dem} = -\nabla U_D$. In the original approach from Döring [**?**] the demagnetization energy was evaluated as:

$$E_{dem} = \frac{\mu_0}{2}\int_V |\mathbf{H}_{dem}|^2 \, d\mathbf{r},$$

an equilibrium angle $\gamma = -\arccos\left(p \cdot \frac{11}{29}\right)$ was found as the lowest energy configuration. This approach was later refined [**?**, **?**, **?**] in order to take in consideration the stray field generated outside of the small sphere V, evaluating the demagnetization energy as:

$$E_{dem} = \frac{\mu_0}{2}\int_V \mathbf{M} \cdot \mathbf{H}_{dem} \, d\mathbf{r}.$$

This calculation resulted in a configuration with an angle $\gamma = -\arccos(p/4)$.

Other approaches towards the evaluation of the structure of a Bloch point included models with variable M_s [**?**, **?**], nevertheless, analytical [**?**] and computational [**?**] studies showed that in a discrete system, Bloch points tend to be localized between lattice sites. According to these descriptions, models that consider a local reduction in the magnetic moments are not necessary.

Chapter 4

Computational background

As a fundamental tool to derive accurate results from analytical theories, computational physics proposes to employ algorithms in order to solve problems that could not be solved otherwise. The fundamental rule in this field, is that for any given algorithm, the more computational power one uses, either by increasing its iterations or the number of variables, the better it approximates exact results. In spite of being established as a research field only during the 20th century, due to the large scale employment of electronic calculators, the history of computational physics can be traced back to the early times of human civilization, when numeric systems were invented in order to keep track of commercial transactions and the motion of stars [**?**]. Notably, millennia later, economy and astrophysics still are among the fields where computational physics is mostly employed. One of the earliest attempts of computational physics, devised to approximate π from the perimeter of a regular polygon, was made in the third century by Chinese mathematician Liu Hui [**?**]. By using two polygons, approximating a circle of radius r, from the inside and from the outside [see Fig. **??**], Liu Hui could predict a lower and upper bounds for π given by the perimeter of the two polygons, whose precision increased with the number of sides in the polygon. Liu Hui used for his calculations a 3072-sided polygon to obtain 3,1410$< \pi <$3,1427, two centuries later two further Chinese mathematicians, Zu Chongzhi and his son Zu Gengzhi, employed a 24576-sided polygon in order to improve the approximation to obtain 3,1415926$< \pi <$3,1415927. Using a computer and modern computational physics, it is possible to devise an algorithm which relies on a similar technique to obtain more accurate results by using polygons with a manageable amount of sides.

Let k be the number of sides of a given regular polygon and π_k the ratio between its perimeter and the diameter of the circle the polygon is inscribed

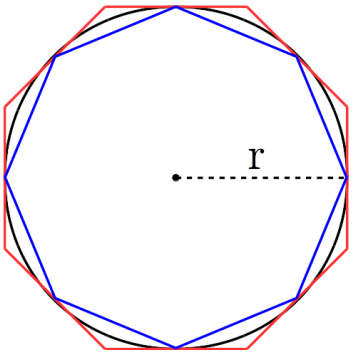

Figure 4.1: The system used by Liu Hui to approximate π.

within. The correct value for π is given by the expansion:

$$\pi_k = \pi + \sum_{j=1}^{\infty} \frac{c_j}{k^j},$$

whose coefficients do not depend on k. An approximation of π can then be evaluated by solving the set of equations:

$$\sum_{j=1}^{N} a_j x_j = \pi_k$$

if the expansion is truncated at the N-th order in $1/k$, with $a_j = 1/k^{j-1}$, $x_1 = \pi$, and $x_j = c_{j-1}$ for N different values of π_k. For $N = 3$ and $k = 32$, 64, 128, 256 the value of π can be evaluated with five digits of accuracy, comparable to the results found by the Zus using a 24576-sided polygon [**?**].

In modern physics powerful computational techniques are implemented with the aid of computers. As a consequence of the digital revolution, computational physics was established as a research field. Numerical calculation is a prerogative of modern research. The aim of the following chapters is to present the algorithms that were used in the multiscale approach object of this thesis.

The basic mathematics presented in this chapter, and in particular the algorithms used to evaluate derivatives, solve differential equations, and interpolate functions refer to Ref. [**?**].

4.1 Solution of differential equations

The LLG equation written in Eq. **??**, as well as the versions of the equation presenting spin torques presented in section **??** are ordinary differential

equations of the first order in the time coordinate. Furthermore, in the micromagnetic model partial derivatives and integrals of $\mathbf{M}$ in the spatial coordinates occur when evaluating the exchange and the demagnetization effective field respectively. In particular, solving the LLG equation in order to describe the time evolution of a magnetic system constitutes an initial-value problem.

A generic initial-value problem can be expressed as:

$$\begin{cases} \dfrac{d\mathbf{M}(\mathbf{r},t)}{dt} = \mathbf{G}(\mathbf{r},t,\,\mathbf{M}(\mathbf{r},t)) \\ \\ \mathbf{M}(\mathbf{r},0) = \mathbf{M}_0(\mathbf{r}) \end{cases} \tag{4.1}$$

where the field $\mathbf{G}$ on the right-hand side is the generalized velocity vector.

In order to describe the computational methods commonly employed to solve a differential equation we will refer in the following to a simpler case, such as the motion of a particle under an elastic force, this problem reads:

$$\begin{cases} \dfrac{d^2x}{dt^2} = -\dfrac{kx}{m} \\ \\ x(0) = x_0, \quad v(0) = v_0 \end{cases} \tag{4.2}$$

or

$$\begin{cases} \dfrac{dx}{dt} = v(t) \\ \\ \dfrac{dv}{dt} = -\dfrac{kx}{m} \\ \\ x(0) = x_0, \quad v(0) = v_0 \end{cases} \tag{4.3}$$

where x denotes the position of the particle, v its velocity, m its mass, and k the elastic constant. In this case, an equation of the second order was written as a set of two first order equations, this is a fundamental step when computationally solving a differential equation of order higher than one. From a computational point of view, such a set of equations is analogous to a set showing the components of a vector on each equation, as in the case of the LLG equation.

4.1.1 The Euler and Picard methods

The core idea behind the computational solution of differential equations consists in iteratively evaluate the unknown function $x(t)$, in a discrete set of

time instants $\{t_i\}_{i\in\mathbb{N}}$, with $\mathbb{N}$ the set of the natural numbers. For the sake of simplicity we will consider $t_{i+1}-t_i=\Delta t,\ \forall i$. For this purpose the derivatives of x are approximated at the same time instants. The simplest approximation for the derivative of a function consists in the two-point formula:

$$\left.\frac{dx}{dt}\right|_{t_{i+1}} = \lim_{\Delta t\to 0}\frac{x_{i+1}-x_i}{\Delta t} = \frac{x_{i+1}-x_i}{\Delta t} + \mathcal{O}\left(\Delta t\right) = v_{i+1}, \tag{4.4}$$

where $x_i = x\left(t_i\right)$ and $v_i = v\left(t_i\right)$. In the Euler method this formula is inverted and applied to the differential equation **??** to evaluate its left-hand side as:

$$\begin{cases} x_{i+1} = x_i + v_i\Delta t + \mathcal{O}\left(\Delta t^2\right) \\ \\ v_{i+1} = v_i - \dfrac{kx_i}{m}\Delta t + \mathcal{O}\left(\Delta t^2\right) \end{cases} \tag{4.5}$$

This method is analogous to considering the first order Taylor approximation of the unknown function, it is the simplest method to solve an ordinary differential equation and this simplicity strongly impacts the accuracy of the prediction, since the accumulated error after n computational steps amounts to $n\,\mathcal{O}\left(\Delta t^2\right) \simeq \mathcal{O}\left(\Delta t\right)$.

In order to increase the accuracy of the Euler method, Eq. **??** can be rewritten as:

$$\begin{cases} x_{i+j} = x_i + \displaystyle\int_{t_i}^{t_{i+j}} v\left(x,t\right)\,dt \\ \\ v_{i+j} = v_i - \dfrac{k}{m}\displaystyle\int_{t_i}^{t_{i+j}} x\left(t\right)\,dt \end{cases} \tag{4.6}$$

for any given couple of integers i and j. The Picard method proposes to use the trapezoid rule to approximate the integrals in **??**, this reduces the error at each iteration to $\mathcal{O}\left(\Delta t^3\right)$. This consists in approximating the integrand function with a straight line between t_i and t_{i+j}, in order to do this an initial prediction of x_{i+1} and v_{i+1} is needed, this can be evaluated in the Euler method and then refined so that:

$$\begin{cases} x_{i+1}^{(1)} = x_i + \left(v_{i+1}^{(0)} - v_i\right)\dfrac{\Delta t}{2} + \mathcal{O}\left(\Delta t^3\right) \\ \\ v_{i+1}^{(1)} = v_i - \dfrac{k}{m}\left(x_{i+1}^{(0)} - x_i\right)\dfrac{\Delta t}{2} + \mathcal{O}\left(\Delta t^3\right) \end{cases}, \tag{4.7}$$

where the values $x_{i+1}^{(0)}$, and $v_{i+1}^{(0)}$ can be calculated using the Euler method as shown in Eq. **??**, or can be predicted by making an ansatz for the solution

the differential equation. The calculated values, $x_{i+1}^{(1)}$, and $v_{i+1}^{(1)}$ can either be used to evaluate the next step, labeled with $i+2$ or to refine the prediction at the step $i+1$. In order to obtain a more accurate prediction. When refining the result of a fixed time step, a convergence criterion can be used to obtain a number of iterations suitable for the expected accuracy. The accuracy of the Picard method is strongly influenced by the prediction in the earliest iterations. In particular, an inaccurate prediction of the unknown function in the early steps can lead to slowly or non-converging results, or to large inaccuracies after many iterations.

A state of the art method for solving differential equations is the Runge-Kutta method [**?**]. Like the Cauchy problem, this method needs only the initial condition of the unknown function to reach a solution, therefore it is not so susceptible to the predictions for the earliest time-steps as the Picard method. Furthermore the Runge-Kutta method is particularly relevant in the context of this thesis since such a method was employed in the solving routine of our multiscale approach. A second order predictor-corrector approach of the Adams type [**?**] is used in the widely employed OOMMF package [**?**]. A fourth order Runge-Kutta is used in this package if the predictor corrector approach fails.

4.1.2 The Runge-Kutta method

The Runge-Kutta method is based on a double Taylor expansion of the unknown function. In order to describe this method we will refer to the generic first-order differential equation:

$$\frac{df}{dt} = g\left(f, t\right),$$

where g is the generalized velocity of the unknown function f that can in principle be any analytic function of f and of the time variable.

The unknown function can be approximated at a given time instant $t+\Delta t$

as :

$$
\begin{aligned}
& f\left(t+\Delta t\right) = \\
& = f\left(t\right) + \Delta t f'\left(t\right) + \frac{\Delta t^2}{2} f''\left(t\right) + \frac{\Delta t^3}{3!} f'''\left(t\right) + \cdots = \\
& = f\left(t\right) + \Delta t g\left(t\right) + \frac{\Delta t^2}{2}\left[\left.\frac{dg}{dt}\right|_t + \left.\frac{dg}{df}\right|_t g\left(t\right)\right] + \\
& + \frac{\Delta t^3}{6}\left[\left.\frac{d^2g}{dt^2}\right|_t + 2\left.\frac{d^2g}{dtdf}\right|_t g\left(t\right) + 2\left.\frac{d^2g}{df^2}\right|_t g^2\left(t\right) + 2\left(\left.\frac{dg}{df}\right|_t\right)^2 g\left(t\right) + \left.\frac{dg}{df}\right|_t \left.\frac{dg}{dt}\right|_t\right] + \\
& + \cdots .
\end{aligned}
\tag{4.8}
$$

The formula **??** can be formally written, up to the m-th order in Δt, as:

$$
f\left(t+\Delta t\right) = f\left(t\right) + \sum_{i=1}^{m} \alpha_i c_i + \mathcal{O}\left(\Delta t^{m+1}\right) \tag{4.9}
$$

with the parameters c_i:

$$
\begin{aligned}
& c_1 = \Delta t\; g\left(f, t\right) \\
& c_2 = \Delta t\; g\left(f + \nu_{21} c_1,\; t + \Delta t \nu_{21}\right) \\
& c_3 = \Delta t\; g\left(f + \nu_{31} c_1 + \nu_{32} c_2,\; t + \Delta t\left(\nu_{31} + \nu_{21}\right)\right) \\
& \vdots \\
& c_m = \Delta t\; g\left(f + \textstyle\sum_{i=1}^{m-1} \nu_{mi} c_i,\; t + \Delta t \sum_{i=1}^{m-1} \nu_{mi}\right),
\end{aligned}
\tag{4.10}
$$

where α_i (for $i < m$) and ν_{ij} (for $j < i$) are parameters to be determined.

Carrying out a Taylor expansion for all c_i, Eq. **??** can be written in terms of series of powers of Δt. This expression can be then compared term by term to Eq. **??**. This provides a set of equations for α_i and ν_{ij}. This is a set of m equations for $m + m\left(m+1\right)/2$ parameters to be determined, therefore its solution is not unique.

Let us illustrate the case for $m = 2$: in this case Eq. **??** reads:

$$
f\left(t+\Delta t\right) = f\left(t\right) + \Delta t g\left(t\right) + \frac{\Delta t^2}{2}\left[\left.\frac{dg}{dt}\right|_t + \left.\frac{dg}{df}\right|_t g\left(t\right)\right]. \tag{4.11}
$$

By truncating Eq. **??** at the second order, another expression for the unknown function is recovered:

$$
f\left(t+\Delta t\right) = f\left(t\right) + \alpha_1 c_1 + \alpha_2 c_2, \tag{4.12}
$$

since the term c_2 can be expanded in a Taylor series, up to $\mathcal{O}(\Delta t)^2$ as:

$$c_2 = \Delta t\, g\left(f + \nu_{21} c_1,\ t + \Delta t \nu_{21}\right) = \Delta t\, g + \Delta t^2 \nu_{21} \left[\left.\frac{dg}{dt}\right|_t + \left.\frac{dg}{df}\right|_t g\left(t\right) \right]. \tag{4.13}$$

In this terms Eq. **??** reads:

$$f\left(t + \Delta t\right) = f\left(t\right) + \Delta t \left(\alpha_1 + \alpha_2\right) g + \Delta t^2 \alpha_2 \nu_{21} \left[\left.\frac{dg}{dt}\right|_t + \left.\frac{dg}{df}\right|_t g\left(t\right) \right]. \tag{4.14}$$

By comparing eqs. **??** and **??** a set of two equations for three parameters can be written:

$$\begin{cases} \alpha_1 + \alpha_2 = 1 \\ \alpha_2 \nu_{21} = \frac{1}{2} \end{cases}. \tag{4.15}$$

As pointed out earlier in the text no unique solution exists for the equation set **??**, therefore one parameter can be chosen arbitrarily. This flexibility allows the user to improve on the accuracy of the method by choosing the free parameters according to the particular problem to be solved.

4.2 Discretization of the equation

The dynamics of a point particle constitutes a practical example when discussing methods to solve differential equations numerically. Alongside the discretization of the time domain, in the case of the dynamics of a field, such as the magnetization in the LLG equation, the discretization of the spatial coordinates needs to take place as well, in order for the computational algorithms to be implemented.

In the finite difference method (FDM), the space occupied by the physical system of interest is divided in a discrete set of cells. The cells are labeled according to the coordinates of their centers. In the discretized space the cell labeled by (i, j, k), with i, j, and k natural numbers, is located on the point with coordinates (x_i, y_j, z_k) in the continuous space. Such positions are separated along each axis by a fixed interval, so that for the generic component $\xi = x, y, z$, the relation $\xi_{i+1} = \xi_i + \Delta\xi$ holds. As a consequence, all the cells are identical rectangles with sides $(\Delta x, \Delta y, \Delta z)$.

Just like the discretization in time, the discretization of space introduces inaccuracies that are reduced if the cells are refined, therefore increasing their number as well as the computational effort necessary for executing an algorithm. One further source of inaccuracy occurs when modeling curved systems. In this case, a curved body, such as a sphere or a circle, is approximated by a set of rectangular cells, introducing effects that are not present

in the ideal analytical case and decreasing the symmetry of the system [see Fig. **??**].

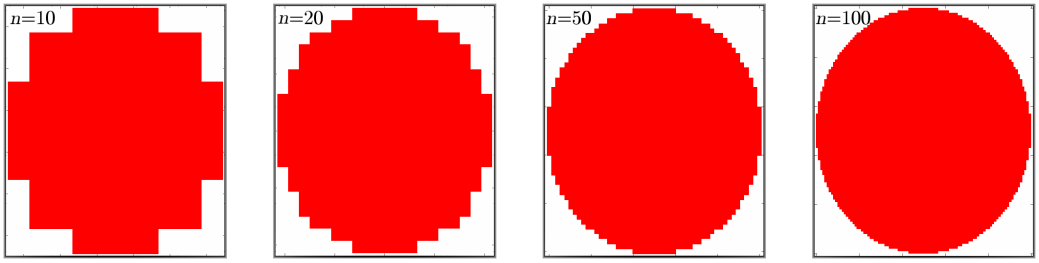

Figure 4.2: Circular system modeled using the finite different method with a different number of cells per side n.

In some differential equations, the generalized velocity can be expressed in terms of the partial derivatives of the unknown function. This is the case for the LLG equation in the micromagnetic model, where the exchange field is calculated as the derivative of $\mathbf{M}$ [see Eq. **??**]. In order to calculate a partial derivative of a discretized function a further approximation is necessary.

The first order partial derivative can be evaluated using the two-point formula as shown in Eq. **??**:

$$\frac{\partial \mathbf{M}\left(x_i, y_j, z_k, t\right)}{\partial x} = \frac{\mathbf{M}\left(x_{i+1}, y_j, z_k, t\right) - \mathbf{M}\left(x_i, y_j, z_k, t\right)}{\Delta x} + \mathcal{O}\left(\Delta x\right), \quad (4.16)$$

or the three-point formula, which improves the accuracy by one order of magnitude in Δx:

$$\frac{\partial \mathbf{M}\left(x_i\right)}{\partial x} = \frac{\mathbf{M}\left(x_{i+1}\right) - \mathbf{M}\left(x_{i-1}\right)}{2\Delta x} + \mathcal{O}\left(\Delta x^2\right), \quad (4.17)$$

where the y, z, and t variables are not shown for the sake of tidiness. It is in principle possible to further improve the accuracy of the derivation algorithm by using more points to evaluate the derivative, such as in the case of the five-point formula:

$$\frac{\partial \mathbf{M}\left(x_i\right)}{\partial x} = \frac{\mathbf{M}\left(x_{i-2}\right) - 8\mathbf{M}\left(x_{i-1}\right) + 8\mathbf{M}\left(x_{i+1}\right) - \mathbf{M}\left(x_{i+2}\right)}{12\Delta x} + \mathcal{O}\left(\Delta x^4\right). \quad (4.18)$$

In order to evaluate second order derivatives a minimum of three points is needed:

$$\frac{\partial^2 \mathbf{M}\left(x_i, y_j, z_k, t\right)}{\partial x^2} = \frac{\mathbf{M}\left(x_{i+1}\right) - 2\mathbf{M}\left(x_i\right) + \mathbf{M}\left(x_{i-1}\right)}{\Delta x^2} + \mathcal{O}\left(\Delta x^2\right). \quad (4.19)$$

As shown in **??**, the micromagnetic evaluation of the exchange effective field is intrinsically limited by the model itself, exponentially decreasing in accuracy when the magnetization changes on the scale of the atomic lattice. A stronger limitation is introduced by the algorithms used to evaluate the derivatives, since their accuracy depends on the discretization. Since the chosen cell size is usually larger than the elementary cell of the ferromagnetic material, the user must make sure that the magnetization does not change at the scale of the computational cell, in order to ensure an accurate solution of the equation.

4.3 Interpolation

The discretization of a function is a fundamental step towards the implementation of computational algorithms. In some cases it is necessary to evaluate a function at an intermediate position between two cells, or at an instant between two steps in the solution of a differential equation. Interpolation algorithms are used to approximate a function in such occasions.

The simplest example of an interpolation scheme consists of the linear interpolation algorithm. By means of this algorithm, functions of a single variable are approximated as a straight line between two points where their value is known. Let $f_i = f(x_i)$ be a discretized function for any $i \in \mathbb{N}$. The value $f(x)$ that such a function takes in $x \in [x_i, x_{i+1}]$, is given by:

$$f(x) = f_i + \frac{x - x_i}{x_{i+1} - x_i}(f_{i+1} - f_i) + \Delta f = f_x + \Delta f, \tag{4.20}$$

with Δf the difference between the actual value of $f(x)$ and its approximation f_x. It can be easily noticed that $\Delta f = 0$ in x_i and x_{i+1}. Furthermore, the dependence of Δf on x must be at least quadratic, therefore it can be approximated as

$$\Delta f\ (x) = \frac{\gamma}{2}(x - x_i)(x - x_{i+1}), \tag{4.21}$$

where γ is a parameter depending on the particular form of $f(x)$. An upper bound for the parameter γ can be evaluated as

$$\gamma_{max} = \max(f''(x)), \tag{4.22}$$

with $x \in [x_i, x_{i+1}]$. A second order Taylor expansion can be used to estimate the upper bound for the error Δf as:

$$|\Delta f(x)| \leq \frac{\gamma_{max}}{8}(x_{i+1} - x_i)^2. \tag{4.23}$$

The error can be decreased by refining the set $\{x_i\}$, which in most cases is not a practical choice. Another possibility consists in increasing the order of the interpolation by using a higher order polynomial, therefore a curve of an higher order, to approximate the function. In principle, the maximum interpolation order is limited by the number of data points available for the function. For a set of n data points the maximum interpolation order available is $n-1$.

4.3.1 Interpolating functions of two variables

The bilinear interpolation constitutes an immediate extension on the one-dimensional concept of linear interpolation when approximating a discretized function of two variables $f(x_i, y_j)$. The key idea behind the bilinear interpolation scheme consists of performing linear interpolations of $f(x_i, y_j)$ along the direction of one of the two axes, then one further interpolation between the two interpolated values along the other axis. In order to calculate the approximated value $f_{x,y}$ for $x \in [x_i, x_{i+1}]$, and $y \in [y_j, y_{j+1}]$, first one evaluates $f_{x,j}$ and $f_{x,j+1}$ as:

$$\begin{aligned} f_{x,j} &= f_{i,j} + \frac{x - x_i}{x_{i+1} - x_i}\left(f_{i+1,j} - f_{i,j}\right) \\ f_{x,j+1} &= f_{i,j+1} + \frac{x - x_i}{x_{i+1} - x_i}\left(f_{i+1,j+1} - f_{i,j+1}\right) \end{aligned}, \tag{4.24}$$

then, as the interpolation of the two values calculated in eq. (**??**):

$$f_{x,y} = f_{x,j} + \frac{y - y_j}{y_{j+1} - y_j}\left(f_{x,j+1} - f_{x,j}\right). \tag{4.25}$$

The order in which the axes are interpolated does not influence the result of the approximation, an identical result can be evaluated as the interpolation of $f_{i,y}$ and $f_{i+1,y}$ given by:

$$\begin{aligned} f_{i,y} &= f_{i,j} + \frac{y - y_j}{y_{j+1} - y_j}\left(f_{i,j+1} - f_{i,j}\right) \\ f_{i+1,y} &= f_{i+1,j} + \frac{y - y_j}{y_{j+1} - y_j}\left(f_{i+1,j+1} - f_{i+1,j}\right) \end{aligned}. \tag{4.26}$$

The bilinear interpolation is quadratic in order since it involves the product of two linear functions. Furthermore it is linear in amplitude, this means that the interpolated function is linear along any direction in the

two-dimensional space (the particular case for the directions parallel to the axes is obvious). The obvious extension of this method for functions of three variables, the trilinear interpolation, involves the linear interpolation of two values, calculated on parallel planes, using bilinear interpolations.

Linear interpolation schemes can be interpreted as the weighted average of f_i and f_{i+1}. The weights for each value are the normalized distances along the interpolation axis of the interpolated point from the coordinate of the opposite known value. This is easily noticed by rearranging the terms in eq. (**??**). Namely, the weight of f_i is $(x_{i+1} - x) / (x_{i+1} - x_i)$ and the weight of f_{i+1} is $(x - x_i) / (x_{i+1} - x_i)$. This interpretation can be generalized to a larger number of dimensions as shown in Fig. **??** (b) in the case of the bilinear interpolation. In this case the weight is given by the normalized area of the rectangle opposite to the point where the value of f is known.

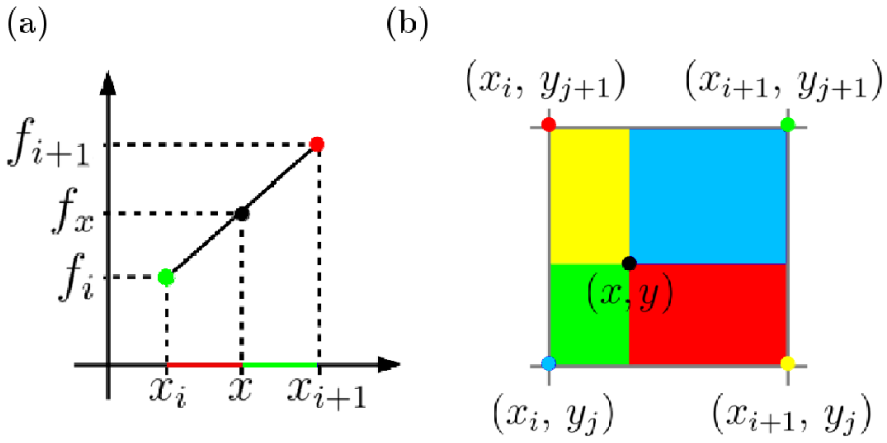

Figure 4.3: Interpretation of the linear (a) and bilinear (b) interpolation as weighted averages. The black dot shows the coordinate where the function is interpolated. (a) The length of the colored segments constitutes the weight for the known value of f in the point marked with the same color. (b) In the bilinear interpolation the area of the each rectangle constitutes the weight for the corresponding known value of f.

4.3.2 Interpolation in the multiscale approach

The multiscale approach that is the focus of this thesis, proposes to use the Runge-Kutta algorithm to solve the LLG equation on two different grids. On one grid the finite difference method is applied to the micromagnetic model to describe the magnetic system in its entirety. The second, finer, grid

is located on regions of the system where a singularity can arise or where anyway more precision is required; on this grid the classical simulation of the LLG equation is performed in the Heisenberg spin model. The cell size of the finer grid corresponds to the elementary cell of the material chosen for the simulation, thus each cell of this grid can be considered as a lattice site. For the sake of the portability of the algorithms from one grid to the other, the atomic lattice is always considered to be simple cubic. To improve on the quality of this approach, the size of the micromagnetic cell is chosen in order to contain an odd number of atomistic cells, this way a fixed amount of atomistic sites is in every micromagnetic cell. Furthermore one atomistic site occupies the center of each micromagnetic cell. In this context, interpolation algorithms are used to approximate the value of functions discretized on the micromagnetic grid to the corresponding atomistic sites. If the interpolated function is $\mathbf{M}$, the interpolated value is rescaled according to eq. (**??**) in order to obtain the magnetic moment μ. The interpolation algorithms used for this purpose are linear, bilinear or trilinear according to the dimensions of the micromagnetic grid. While the interpolation always introduces an error, as stated in eq. (**??**), these inaccuracies are considered to disappear during the course of the simulation. This assumption is based on the fact that in the variational approach, on which the LLG equation is based [see eq. (**??**)], small perturbations on the magnetic state of the system lead to the same lowest energy configuration.

Chapter 5

The necessity of a multiscale approach

To model magnetization dynamics, currently two paradigms analyzed in depth in chapter **??** are commonly used: the micromagnetic model and the classical Heisenberg spin model. In contrast to the Heisenberg model, the micromagnetic model [**?**] is ideal when simulating systems with linear dimensions of the order of a few nanometers or larger; since it is a continuous model that is discretized for computational application. The immediate advantage of approximating a large number of lattice sites with a single cell [see section **??**] consists in a sizeable decrease in terms of computational effort. Nonetheless, many magnetic structures and phenomena of general interest cannot be realistically simulated in this model. As shown in the previous chapters of this thesis, a twofold limitation occurs when the micromagnetic model is used to simulate magnetic structures which change on short length scales. The computational limitation of the algorithms used to evaluate the derivatives of $\mathbf{M}$ [see section **??**], which are needed when evaluating the exchange interaction effective field [see section **??**], produce an upper bound to the possible size of a micromagnetic cell. While this limitation can in principle be lifted by refining the mesh, this practice would increase the computational effort needed for a simulation, removing the main advantage of micromagnetics compared to the Heisenberg model. A stronger, fundamental limitation, is given by the intrinsic approximation of the model [see section **??** for details of the errors introduced by the micromagnetic model for rapidly varying spin structures]. This limitation does not depend on the numeric implementation, rather it affects micromagnetism in its original, analytical formulation, making accurate analyses of magnetic structures that change on the length scale of the atomic lattice unattainable. A textbook example for this scenario is offered by Bloch points [**?**] [see Fig. **??** and section **??**]. Certain domain

walls and spin waves also belong to this category for particular values of the material parameters.

As a discrete description, where with every atom in the lattice of the ferromagnet a magnetic moment is associated, the capability for Heisenberg model to simulate any magnetic structure is not limited by computational artifacts originating from the discretization of a continuous model. On the other hand, the Heisenberg model cannot be efficiently used to simulate systems larger than a few nanometers due to the computational time increasing faster than linearly with the number of lattice sites [?,?]. In the presented approach, the entire system is simulated using the micromagnetic model while one or more regions of which contain structures that exhibit a large gradient (e.g. Bloch points), are simulated using the discrete Heisenberg model. The main obstacle for the development of a combined multiscale technique consists of devising accurate conditions to make the interface between regions on two different scales magnetically smooth, in order to prevent any interface related artifacts.

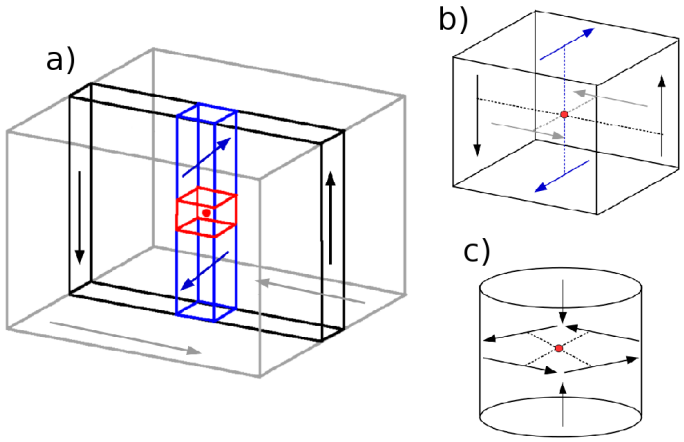

Figure 5.1: (a) Schematic of a magnetization structure with a micromagnetic singularity (Bloch point). The two domains depicted by grey arrows are separated by two Bloch walls (black). The Bloch walls have opposite sense of rotation and are separated by two Néel/Bloch lines (blue). Between the two Néel/Bloch lines with opposite orientations, a micromagnetic singularity (red) is formed. A magnification of the red square is shown in (b). (c) A micromagnetic singularity also occurs during the reversal of a magnetic vortex core [?,?]. These diagrams were adapted from Ref. [?].

5.1 Skyrmion annihilation in a constant field

As a demonstration for the necessity of a multiscale approach to magnetization dynamics, simulations of Skyrmions shrinking and annihilating in an external magnetic field were performed. The content of this chapter refers to Ref. [**?**]. The implementation of the multiscale approach is presented in detail in chapter **??**.

The chosen system is a ferromagnetic disk with a radius of 53 nm and thickness of 3 nm, the saturation magnetization $M_s = 10^6$ A/m, out-of-plane anisotropy constant $K_z = 1.3 \times 10^6$ J/m^3, and the exchange constant $A = 1.1 \times 10^{-11}$ J/m. These parameters are comparable to those of CoFeB [**?**] in multilayer stacks that are widely used in thin film nanostructures that exhibit Skyrmions [**?**]. The central part of the system was simulated in the Heisenberg model (fine scale region), while the remaining part was simulated using the micromagnetic model (coarse scale region). The size of the fine scale region was chosen in order to fit the entire Skyrmion at rest, but without sacrificing too much computational time. It should be stressed that larger Skyrmions can still be simulated accurately as far as no discontinuities occur in the coarse scale region.

First, magnetic Néel Skyrmion states were relaxed for different values of the Dzyaloshinskii-Moriya interaction (DMI), then simulations with a constant uniform magnetic field, applied in the direction opposite to the magnetization inside the Skyrmion were performed. All the micromagnetic parameters were kept fixed, whereas the atomistic ones were changed. In particular, the distance a between two neighboring nodes of the mesh was changed, in order to increase the density of spins. While a can be interpreted as the lattice constant of the material, it is treated in this case just as a computational parameter. As a result, the magnetic moment of the spins μ and the exchange constant J were rescaled according to $\mu = a^3 M_s$ and $J = aA$. These all effectively simulate a single material that is described with the same micromagnetic parameters, which are used for the coarse scale region.

In Fig. **??**(a) we show that an application of an external out-of-plane magnetic field leads to the Skyrmion shrinking until it reaches its new equilibrium size. This behavior is reproduced for magnetic fields up to a critical value H_{del}. For fields larger than H_{del}, the Skyrmion shrinks until it completely annihilates. The analysis of the Skyrmion dynamics in nonzero out-of-plane fields shows that the spins magnetized in plane, corresponding to the center of the Skyrmion's circular domain wall, tilt clockwise while the Skyrmion shrinks [see Figs. **??**(b) and **??**]. When the shrinking stops, i.e. the Skyrmion reaches a new equilibrium size, the magnetization in the domain wall aligns along the radial direction again, recovering the Néel Skyrmion character.

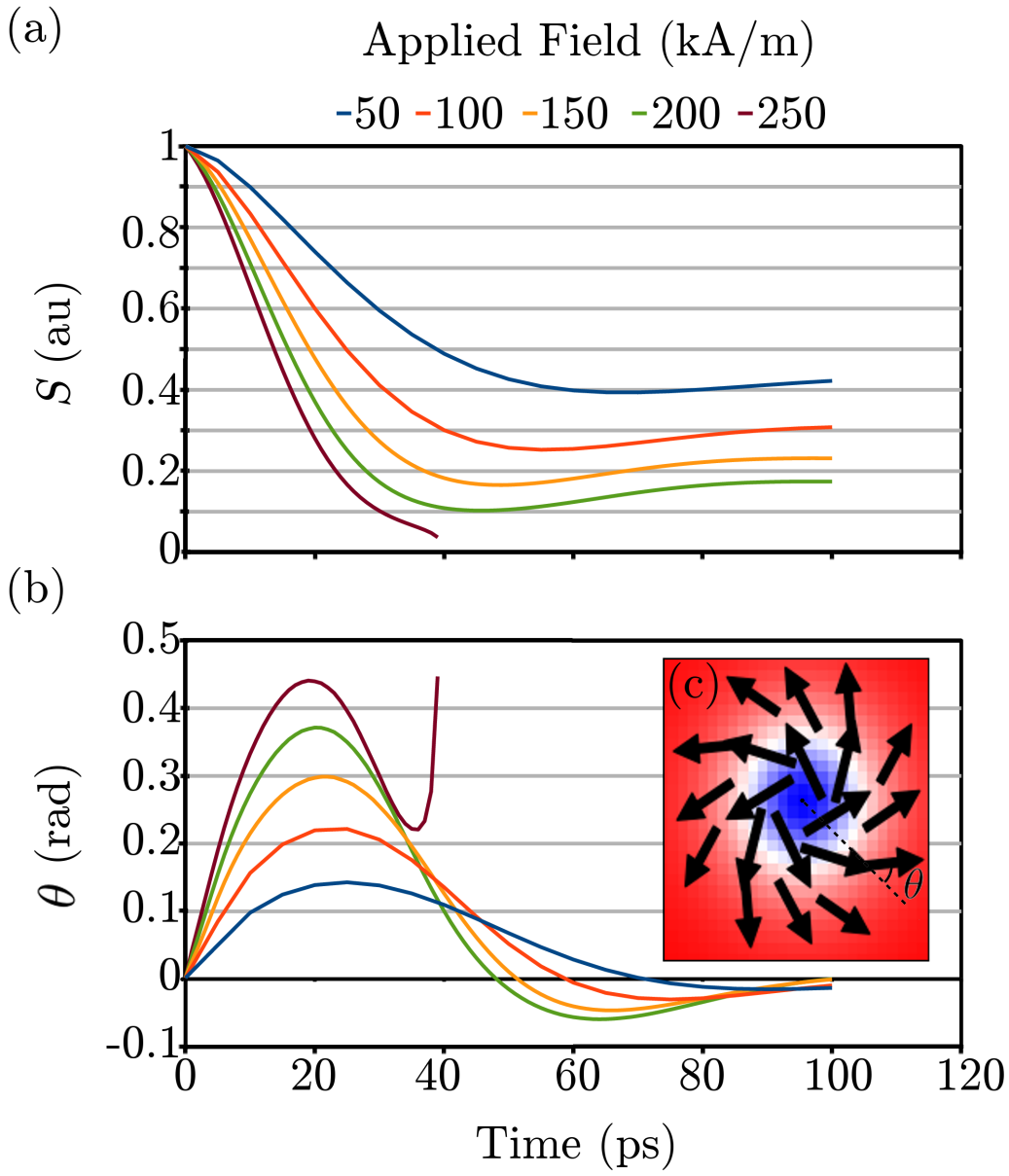

Figure 5.2: Dynamics of a Skyrmion for different values of a constant out-of-plane field. The system shows an oscillatory behavior, where both (a) its size, expressed in terms of the Skyrmion magnetic moment S, and (b) the angle θ between the in-plane magnetization components of the domain wall and the radial direction, reach a certain nonzero value before relaxing back to the equilibrium. The data corresponding to 250 kA/m shows the Skyrmion annihilation. The inset (c) illustrates how the angle θ is defined. The color code showing the out of plane component of $\mathbf{M}$ is clarified in Fig. **??**.

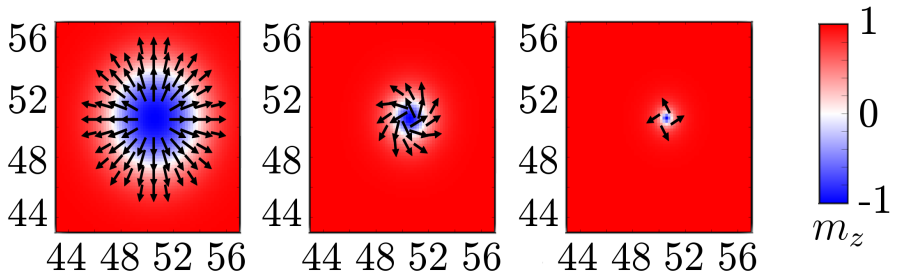

Figure 5.3: Dynamic snapshots at various stages of the annihilation process in 300 kA/m external magnetic field. The initial configuration of a Néel Skyrmion is changed when the structure is shrinking. The scale on the axes is expressed in units of the micromagnetic computational cell (3 nm).

As a measure of the Skyrmion size we use the total magnetic moment S inside the Skyrmion's domain wall. It is proportional to $\sum_i (m_{z,i} - 1)$, where $m_{z,i}$ is the out-of-plane component of the normalized magnetization at the lattice site i, and the sum runs over all sites in the fine scale region, which always completely includes the Skyrmion's domain wall. For fields below H_{del}, we observe that S reaches a minimum, depending on Gilbert damping α, before relaxing back to a slightly larger value [Fig. **??**(a)]. While the Skyrmion increases in size, the magnetization in the domain wall tilts counterclockwise [Fig. **??**(b)]. The aim here is to demonstrate how the simulation results can be influenced by the refinement of the mesh rather than testing the stability of the Skyrmion for different material parameters, as previously investigated e.g. in Ref. [**?**].

We find that decreasing a, i.e. increasing the density of magnetic moments, leads to an increase of H_{del} [see Fig. **??**]. This is in agreement with Ref. [**?**] and shows how the minimum size which a Skyrmion can reach before the annihilation strongly depends on the lattice constant. Furthermore, these results agree with the asymptotic behavior of indestructible Skyrmions in a continuous model [**?**, **?**]. Topological protection can thus be considered a limiting case of the energy barrier [**?**] separating the metastable Skyrmion state from the ferromagnetic state.

The energy barrier is shown in Fig. **??**, where the internal energy E_{int} of a Skyrmion shrinking under the influence of a constant magnetic field is plotted as a function of time. It can be noticed that E_{int}, consisting of the exchange, anisotropy, dipolar energy, and DMI contribution, increases until the annihilation occurs. The energy barrier is overcome by the application of the Zeeman energy. The Skyrmion moment S is also shown, to stress that once the Skyrmion reaches its minimum size, the topological barrier is overcome,

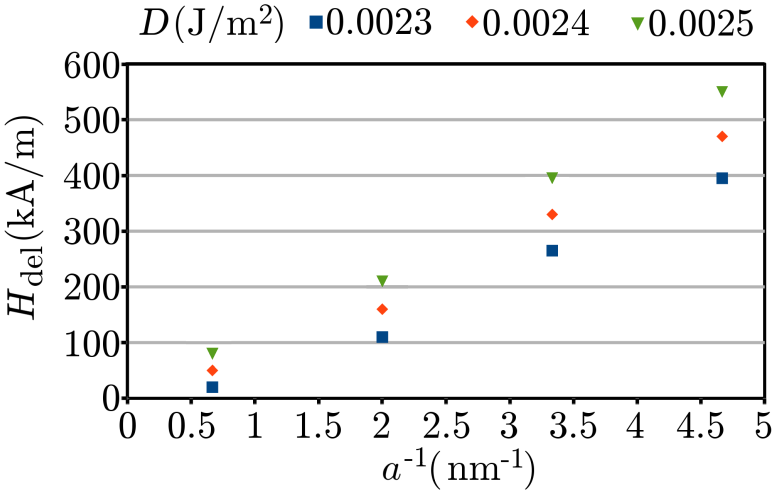

Figure 5.4: The minimum magnetic field H_{del} necessary to adiabatically annihilate a Skyrmion for different values of the DMI constant D and linear spin density a^{-1}. H_{del} is shown to linearly increase as a function of the spin density. Data points corresponding to the lowest value of a^{-1} were simulated in purely micromagnetic simulations.

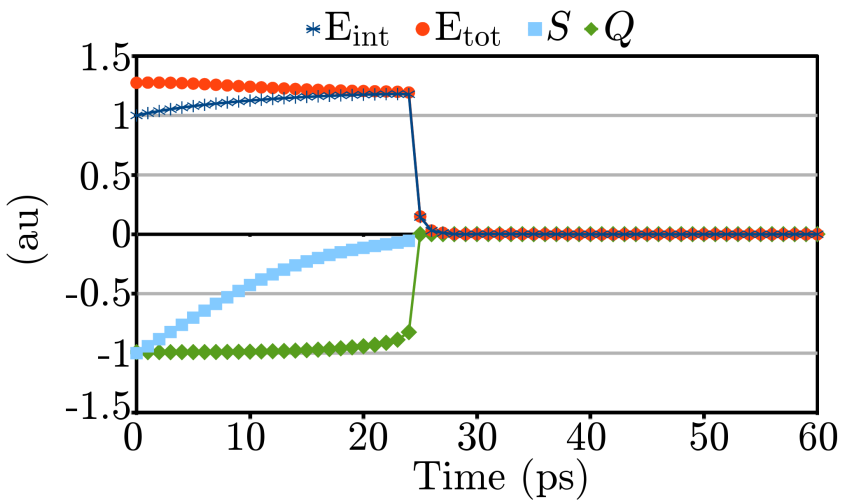

Figure 5.5: Path to annihilation of a Skyrmion in 300 kA/m external magnetic field. The internal energy E_{int} of the system and the total energy (internal plus Zeeman energies) are compared as functions of time. A potential barrier exists for the internal energy which has to be overcome by the application of an external field. The size S and the topological charge Q are shown. All the quantities are presented in arbitrary units.

and the system relaxes in the more stable uniform ferromagnetic state. It can be further noticed that the Skyrmion charge Q instantly switches to zero when the barrier is overcome. A purely micromagnetic simulation with a 1.5 nm cell size ($a^{-1} \simeq 0.667$ nm^{-1}) was included for comparison. It cannot be understated that a multiscale approach is able to simulate the singularities atomistically using realistic material parameters, and the uniformly magnetized external region in the micromagnetic model, allows one to predict the dynamics of a similar system with better quantitative accuracy than obtainable using only the micromagnetic model.

Determining the stability using a multiscale approach demonstrates that the annihilation of Skyrmions is strongly influenced by computational parameters, such as the mesh size. Using the multiscale approach overcomes this problem, and allows one to obtain the realistic stability parameters. The cell size here is fixed by the appropriate lattice constant of the simulated material, and the computational efforts are far lower than those of a purely atomistic simulation. Furthermore, this approach reproduces the dynamics including the spin spectrum realistically, which even allows in the future to include thermal effects.

Chapter 6

Implementation

The multiscale approach, implemented as an expansion of the MicroMagnum micromagnetic simulator [**?**], solves the Landau-Lifshitz-Gilbert equation numerically for two different models: the coarse grained micromagnetic model, which simulates the whole sample; and the classical Heisenberg spin model, which is used for magnetic structures that cannot be accurately described by the micromagnetic model, discretizing the magnetization field at atomic resolution [see Fig. **??**]. Parts of this chapter have been published in Ref. [**?**]

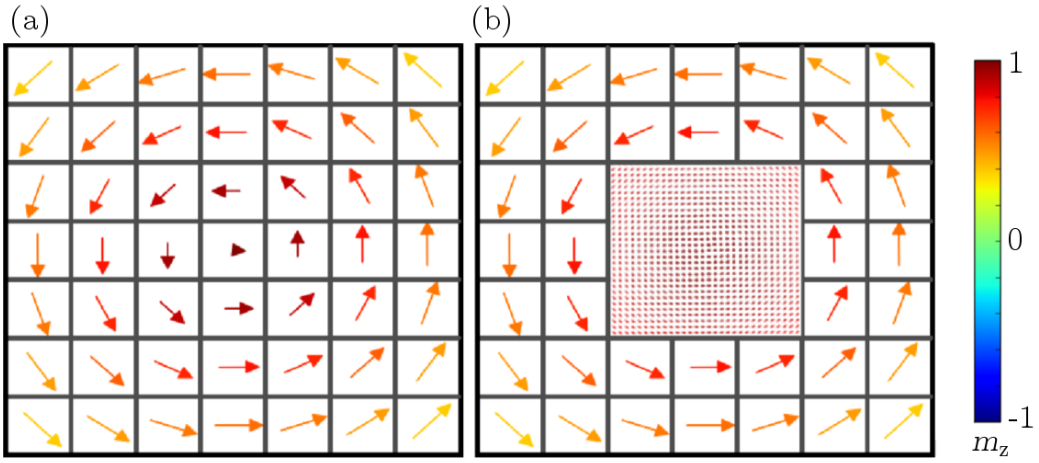

Figure 6.1: The basis of the multiscale model. a) Purely micromagnetic simulation: each cell in the vortex core region is simulated in the coarse scale. b) The multiscale simulation, where a small region (central 9 cells) is simulated using the atomistic model, while the rest of the sample is simulated using the micromagnetic model. The color code shows the out of plane component of the unit magnetization.

The software executes in parallel two independent solving routines, one for each model (it is in principle possible to execute any number of fine scale solving routines), performing one full computational step on the coarse scale one and then a short series of steps on the fine scale one centered around the time coordinate of the coarse one [see Fig. **??**].

The main task towards the development of this technique consisted in modeling the interaction between different regions. This was achieved by applying, after each coarse scale step, a set of magnetic fields designed to approximate the effect of the non-local terms of the effective magnetic field from one region on the other, see Fig. **??**, namely exchange and stray field.

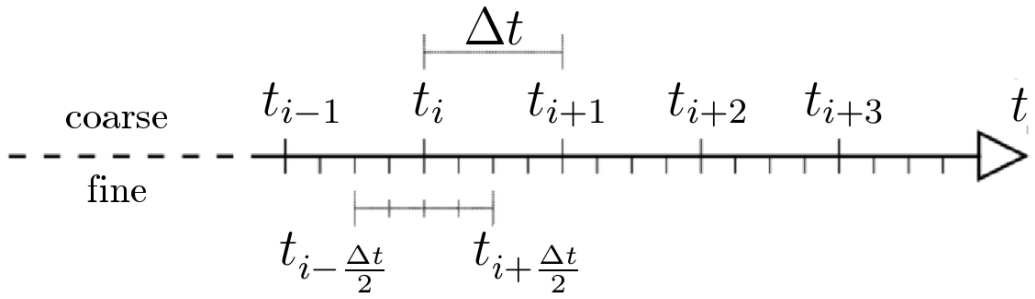

Figure 6.2: The multiscale model in the time domain: after each coarse computational time step the corrections to the effective field in the fine scale region, generated by the coarse one are evaluated, a short series of fine steps centered around the latest coarse step, of length h, is executed, then corrections to the coarse scale effective field (generated by the Heisenberg fine scale one) are evaluated.

6.1 Exchange field

The exchange field, generated by the fine scale magnetic moments closest to the interface ('interfacial moments'), on their 'neighboring' cells in the coarse scale ('interfacial cells') is evaluated by averaging all the interfacial moments inside each coarse scale cell [see Fig. **??**]. The average vector is rescaled by the volume $V_a = c_s a^3$ [see Eq. **??**] of a cell in the atomic lattice, in order to obtain the magnetization (A/m), rather than the magnetic moment (Am^2). A new finite difference mesh, with coarse scale discretization is created and the cells corresponding to the internal surface of the fine scale region are filled with the difference between the magnetization of the same cell in the original coarse mesh and the new vectors. In this way, the linearity of the exchange field with respect to the magnetization is exploited to evaluate a correction

to the field, calculated in the micromagnetic formulation, generated by the original coarse scale cells alone. The corrected exchange field, exerted by the multiscale cell j on the micromagnetic cell i is calculated as:

$$\mathbf{H}_{ex,\,corr}\left(\mathbf{M}_j\right) = \mathbf{H}_{ex}\left(\mathbf{M}_{int,j} - \mathbf{M}_j\right) + \mathbf{H}_{ex}\left(\mathbf{M}_j\right). \tag{6.1}$$

Here $\mathbf{M}_j$ denotes the magnetization in the cell j in the purely micromagnetic simulation, while $\mathbf{M}_{int,j}$ is defined as:

$$\mathbf{M}_{int,j} = \frac{M_s}{|\boldsymbol{\mu}|\, N_{int}} \sum_{k}^{N_{int}} \boldsymbol{\mu}_k = \frac{\sum_k^{N_{int}} \boldsymbol{\mu}_k}{V_a N_{int}}, \tag{6.2}$$

where the sum runs over all the magnetic moments μ located along the interface on the side of cell j that is neighboring cell i. This formula is only fully valid in the case of complete cells, without additional or missing atoms. This effective field term is evaluated in the micromagnetic model.

Likewise, to evaluate the exchange field generated by interfacial cells on interfacial moments, interpolation is employed in order to define a set of new magnetic moments ('ghost moments' [**?**]) to act as first neighbors to the interfacial ones. The exchange field generated by the ghost moments is evaluated in the Heisenberg spin model. A combination of fine scale moments and coarse scale magnetization is used in the interpolation in order to ensure a smooth transition in the magnetic pattern across the interface. This means that each ghost moment results from the interpolation of atomistic and aptly renormalized micromagnetic vectors. The same techniques, based on the average of interfacial magnetic moments, and the calculation of ghost moments through interpolation across the interface, are employed when evaluating antisymmetric exchange (Dzyaloshinskii-Moriya interaction) across the scale interface.

6.2 Demagnetization field

The stray field contains all the long range contributions to the effective fields. The implementation of this field constitutes one of the main differences between the two models. In both scales the demagnetization tensor formulation was employed, [**?**] as well as the calculation method based on FFT for efficient calculation [**?**]. While for the coarse cells the demagnetization tensor describes the interaction between two uniformly magnetized solid rectangles, according to the calculations carried on by Newell *et al.*, [**?**] the demagnetization tensor used for two full magnetic moments in the fine scale, is defined

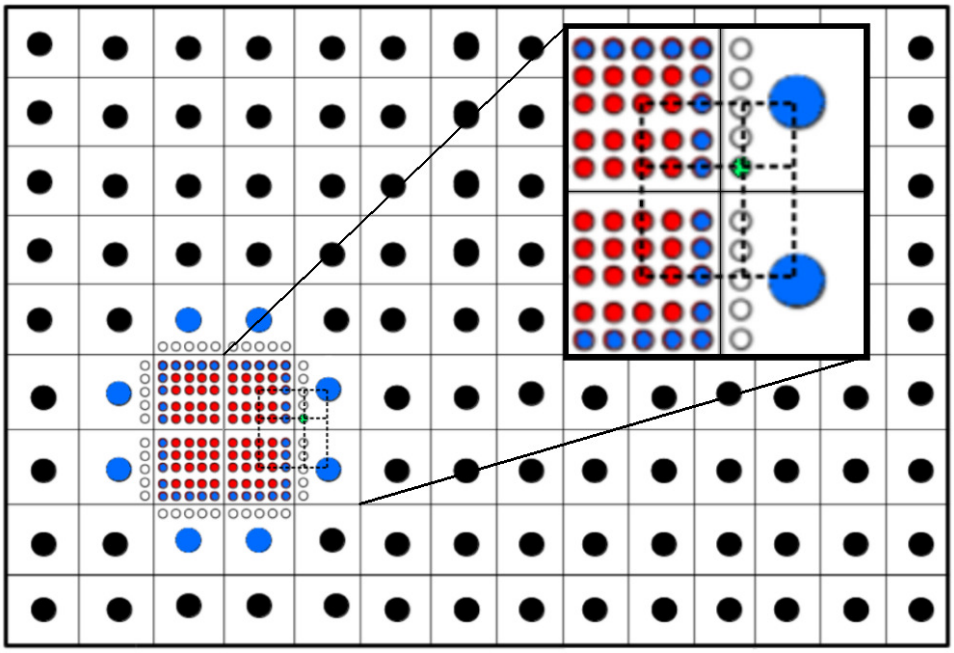

Figure 6.3: The key components in the evaluation of the cross-scale effective field terms: magnetic moments (red), micromagnetic cells (black), interfacial moments and cells (highlited in blue), ghost moments, which are not part of the LLG solving routine (white). The dashed lines show how the ghost moments, and in particular the one marked in green, are evaluated as the bilinear interpolation of fine scale moments and coarse scale magnetization. (Inset) Zoom on the square formed by the dashed interpolation lines, which is a practical case of the one shown in figure **??**(b).

as:

$$\frac{1}{4\pi}\left[\frac{\mathbb{1}}{|\mathbf{r}_i-\mathbf{r}_j|^3}-3\frac{(\mathbf{r}_i-\mathbf{r}_j)\otimes(\mathbf{r}_i-\mathbf{r}_j)}{|\mathbf{r}_i-\mathbf{r}_j|^5}\right], \tag{6.3}$$

where $\mathbf{r}_i$ and $\mathbf{r}_j$ are the position of two magnetic moments, $\mathbb{1}$ is 3×3 identity matrix, and symbol $\otimes$ denotes the tensor product.

Similarly to the exchange field, the stray field is linear in the magnetization vector and this property is exploited likewise. The correction to the stray field generated in the micromagnetic system by fine scale regions is evaluated using the averaged value of magnetic moments in each cell. In order to evaluate the complete demagnetization field acting on the fine scale system, the coarse scale magnetization structure is copied into a new mesh and the cells corresponding to the fine scale region are filled with null vectors. The stray field generated by this system is evaluated. This technique is employed in order for the field generated by the fine scale region on itself not to be evaluated twice. Since the field has the same discretization as the structure generating it, the result is then interpolated, in order for it to have the discretization of the fine scale mesh. The type of linear interpolation depends, as for the ghost moments, on the dimensionality of the mesh. This is the only case for an effective field term evaluated micromagnetically to be applied on the fine scale region. This approximation is made necessary by the computational complexity of the algorithm calculating the field, increasing with $N\log(N)$ where N is the number of cells. This dependence is due to the method employed for calculating the demagnetization tensor based on Fast Fourier Transform (FFT) [**?**, **?**].

6.3 Tests

Having implemented the approach, a series of tests was performed as a demonstration of the validity of this method. First, some basic tests were run, in order to make sure that the effective field terms were evaluated correctly. This was achieved mainly by comparing the numerical results to the analytical theory for small systems and comparing micromagnetic and atomistic results for larger systems. The results for the dynamics of a single magnetic moment in an external field derived in **??** were compared to the numerical results generated by the multiscale approach in order to make sure that the Runge-Kutta algorithm was implemented correctly in both scales.

In order to test the interface conditions at the interface two customized tests were performed. These results are published in [**?**] along with the details of the implementation of such interface conditions.

6.3.1 Spin wave transmission

A one-dimensional nanowire, 1.8 μm long with a square 0.3×0.3 nm^2 section was simulated. The fine scale domain was 90 nm long [see Fig. **??**], the material parameters for this system are those commonly used for permalloy, namely: $M_s = 8 \times 10^5$ A/m, exchange constant $A = 1.3 \times 10^{-11}$ J/m, and Gilbert damping constant $\alpha = 0.01$ [**?**]. The lattice constant chosen for the atomistic region was $l = 0.3$ nm, comparable to the ones of iron and nickel.

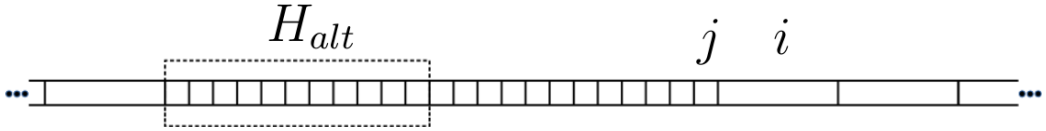

Figure 6.4: The fine scale region of the nanowire and its immediate surroundings. An oscillating magnetic field $H_{\rm alt}$ is applied to a section of the fine scale region to excite spin waves. The amplitude of the spin wave is evaluated in the atomistic fine scale cell j and the coarse scale cell i which is described micromagnetically.

Spin waves of different frequencies ω_0 were excited applying an alternating transversal magnetic field, $H_{\rm alt}$, to a short (3 nm long) section of the wire. The magnetization as a function of time was measured on the atomistic moment furthest from the region where $H_{\rm alt}$ is applied ($\boldsymbol{\mu}_j(t)$), and on the neighboring micromagnetic cell ($\mathbf{M}_i(t)$), the transversal component of the two arrays was normalized, and then analyzed using FFT in order to find $\mu_j(\omega)$ and $M_i(\omega)$. Peaks with frequency corresponding to the frequency of $H_{\rm alt}$ were easily identifiable. The height of such peaks increased linearly with the amplitude of $H_{\rm alt}$. The peaks, $\mu_j(\omega_0)$ and $M_i(\omega_0)$, were squared and the transmission coefficient T across the interface has been evaluated by calculating the ratio between the two:

$$T(\omega_0) = \frac{|\mu_j(\omega_0)|^2}{|M_i(\omega_0)|^2}. \tag{6.4}$$

For some values of the frequency, a purely atomistic simulation was performed for comparison, and with the aim of obtaining the relation between frequency and wavelength. Using FFT in the space domain, the corresponding wavenumber k was measured for each value of the excitation frequency. In particular, such Fourier transforms were evaluated at different time instants and then averaged. Once again peaks were easily identifiable. By means of linear regression [see Fig. **??**] the dependence $k^2(\omega)$ was measured

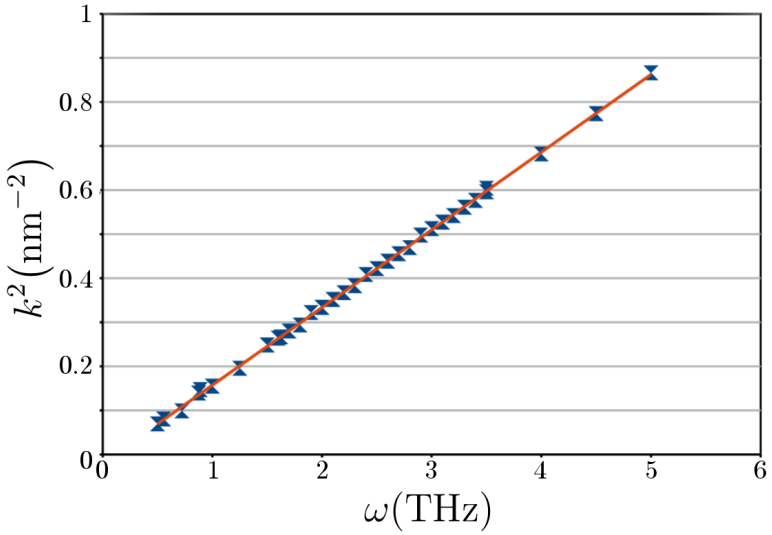

Figure 6.5: Linear regression used to measure the relation between excited wavevector k and the excitation frequency ω.

and the wavelength corresponding to each value of the excitation frequency was calculated as $\lambda(\omega) = 2\pi/k(\omega)$.

Three sets of simulations were performed, with different lengths of the micromagnetic cells, corresponding to ten, twenty and thirty times the atomic lattice constant. The data show ideal transmission for frequency values smaller than a sharply defined cut-off frequency. The same data, as a function of the wavelength, show consistently that the transmission drops to zero at a cut-off wavelength corresponding to a specific value of the coarse cell size [Fig. **??**].

Considering the cut-off as a consequence of the coarse scale not being able to resolve waves with such a small wavelength, a similar system was simulated, this time with the excitation being applied on the coarse scale region only. Here the waves propagate into and then out of the fine scale region and the transmission is measured for waves leaving the fine scale region [Fig. **??**(a)]. The test was repeated using periodic boundary conditions to make sure that the sharp cut-off was not caused by the waves being reflected at the end of the wire. Both tests were then repeated for different values of the exchange constant. In order to measure the cut-off frequencies, a linear regression was executed on all the transmission values between 0.1 and 0.9, the intersection of this line with the transmission value of 0.5 was defined as the cut-off frequency.

The cut-off wavelength of the order of a few computational cells is at-

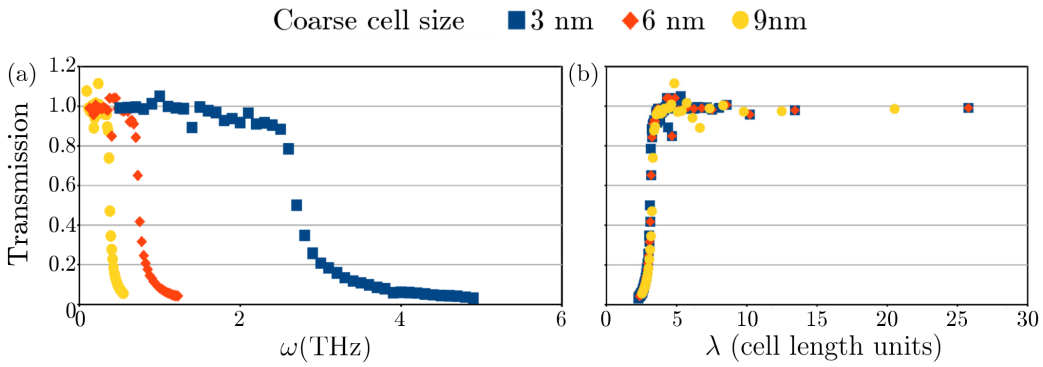

Figure 6.6: The measured transmission for waves excited in the fine scale region with open boundary conditions as a function of their frequency ω (a) and wavelength λ (b). A transmission of 1 (100%) for a wide range of wavelengths demonstrates the numerical validity of the model.

tributed to the approximation performed in evaluating the exchange interaction, which is due to the limited accuracy of the algorithms used to calculate the derivatives of **M** [see sections **??** and **??**]. This universal behavior can be considered as a limitation of computational micromagnetism, which does not allow one to simulate very short wavelength spin waves without refining the mesh, introducing therefore a dramatic increase in the computation time. The dependence of the cut-off frequency on the exchange constant supports this hypothesis [see Fig. **??**(b)].

The transmission data for the spin waves shows that information about magnetic structures in the fine region can cross perfectly the scale interface, thus demonstrating the reliability and numerical validity of the model. A thorough analysis of the cut-off phenomenon found for spin wave transmission shows that in the presence of spin waves with a short wavelength the multiscale approach can be reliably used under the condition that the waves do not leave the fine scale region. Meanwhile, the traditional approach – a refinement of the whole mesh – would increase the computational time dramatically.

6.3.2 Continuity of a DMI spiral

To demonstrate the reliability of the method used to evaluate effective fields across the interface by direct comparison to analytical theory, a system exhibiting antisymmetric exchange [**?**, **?**] was simulated, as this leads to a spin structure that can be analytically calculated. A nanowire, similar in shape to the one used to test spin wave transmission, with the parameters

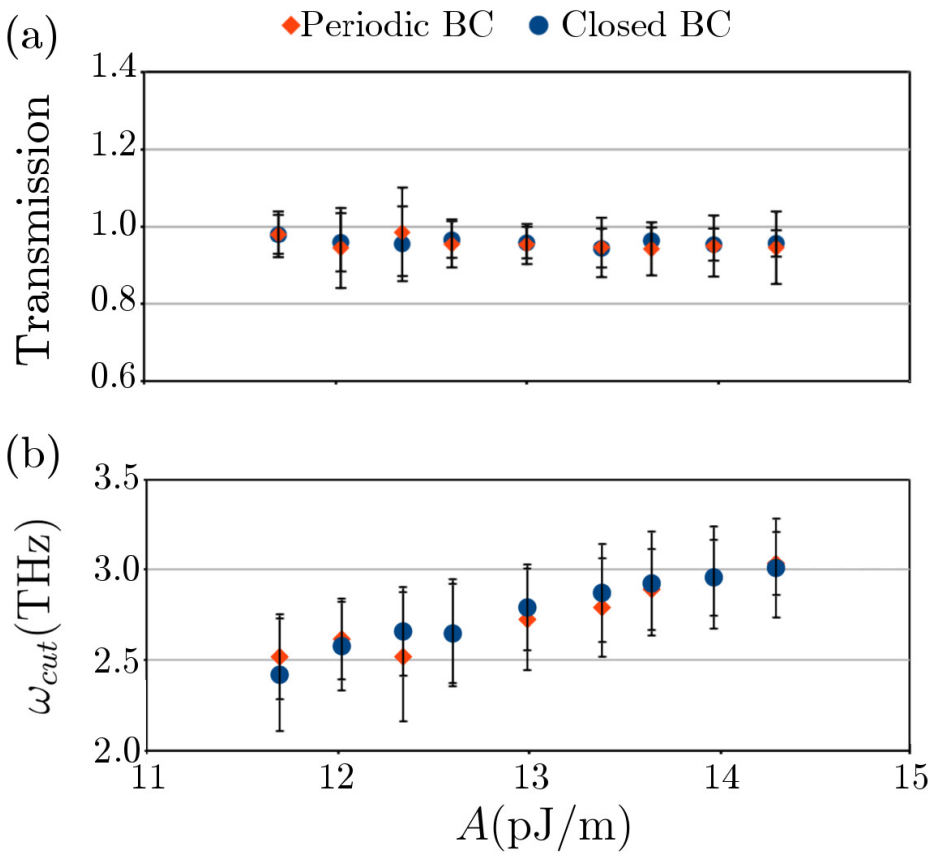

Figure 6.7: (a) The average transmission for waves of all possible frequencies excited in the coarse scale region, before entering the fine scale one, with closed and periodic boundary conditions (BC) for different values of the exchange constant A. The data shown is the result of an average on all the frequencies. Peaks with frequency higher than 3.5 THz were not visible in the Fourier transform, underlining the fact that the cut-off is a consequence of the waves not being resolved for the chosen cell-size. The observed transmission of approximately 1 shows the validity of the method with no artificial attenuation at the interface between the regions where different models are used. (b) The cut-off frequency ω_{cut} for waves excited in the fine scale region with closed and periodic boundary conditions (BC) for different values of the exchange constant A. A cut-off frequency depending on the exchange constant demonstrates that this phenomenon is strictly micromagnetic and is not introduced by the multi-scale approach.

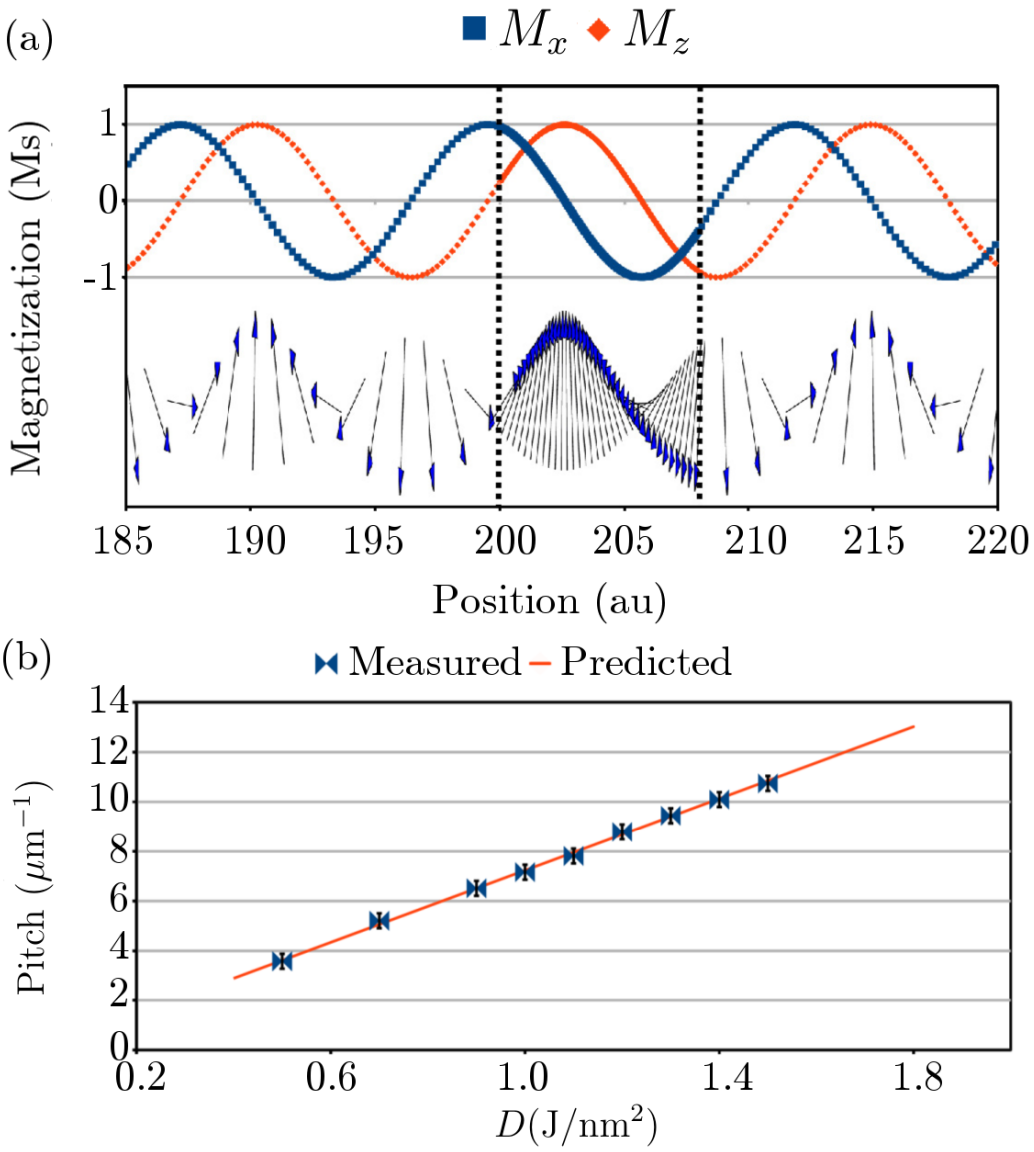

Figure 6.8: (a) The two components of the magnetization for a multiscale DMI helix in the xz plane, showing continuity and consistency of the period in the coarse and fine scale. The dashed lines show the position of the fine scale region. (b) The pitch of the helix increases linearly with the DMI constant and is consistent with the value expected from an analytical calculation [**?**].

$M_s = 1.05 \times 10^6$ A/m, exchange constant $A = 11 \times 10^{11}$ J/m. Different values of $D = |\mathbf{D}_{ij}|$ were used. The vector $\mathbf{D}_{ij}$ scales the energy density of the Dzyaloshinskii-Moriya interaction (DMI) as calculated in Ref. [**?**] and shown in **??**:

$$e_{DMI} = \mathbf{D}_{ij} \cdot (\boldsymbol{\mu}_i \times \boldsymbol{\mu}_j) \,/\, |\mu|^2 \,.$$

The system was relaxed in a coarse scale simulation, then a fine scale region was applied on a section of the wire and the system was relaxed again. The relaxed state [see Fig. **??**] showing continuity in the helix structure, typical of systems exhibiting DMI, with a pitch in agreement with the predicted [**?**] value of $D/(4\pi A)$. The pitch was evaluated from the Fourier transform in the space domain for the two components of the helix, using the data points from both scales and taking the peak value from the Fourier transform. The components of $\mathbf{M}$ evidently have a perfectly sinusoidal shape, see Fig. **??**.

This data further shows that the method employed for evaluating cross scale interactions ensures continuity between the regions of different scales and yield quantitative agreement with the analytical theory.

6.4 Tracking

A tracking algorithm was devised in order to keep the fine scale region as small as possible, it scans the fine scale region for the position of the structure of interest (SOI), usually where a singularity is likely to occur, and shifts the fine scale region by an integer number of coarse scale cells units, in order to always have the SOI close to its center. When micromagnetic cells previously not part of the fine scale region become included, interpolation is applied in order to fill in the fine scale mesh with magnetic moments that accurately reproduce the coarse scale magnetization and are continuous within and across the scale interface.

To show that the fine scale area can be reliably moved, a test was performed. This test simulated domain wall motion in a nanostrip ($3\,\mu$m $\times$ $33\,$nm $\times 0.3\,$nm) induced by a unidirectional magnetic field. The material parameters of the strip are the same as the nanowire from the previous test with the only exception of Gilbert damping $\alpha = 0.1$. The domain wall is initially in the center of the fine scale region, when the distance from the starting position becomes larger than a certain threshold (tracking distance), the whole fine scale region is shifted, in order to keep it centered. The test was repeated for different tracking distances to show that this process does not influence the dynamics of the system (Fig. **??**). These results indicate the reliability of the tracking algorithm and its effectiveness as a method to keep the size of

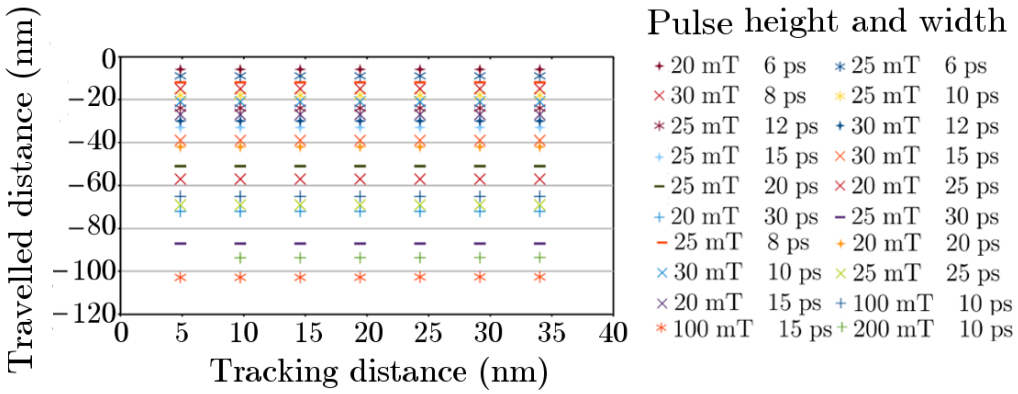

Figure 6.9: Domain wall displacement after the application of a unidirectional Gaussian-shape magnetic field pulse with different values of height and width as a function of the tracking distance. This is the distance traveled by the domain wall before the fine scale region is centered around it. We expect this parameter not to influence the dynamics of the system and the data confirms this assumption.

the fine scale regions at a minimum and not introducing significant artifacts to the simulated results.

Chapter 7

Topological transformations in magnetic Skyrmions

Magnetic Skyrmions are one of the most interesting spin structures for the development of future information technology as they have been predicted to be topologically protected. As shown in Ref. [?] a BL can be formed and annihilated in a Bloch Skyrmion via application of a field gradient. Since the process of annihilating a Skyrmion is a key operation for devices, the effect of a spin polarized current pulse was analyzed to see that Skyrmions can be reliably deleted by designing the pulse shape. For this purpose current pulses that generate spin-orbit torques [?, ?, ?] were employed, in order to show how the shape of these pulses influences the Skyrmion and induces changes to the topology. In general, using spin currents is more advantageous than using fields to manipulate magnetization due to more favorable scaling. The influence of the spin-orbit torques on Skyrmions [?, ?], in particular yields many promising possibilities towards the implementation of Skyrmions as information bits.

As the annihilation of a Skyrmion includes the annihilation of a Bloch line (BL) [?], this phenomenon cannot be properly simulated in the micromagnetic framework. Because of this change in topology of the spin structure during the process [?], the charge Q [see eq. (??)] of the system changes from ± 1 to 0, thus lifting the topological protection.

Within the multiscale approach the core of an isolated Skyrmion was simulated atomistically, while the remaining part of a nanodisk hosting the Skyrmion was simulated using the Heisenberg model. The material parameters employed for this simulation were the same as the stability simulations presented in ?? with the damping constant $\alpha = 0.1$. Furthermore the Hall angle $\alpha_H = 0.1$ and the constant $\xi = 0.5$ were used.

The LLG equation implemented to include the effect of a spin-polarized

current, generated for instance via the inverse spin galvanic effect or the spin-Hall effect, is eq. (??) presented in chapter ?? derived from Ref. [?], and reads:

$$\begin{aligned}\frac{d\mathbf{m}}{dt} = &-\gamma'\left[\mathbf{m}\times\mathbf{H}_{eff}+\alpha\left(\mathbf{m}\times\left(\mathbf{m}\times\mathbf{H}_{eff}\right)\right)\right]\\ &-\gamma' a_J\left[\left(\xi-\alpha\right)\left(\mathbf{m}\times\mathbf{p}\right)+\left(1+\alpha\xi\right)\left(\mathbf{m}\times\left(\mathbf{m}\times\mathbf{p}\right)\right)\right],\end{aligned} \tag{??}$$

where $\gamma' = \gamma/\left(1+\alpha^2\right)$ with γ being the gyromagnetic ratio, $\mathbf{H}_{eff}$ is the effective field, $\mathbf{p}$ the average polarization of the current generated by the spin-Hall effect, a_J the damping-like term constant [?, ?, ?], and ξ the ratio between damping-like and field-like torques. Current density pulses of Gaussian shape, $J(t) = J_0 \exp[-t^2/(2\sigma^2)]$ were applied along the x-direction.

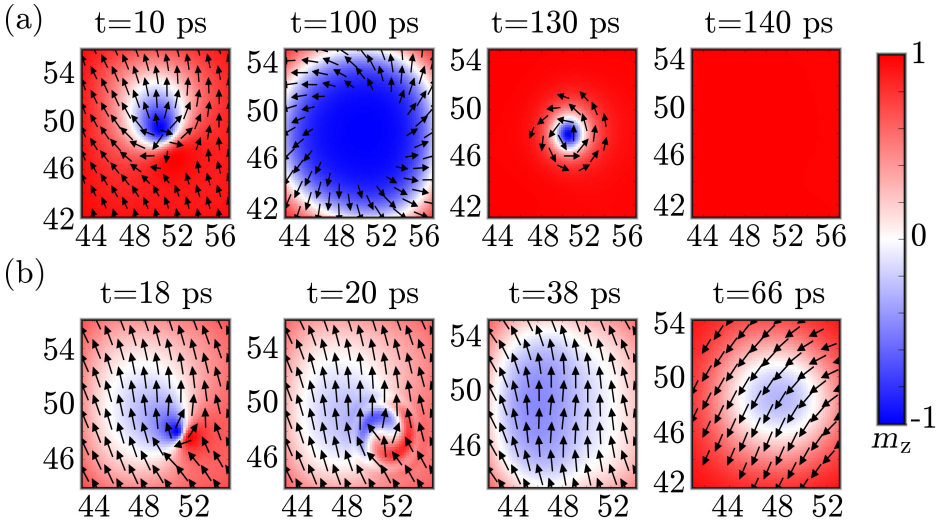

Figure 7.1: Spin structure of the Skyrmion during the annihilation process in cases I and II. The color code for the arrows shows the out-of-plane component, from red, to white to blue. The initial state corresponds to a relaxed Skyrmion centered on the cell with coordinates (50, 50). (a) Case I: A BL is formed in the domain wall of the Skyrmion within a vortex-antivortex pair. The spins in the domain wall turn clockwise starting from the position of the pair, meanwhile, the Skyrmion increases in size and reaches a maximum then starts shrinking in size. As the Skyrmion shrinks below the minimum size, it is finally annihilated. The system relaxes into the ferromagnetic ground state. (b) Case II: The vortex-antivortex pair annihilates, the Skyrmion number immediately turns to zero, the system quickly relaxes back to the ferromagnetic state.

The results show that during the application of the pulse the topological

charge density, defined as

$$q = \frac{1}{4\pi}\mathbf{m} \cdot \left(\frac{\partial \mathbf{m}}{\partial x} \times \frac{\partial \mathbf{m}}{\partial y} \right),$$

accumulates in a vortex antivortex couple. It is indeed possible to form a vertical BL, as a vortex-antivortex couple within the domain wall of the Skyrmion. In the process the domain wall deforms, increases in width on one side of the Skyrmion and decreases on the opposite side. The duration of the pulse plays a fundamental role, since a pulse that is too short would not deform the domain wall enough, while a pulse too long would act adiabatically on the whole Skyrmion and push it beyond the edge of the magnetic system. Intermediate values result in the formation of the BL that can either annihilate or relax. While the annihilation is a topological transformation and leads to the annihilation of the Skyrmion, the relaxation of the BL results in its rapid expansion. We can explain the rapid expansion of the Skyrmion as a consequence of the large exchange energy density of the BL being dissipated in the breathing mode excitation of the Skyrmion.

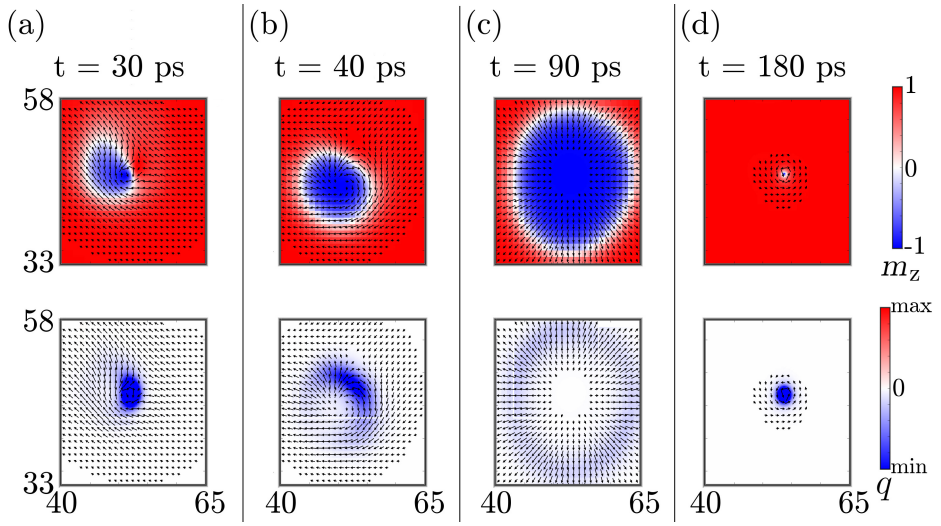

Figure 7.2: Details of the case I annihilation process. (a) The topological charge density is accumulated in a vortex-antivortex pair. (b) The system relaxes. (c) The Skyrmion size increases until the Néel character is recovered. (d) The Skyrmion shrinks and then annihilates.

It is possible to distinguish three different regimes [see Fig. **??**]. In the nonannihilating regime the relaxation of the BL is accompanied by size oscillations of the Skyrmion, which do not lead to collapse. As was noted in **??**,

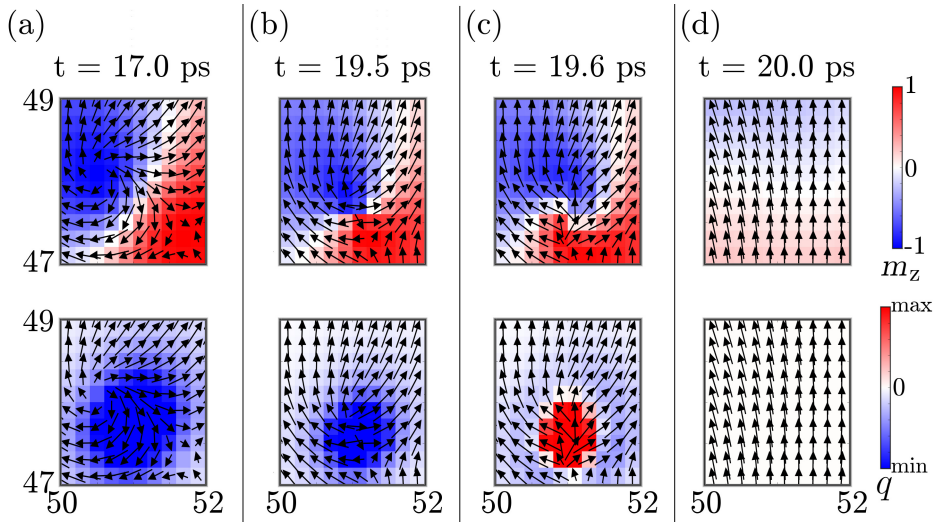

Figure 7.3: Zoom on the case II annihilation process shown in Fig. **??**(b). (a) The topological charge density is accumulated in a vortex-antivortex pair. (b) A Bloch line is formed. (c) The Bloch line annihilates, generating a topological charge density of the opposite sign. (d) The system relaxes into the ferromagnetic state.

Skyrmions collapse once their size becomes too small to stabilize them in the antiparallelly aligned surrounding magnetization. This occurs in the annihilation regime of case I [Fig. **??**(a)], which (while qualitatively similar to the nonannihilating regime) results in stronger size oscillations that annihilate the Skyrmion due to overshooting in the shrinking phase. The annihilation regime of case II, see Fig. **??**(b), is indeed qualitatively different since the vortex-antivortex pair with opposite polarities forms and subsequently annihilates [**?**, **?**], leading to the immediate annihilation of the Skyrmion. This regime could thus be exploited for practical applications since it allows one to lift the topological protection of Skyrmions in a quick and reliable manner.

Some considerations can be inferred about the energetic landscape of the Skyrmion in the three regimes. In the nonannihilating regime, the injected pulse does not provide enough energy to overcome the potential barrier discussed in chapter **??**. Topological charge density accumulates on one side of the domain wall and is then redistributed to the whole Skyrmion. During this process the size of the Skyrmion increases. The energy provided by the pulse is then dissipated as the size of the Skyrmion fluctuates until it reaches equilibrium. If the energy provided by the pulse is higher than the potential barrier, the size oscillations of the Skyrmion are large enough to annihilate the Skyrmion in the case I regime. A larger amount of energy needed to

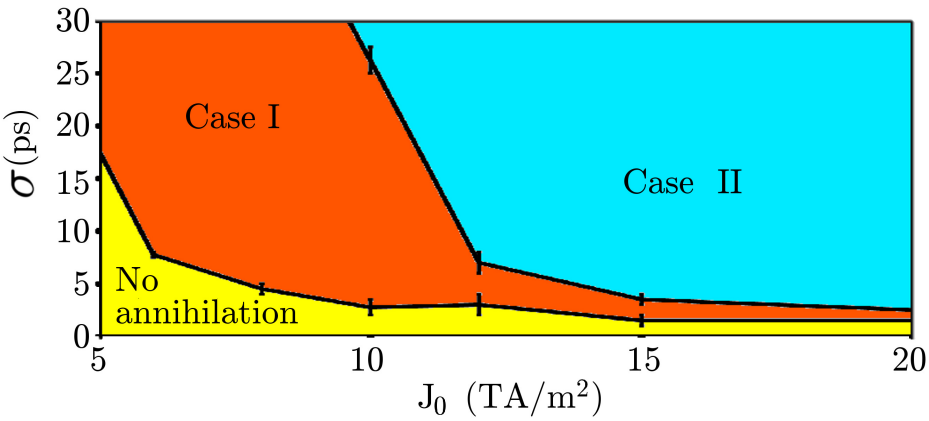

Figure 7.4: Different regimes depending on the peak height J_0 and half-width σ of the Gaussian pulse. The error bars were evaluated by performing simulations with different values of σ.

form and annihilate a Bloch line on the domain wall, as it happens in the case II regime. In this case the energy is not dissipated by relaxing the structure, increasing the size of the Skyrmion. Rather, due to the instability of the topological charge being accumulated on a few magnetic moments [see Fig. **??**] the Bloch line is immediately annihilated. During the annihilation of the Bloch line a topological charge of the opposite sign is generating. As a consequence, the topological protection is overcome and the system quickly relaxes into the ferromagnetic state.

The application of spin-orbit torques due to spin-polarized current pulses was shown to be a very fast and efficient method to delete isolated Skyrmions as required for applications, since certain combinations of pulse parameters exist, which robustly annihilate the Skyrmion. This may open up a path to delete Skyrmions reliably as required for future spintronic memory.

Chapter 8

Summary and outlook

The extensive attention given to the theory in the early chapters of this thesis, is aimed to provide the reader with all the necessary information to understand the need for a multiscale approach, and the main challenges towards its implementation.

The main observables in the theory, the spin **S** and the magnetization **M**, are presented in the first chapter. The LLG equation, determining their dynamics, is derived from basic quantum mechanical calculations and phenomenological observations.

In the second chapter the effective field terms of the LLG equation are evaluated in the micromagnetic model as a continuum approximation of the classical Heisenberg spin model. Particular focus is dedicated to the nonlocal terms, the exchange and demagnetization fields. The former imposes the main shortcoming on the micromagnetic model, since it cannot be evaluated accurately for tightly wound magnetization structures. The latter accounts for the long range interaction of all the spins in the magnetic system with each other. The computational complexity of the algorithms needed to evaluate the demagnetization field constitutes the main disadvantage of atomistic models when simulating systems of a size comparable to that of certain devices of technological interest. Furthermore, the Dzyaloshinskii-Moriya interaction, responsible for the stabilization of Skyrmions, and the spin-Hall torque, commonly used to excite this structures, are presented in detail.

The third chapter focuses on some magnetic structures of interest. Chiral structures such as vortices and Skyrmions are described and their topological properties are explained. In order to underline the need for a multiscale approach, structures and phenomena that cannot be simulated in the micromagnetic model, such as Bloch points and unwinding Bloch lines, are detailed.

The fourth chapter presents different algorithms employed in the ap-

proach. The Runge-Kutta algorithm, used to calculate the solution of differential equations is the fundamental computational tool when running a simulation. The finite difference method, which discretizes a continuous model provides one further limitation to the micromagnetic model, whose accuracy in evaluating the exchange field, is not only intrinsically limited by the micromagnetic approximation, but by the effect that the refinement of the mesh has on the evaluation of the spatial derivatives as well. Interpolation algorithms, employed to approximate atomistic quantities from micromagnetism are essential in order to understand how the multiscale approach was implemented.

The arguments in favor of a multiscale approach are summarized in the fifth chapter. As a further proof of concept, the stability of Skyrmions was evaluated for different sets of computational and physical parameters in order to show how an accurate atomistic model is needed to accurately simulating Skyrmion annihilation.

The implementation of the approach is the focus of the sixth chapter. Here the model used to evaluate the exchange and demagnetization fields between regions on a different scale is detailed. The validity of the approach was tested by evaluating the transmission coefficient for spin waves traveling through the interface between the two regions. One further demonstration is provided by the simulation of a DMI spiral. This structure arises as a consequence of the interplay between isotropic and antisymmetric exchange interaction (DMI). The correct evaluation of the spiral relies on an accurate implementation of this effect across the model interface. The tracking algorithm was tested as well by simulating domain wall motion. The importance of tracking the structure to simulate atomistically, in this case the domain wall, cannot be understated since it allows to greatly reduce the size of the fine scale region.

The seventh chapter presents the first application of the multiscale approach. Skyrmions are excited and annihilated by using spin-Hall torques. The topological aspects of the Skyrmion annihilation are analyzed with unprecedented detail for a numerical approach. The operating range of a memory device based on this technology is evaluated quantitatively, identifying a regime where Skyrmions, encoding an information bit, can be annihilated quickly and reliably.

Future developments on this multiscale approach include the implementation of atomic lattices other than the simple cubic one and thermal effects. In particular, simulating lattices other than the simple cubic one would allow for a more realistic implementation of the DMI and of the thermal effects, which cannot be accurately simulated in a discretized micromagnetic model, since the computational grid would induce an artificial cut-off wavelength

to the magnon spectrum. One further direction for improvement consists in employing higher order interpolation algorithms, in order to ensure an even smoother transition between the two models.

Furthermore, the basic elements of the multiscale approach, such as the interpolation of ghost moments or the tracking algorithm, could be applied to other fields of physics involving equations similar to the LLG.

The current interest towards structures with topological properties could generate several applications of the multiscale approach, since transformations involving changes in the topology of a system can only be simulated accurately in an atomistic model. This opens the path for a wide variety of investigations of both fundamental and technological interest.

Bibliography

[1] W. F. Brown, *Micromagnetics: Successor to domain theory?*. J. Phys. Radium **20**, 101-104 (1959).

[2] W. F. Brown, *Magnetostatic Principles in Ferromagnetism*. (North Holland Publishing Company, Amsterdam, 1962).

[3] W. F. Brown, *Micromagnetics*. (John Wiley and Sons, Hoboken NJ, 1962).

[4] L. D. Landau and E. M. Lifshitz, *Theory of the Dispersion of Magnetic Permeability in Ferromagnetic Bodies*. Phys. Z. Sowjetunion **8**, 153 (1935).

[5] F. Bloch, *Zur Theorie des Austauschproblems und der Remanenzerscheinung der Ferromagnetika*. Z. Phys. **74**, 295 (1932).

[6] L. Néel, *Énergie des parois de Bloch dans les couches minces*. C. R. Acad. Sci. **241**, 533 (1955).

[7] E. E. Huber Jr., D.O. Smith, J. B. Goodenough, *Domain Wall Structure in Permalloy Films*. J. Appl. Phys. **29**, 294 (1958).

[8] S. Middelhoek, *Magnetic Domain Walls in Thin Ni-Fe Films*. J. Appl. Phys. **34**, 1054 (1963).

[9] A. Hubert and R. Schäfer, *Magnetic Domains - the Analysis of Magnetic Microstructures*. (Springer-Verlag, Berlin, 1998).

[10] J. Raabe, R. Pulwey, R. Sattler, T. Schweinböck, J. Zweck, D. Weiss, *Magnetization pattern of ferromagnetic nanodisks*. J. Appl. Phys. **88**, 4437–4439 (2000).

[11] T. Shinjo, T. Okuno, R. Hassdorf, K. Shigeto, T. Ono, *Magnetic vortex core observation in circular dots of permalloy*. Science **289**, 930–932 (2000).

[12] R. Hertel, S. Gliga, M. Fahnle, C. M. Schneider, *Ultrafast Nanomagnetic Toggle Switching of Vortex Cores*. Phys. Rev. Lett. **98**, 117201 (2007).

[13] A. N. Bogdanov and U. K. Rößler, *Chiral Symmetry Breaking in Magnetic Thin Films and Multilayers*. Phys. Rev. Lett. **87**, 037203 (2001).

[14] U. K. Rößler, A. N. Bogdanov, C. Pfleiderer, *Spontaneous Skyrmion Ground States in Magnetic Metals*. Nature **442**, 797–801 (2006).

[15] J. Iwasaki, M. Mochizuki, N. Nagaosa, *Current-Induced Skyrmion Dynamics in Constricted Geometries*. Nat. Nanotech. **8**, 742-747 (2013).

[16] J. Sampaio, V. Cros, S. Rohart, A. Thiaville, A. Fert, *Skyrmions on the Track*. Nat. Nanotech. **8**, 839-844 (2013).

[17] B. Dupé, M. Hoffmann, C. Paillard, S. Heinze, *Tailoring Magnetic Skyrmions in Ultra-Thin Transition Metal Films*. Nat. Commun. **5**, 5030 (2014).

[18] J. C. Slonczewski, *Theory of Bloch-line and Bloch-wall motion*. J. Appl. Phys. **45**, 6 (1974).

[19] S. Iwatsuka, S. Iida, *Nucleation and punch-through of a horizontal Bloch line detected in dynamic bubble collapse*. Jpn. J. Appl. Phys. **22**, 1855 (1983).

[20] V. G. Bar'yakhtar, E. B. Krotenko, D. A. Yablonskii, *Magnetic symmetry of domain walls with Bloch lines in ferromagnets and ferrites*. Sov. Phys. JETP **64**, 3 (1986).

[21] K. Matsuyama, K. Chikamatsu, H. Asada, *Characteristics of Bloch line memory read operation in 2 μm bubble material*. IEEE Trans. Magn. **26**, 5 (1990).

[22] G. Binasch, P. Grünberg, F. Saurenbach, W. Zinn, *Enhanced magnetoresistance in layered magnetic structures with antiferromagnetic interlayer exchange*. Phys. Rev. B **39**, 7 (1989).

[23] P. Grünberg, *Magnetic field sensor with ferromagnetic thin layers having magnetically antiparallel polarized components* , US Patent 4949039 A, (1989).

[24] M. N. Baibich , J. M. Broto, A. Fert, F. Nguyen Van Dau, F. Petroff, P. Eitenne, G. Creuzet, A. Friederich, J. Chazelas, *Giant Magnetoresistance of* (001)Fe/(001)Cr *Magnetic Superlattices*. Phys. Rev. Lett. **61**, 21 (1988).

[25] T. Miyazaki and N. Tezuka, *Giant magnetic tunneling effect in* $Fe/Al_2O_3/Fe$ *junction*. J. Magn. Magn. Mater. **139**, 3 (1995).

[26] S. S. P. Parkin, M. Hayashi, L. Thomas, *Magnetic Domain-Wall Racetrack Memory*. Science **320**, 5863 (2008).

[27] L. Berger, *Low-field magnetoresistance and domain drag in ferromagnets*. J. Appl. Phys. **49**, 2156 (1978).

[28] L. Berger, *Exchange interaction between ferromagnetic domain wall and electric current in very thin metallic films*. J. Appl. Phys. **55**, 1954 (1984).

[29] L. Berger, *Possible existence of a Josephson effect in ferromagnets*. Phys. Rev. B **33**, 1572 (1986).

[30] L. Berger, *Emission of spin waves by a magnetic multilayer traversed by a current*. Phys. Rev. B **54**, 9353 (1996).

[31] J. C. Slonczewski, *Current-driven excitation of magnetic multilayers*. J. Magn. Magn. Mat. **159**, L1 (1996).

[32] S. Krause and R. Wiesendanger, *Spintronics: Skyrmionics gets hot*. Nat. Mater. **15**, 493-494 (2016).

[33] E. Feldtkeller, *Mikromagnetisch stetige und unstetige Magnetisierungskonfigurationen*. Z. Angew. Phys. **19**, 530 (1965).

[34] W. Döring, *Point singularities in micromagnetism*. J. Appl. Phys.**39**, 1006 (1968).

[35] B. Krüger, *Current-Driven Magnetization Dynamics: Analytical Modeling and Numerical Simulation*, Doctoral dissertation, Universität Hamburg, 2011, http://ediss.sub.uni-hamburg.de/volltexte/2012/5887/pdf/Dissertation.pdf.

[36] C. Mencuccini and V. Silvestrini, *Fisica 2. Elettromagnetismo-ottica.* (Liguori, Napoli, 1998).

[37] T. L. Gilbert, *A Lagrangian Formulation of the Gyromagnetic Equation of the Magnetization Field*. Phys. Rev. **100**, 1243 (1995).

[38] C. Andreas, *Multiscale Multimodel Simulation of Micromagnetic Singularities*, Doctoral dissertation, Forschungszentrum Jülich GmbH, 2014, http://juser.fz-juelich.de/record/201878.

[39] C. A. de Coulomb, *Premier mémoire sur l'électricité et le magnétisme*, Histoire de l'Académie Royale des Sciences, 569-577 (1785).

[40] A. J. Newell, W. Williams, D. J. Dunlop, *A Generalization of the Demagnetizing Tensor for Nonuniform Magnetization*. J. Geophys. Res. **98**, 9551-9555 (1993).

[41] R. Skomski, A. Kashyap, J. Zhou, D. J. Sellmyer, *Anisotropic exchange*. J. Appl. Phys. **97**, 10B302 (2005).

[42] I. Dzyaloshinskii, *A Thermodynamic Theory of "Weak" Ferromagnetism of Antiferromagnetics*. J. Phys. Chem. Solids **4**, 241-255 (1958)

[43] T. Moriya, *Anisotropic Superexchange Interaction and Weak Ferromagnetism*. Phys.Rev. **120**, 91 (1960).

[44] D. Petit, P. R. Seem, M. Tillette, R. Mansell, R. P. Cowburn, *Two-dimensional control of field-driven magnetic bubble movement using Dzyaloshinskii–Moriya interactions*. Appl. Phys. Lett. **106**, 022402 (2015).

[45] S. Chen, S. Zhang, Q. Zhu, X. Liu, C. Jin, J. Wang, Q. Liu, *Effect of Dzyaloshinskii-Moriya interaction on the magnetic vortex oscillator driven by spin-polarized current*. Appl. Phys. Lett. **117**, 17B720 (2015).

[46] F. Zhuo and Z. Z. Sun, *Field-driven Domain Wall Motion in Ferromagnetic Nanowires with Bulk Dzyaloshinskii-Moriya Interaction*. Sci. Rep. **6**, 25122 (2016).

[47] S. Zhang, P. M. Levy, A. Fert, *Mechanisms of spin-polarized current-driven magnetization switching*. Phys. Rev. Lett. **88**, 236601 (2002).

[48] S. Zhang, Z. Li, *Roles of nonequilibrium conduction electrons on the magnetization dynamics of ferromagnets*. Phys. Rev. Lett. **93**, 127204 (2004).

[49] A. Shpiro, P. M. Levy, S. Zhang, *Self-consistent treatment of nonequilibrium spin torques in magnetic multilayers*. Phys. Rev. B **67**, 104430 (2003).

[50] I. M. Miron, K. Garello, G. Gaudin, P. J. Zermatten, M. V. Costache, S. Auffret, S. Bandiera, B. Rodmacq, A. Schuhl, P. Gambardella, *Perpendicular switching of a single ferromagnetic layer induced by in-plane current injection*. Nature **476**, 189 (2011).

[51] I. M. Miron, T. Moore, H. Szambolics, L. D. Buda-Prejbeanu, S. Auffret, B. Rodmacq, S. Pizzini, J. Vogel, M. Bonfim, A. Schuhl, G. Gaudin, *Fast current-induced domain-wall motion controlled by the Rashba effect*. Nat. Mater. **10**, 419 (2011).

[52] K.-W. Kim, S.-M. Seo, J. Ryu, K.-J. Lee, H.-W. Lee, *Magnetization dynamics induced by in-plane currents in ultrathin magnetic nanostructures with Rashba spin-orbit coupling*. Phys. Rev. B **85**, 180404(R) (2012).

[53] T. A. Moore , I. M. Miron, G. Gaudin, G. Serret, S. Auffret, B. Rodmacq, A. Schuhl, S. Pizzini, J. Vogel, M. Bonfim, *High domain wall velocities induced by current in ultrathin* Pt/Co/AlOx *wires with perpendicular magnetic anisotropy*. Appl. Phys. Lett. **93**, 262504 (2008).

[54] J. Sinova, S. O. Valenzuela, J. Wunderlich, C. H. Back, T. Jungwirth, *Spin Hall effects*. Rev. Mod. Phys. **87**, 1213 (2015).

[55] M. I.Dyakonov, V. I.Perel, *Current-induced spin orientation of electrons in semiconductors*. Phys. Lett. A **35**, 459 (1971).

[56] J. E. Hirsch, *Spin Hall Effect*. Phys. Rev. Lett. **83**, 1834 (1999).

[57] S. F. Zhang, *Spin Hall Effect in the Presence of Spin Diffusion*. Phys. Rev. Lett. **85**, 393 (2000).

[58] L. Liu, C.-F. Pai, Y. Li, H. W. Tseng, D. C. Ralph, R. A. Buhrman, *Spin-Torque Switching with the Giant Spin Hall Effect of Tantalum*. Science **336**, 555 (2012).

[59] K.-S. Ryu, L. Thomas, S.-H. Yang, S. Parkin, *Chiral spin torque at magnetic domain walls*. Nat. Nanotech. **8**, 527 (2013).

[60] M. Hayashi, J. Kim, M. Yamanouchi, H. Ohno, *Quantitative characterization of the spin-orbit torque using harmonic Hall voltage measurements*. Phys. Rev. B **89**, 144425 (2014).

[61] R. E. Miller and E. B. Tadmor, *A unified framework and performance benchmark of fourteen multiscale atomistic/continuum coupling methods*. Model. Simulat. Mater. Sci. Eng. **17**, 053001 (2009).

[62] C. Hertel, M. Schümichen, S. Löbig, J. Fröhlich, J. Lang, *Adaptive large eddy simulation with moving grids*. Theor. Comp. Fluid. Dyn. **27**, 817-841 (2012).

[63] C.J. Garcìa-Cervera and A. M. Roma, *Adaptive mesh refinement for micromagnetics simulations*. IEEE Trans. Magn. **42**, 1648-1654 (2006).

[64] K.M. Tako, T. Schrefl, M.A. Wongsam, R.W. Chantrell, *Finite element micromagnetic simulations with adaptive mesh refinement*. J. Appl. Phys. **81**, 4082–4083 (1997).

[65] F. Garcia-Sanchez, O. Chubykalo-Fesenko, O. Mryasov, R. W. Chantrell, K. Y. Guslienko, *Exchange spring structures and coercivity reduction in* FePt/FeRh *bilayers: A comparison of multiscale and micromagnetic calculations*. Appl. Phys. Lett. **87**, 122501 (2005).

[66] F. Garcia-Sanchez, O. Chubykalo-Fesenko, O. Mryasov, R. W. Chantrell, *Multiscale modelling of hysteresis in* FePt/FeRh *bilayer*. Physica B: Condens. Matter **372**, 328 (2006).

[67] F. Garcia-Sanchez, O. Chubykalo-Fesenko, O. Mryasov, R. W. Chantrell, K. Y. Guslienko, *Multiscale versus micromagnetic calculations of the switching field reduction in* FePt/FeRh *bilayers with perpendicular exchange spring*. J. Appl. Phys. **97**, 10J101 (2005).

[68] T. Jourdan, A. Marty, F. Lançon, *Multiscale method for Heisenberg spin simulations*. Phys. Rev. B **77**, 224428 (2008).

[69] T. Jourdan, A. Masseboeuf, A. Marty, F. Lançon, P. Bayle-Guillemaud, *Magnetic bubbles in* FePd *thin films near saturation*. J. Appl. Phys. **106**, 073913 (2009).

[70] C. Andreas, A. Kakay, R. Hertel, *Multiscale and multimodel simulation of Bloch-point dynamics*. Phys. Rev. B **89**, 134403 (2014).

[71] F. Bruckner, M. Feischl, T. Führer, P. Goldenits, M. Page, D. Praetorius, M. Ruggeri, D. Suess, *Multiscale modeling in micromagnetics: Existence of solutions and numerical integration*. Math. Models Methods Appl. Sci. **24**, 2627 (2014).

[72] P. Weinberger, E. Y. Vedmedenko, R. Wieser, R. Wiesendanger, *A multi-scale model of domain wall velocities based on ab initio parameters*. Philos. Mag. **91**, 2248-2262 (2011).

[73] M. Kläui, *Head-to-head domain walls in magnetic nanostructures*. J. Phys. Condens. Matter **20**, 313001 (2008).

[74] W. Rave and A. Hubert, *Magnetic ground state of a thin-film element*. IEEE Trans. Mag. **36**, 3886 -3899 (2000).

[75] J. P. Park, P. Eames, D. M. Engebretson, J. Berezovsky, P. A. Crowell, *Imaging of spin dynamics in closure domain and vortex structures*. Phys. Rev. B **67**, 020403 (2003).

[76] G.-W. Chern, H. Youk, O. Tchernyshyov, *Topological defects in flat nanomagnets: The magnetostatic limit*. J. Appl. Phys.**99**, 08Q505 (2006).

[77] R. Hertel and C. M. Schneider, *Exchange explosions: magnetization dynamics during Vortex-antivortex annihilation*. Phys. Rev. Lett. **97**, 177202 (2006).

[78] O. A. Tretiakov and O. Tchernyshyov, *Vortices in thin ferromagnetic films and the Skyrmion number*. Phys. Rev. B **75**, 012408 (2007).

[79] N. Romming, C. Hanneken, M. Menzel, J. E. Bickel, B. Wolter, K. von Bergmann, A. Kubetzka, R. Wiesendanger, *Writing and Deleting Single Magnetic Skyrmions*. Science **341**, 636-639 (2013).

[80] L. Cai, E. M. Chudnovsky, D. A. Garanin, *Collapse of skyrmions in two-dimensional ferromagnets and antiferromagnets*. Phys. Rev. B **86**, 024429 (2012).

[81] M. Kammerer, M. Weigand, M. Curcic, M. Noske, M. Sproll, A. Vansteenkiste, B. Van Waeyenberge, H. Stoll, G. Woltersdorf, C. H. Back. G. Schuetz, *Magnetic vortex core reversal by excitation of spin waves*. Nat. Commun. **2**, 279 (2011).

[82] T. H. R. Skyrme, *A unified field theory of mesons and baryons*. Nucl. Phys. **31**, 556-569 (1962).

[83] X. Z. Yu, Y. Onose, N. Kanazawa, J. H. Park, J. H. Han, Y. Matsui, N. Nagaosa, Y. Tokura, *Real-space observation of a two-dimensional Skyrmion crystal*. Nature **465**, 901-904 (2010).

[84] S. Seki, X. Z. Yu, S. Ishiwata, Y. Tokura, *Observation of Skyrmions in a multiferroic material*. Science **336** 198-201 (2012).

[85] M. Bode, M. Heide, K. von Bergmann, P. Ferriani, S. Heinze, G. Bihlmayer, A. Kubetzka, O. Pietzsch, S. Blügel, R. Wiesendanger, *Chiral magnetic order at surfaces driven by inversion asymmetry*. Nature **447**, 190-193 (2007).

[86] S. Heinze, K. von Bergmann, M. Menzel, J. Brede, A. Kubetzka, R. Wiesendanger, G. Bihlmayer, S. Blügel, *Spontaneous atomic-scale magnetic Skyrmion lattice in two dimensions*. Nat. Phys. **7**, 713- 718 (2011).

[87] S. Woo, K. Litzius, B. Krüger, M.-Y. Im, L. Caretta, K. Richter, M. Mann, A. Krone, R. M. Reeve, M. Weigand, P. Agrawal, I. Lemesh, M.-A. Mawass, P. Fischer, M. Kläui, G. S. D. Beach, *Observation of room-temperature magnetic Skyrmions and their current-driven dynamics in ultrathin metallic ferromagnets*. Nat. Mater. **15**, 501-506 (2016).

[88] W. Jiang, P. Upadhyaya, W. Zhang, G. Yu, M. B. Jungfleisch, F. Y. Fradin, J. E. Pearson, Y. Tserkovnyak, K. L. Wang, O. Heinonen, S. G. E. te Velthuis, A. Hoffmann, *Blowing magnetic skyrmion bubbles*. Science **349**, 6245 (2015).

[89] O. Boulle, J. Vogel, H. Yang, S. Pizzini, D. de Souza Chaves, A. Locatelli, T. O. Menteş, A. Sala, L. D. Buda-Prejbeanu, O. Klein, M. Belmeguenai, Y. Roussigné, A. Stashkevich, S. M. Chérif, L. Aballe, M. Foerster, M. Chshiev, S. Auffret, I. M. Miron, G. Gaudin, *Room-temperature chiral magnetic skyrmions in ultrathin magnetic nanostructures*. Nat. Nanotech. **11**, 449–454 (2016).

[90] C. Moreau-Luchaire, C. Moutafis, N. Reyren, J. Sampaio, C. A. F. Vaz, N. Van Horne, K. Bouzehouane, K. Garcia, C. Deranlot, P. Warnicke, P. Wohlhüter, J.-M. George, M. Weigand, J. Raabe, V. Cros, A. Fert, *Additive interfacial chiral interaction in multilayers for stabilization of small individual skyrmions at room temperature*. Nat. Nanotech. **11**, 444–448 (2016).

[91] A. Bogdanov and A. Hubert, *Thermodynamically stable magnetic vortex states in magnetic crystals*. J. Magn. Magn. Mater. **138**, 255-269 (1994).

[92] U. K. Rößler, A. N. Bogdanov, C. Pfleiderer, *Spontaneous Skyrmion ground states in magnetic metals*. Nature **442**, 797-801 (2006).

[93] S. Mühlbauer, B. Binz, F. Jonietz, C. Pfleiderer, A. Rosch, A. Neubauer, R. Georgii, P. Böni, *Skyrmion lattice in a chiral magnet*. Science **323**, 915-919 (2009).

[94] S. Rohart and A. Thiaville, *Skyrmion confinement in ultrathin film nanostructures in the presence of Dzyaloshinskii-Moriya interaction*. Phys. Rev. B **88**, 184422 (2013).

[95] A. Fert, J. Sampaio, V. Cros, *Skyrmions on the track*. Nat. Nanotech. **8**, 152-156 (2013).

[96] J. Sampaio, V. Cros, S. Rohart, A. Thiaville, A. Fert, *Nucleation, stability and current-induced motion of isolated magnetic Skyrmions in nanostructures*. Nat. Nanotech. **8**, 839-844 (2013).

[97] G. Finocchio, F. Büttner, R. Tomasello, M. Carpentieri, M. Kläui, *Magnetic Skyrmions: from fundamental to applications*. J. Phys. D: Appl. Phys. **49**, 423001 (2016).

[98] N. Papanicolaou T. N. Tomaras, *Dynamics of magnetic vortices*. Nucl. Phys. B **360**, 425 (1991).

[99] L. Arnaud, B. J. Youssef, D. Challeton, J. Miltat, *Bloch line magnetic memory*, US Patent 5260891 A, (1990).

[100] C. Moutafis, S. Komineas, J. A. C. Bland, *Dynamics and switching processes for magnetic bubbles in nanoelements*. Phys. Rev. B **79**, 224429 (2009).

[101] D. A. Gilbert, B. B. Maranville, A. L. Balk, B. J. Kirby, P. Fischer, D. T. Pierce, J. Unguris, J. A. Borchers, K. Liu, *Realization of ground-state artificial skyrmion lattices at room temperature*. Nat. Commun. **6**, 8462 (2015).

[102] A. Thiaville, J. M. Garcìa, R. Dittrich, J. Miltat, T. Schrefl, *Micromagnetic study of Bloch-point-mediated vortex core reversal*. Phys. Rev. B **67**, 094410 (2003).

[103] O. V. Pylypovskyi, D. D. Sheka, Y. Gaididei, *Bloch point structure in a magnetic nanosphere*. Phys. Rev. B **85**, 224401 (2012).

[104] R. G. Elìas and A. Verga, *Magnetization structure of a Bloch point singularity*. Eur. Phys. J. B **82**, 159–166 (2011).

[105] K. M. Lebecki, D. Hinzke, U. Nowak, O. Chubykalo-Fesenko *Key role of temperature in ferromagnetic Bloch point simulations*. Phys. Rev. B **86**, 094409 (2012).

[106] J. Reinhardt, *Gittertheoretische Behandlung von mikromagnetische Singularitäten*. Int. J. Magn. **5**, 263 (1973).

[107] T. Pang, *An introduction to computational physics*. (Cambridge University Press, Cambridge, 2006).

[108] J. C. Butcher, *Numerical methods for ordinary differential equations in the 20th century*. J. Comput. Appl. Math. **125**, 1-29 (2000).

[109] OOMMF package: http:/math.nist.gov/oommf .

[110] A. Aharoni, *Domain walls and micromagnetics*. J. Phys. Colloq. **32**, 966-971 (1971).

[111] C. Abert, L. Exl, G. Selke, A. Drews, T. Schrefl, *A Fast Finite-Difference Method for Micromagnetics Using the Magnetic Scalar Potential*. IEEE Trans. Magn. **48**, 1105-1109 (2012).

[112] B. Krüger, G. Selke, A. Drews, D. Pfannkuche, *Fast and accurate calculation of the demagnetization tensor for systems with periodic boundary conditions*. IEEE Trans. Magn. **49**, 4749-4755 (2013).

[113] A. De Lucia, K. Litzius, B. Krüger, O. A. Tretiakov, M. Kläui, *Multiscale simulations of topological transformations in magnetic Skyrmions*. arXiv:1702.05767, (2017).

[114] X. Liu, W. Zhang, M. J. Carter, G. Xiao, *Ferromagnetic resonance and damping properties of* CoFeB *thin films as free layers in MgO-based magnetic tunnel junctions*. J. Appl. Phys. **110**, 033910 (2011).

[115] A. Siemens, Y. Zhang, J. Hagemeister, E. Y. Vedmedenko, R. Wiesendanger, *Minimal radius of magnetic skyrmions: statics and dynamics*. New J. Phys. **18**, 045021 (2016).

[116] MicroMagnum software: http://micromagnum.informatik.uni-hamburg.de/.

[117] A. De Lucia, B. Krüger, O. A. Tretiakov, M. Kläui, *Multiscale model approach for magnetization dynamics simulations*. Phys. Rev. B **94**, 184415 (2016).

[118] A. Brataas and K. M. D. Hals, *Spin–orbit torques in action*. Nat. Nanotech. **9**, 86-88 (2014).

[119] I. A. Ado, O. A. Tretiakov, M. Titov, *Microscopic theory of spin-orbit torques in two dimensions*. Phys. Rev. B **95**, 094401 (2017).

[120] R. Tomasello, E. Martinez, R. Zivieri, L. Torres, M. Carpentieri, G. Finocchio, *A strategy for the design of skyrmion racetrack memories*. Sci. Rep. **4**, 6784 (2014).

[121] R. Hertel and C. M. Schneider, *Exchange Explosions: Magnetization Dynamics during Vortex-Antivortex Annihilation*. Phys. Rev. Lett. **97**, 177202 (2006).

Acknowledgments

The results presented in this thesis have been achieved through funding from the following institutions: the Graduate School Material Science in Mainz (GSC 266), SpinNet (DAAD Spintronics network, project number 56268455), the DFG (SFB TRR 173 SPIN+X), and the Carl Zeiss foundation. This work presents the scientific results of my work as a Ph.D. student in the group of Prof. Dr. Mathias Kläui, at the Institute of Physics, Johannes Gutenberg University. I am sincerely grateful to all the people who have given their time and effort to teach and assist me along the way. Thank you to all who have contributed to my experience as a Ph.D. student by any means.

List of publications

S. Finizio, A. Kronenberg, M. Vafaee, M. Foerster, K. Litzius, **A. De Lucia**, T. O. Menteş, L. Aballe, B. Krüger, M. Jourdan, M. Kläui, *Magnetic configurations in nanostructured* Co_2MnGa *thin film elements.* New J. Phys. **17**, 083030 (2015).

A. De Lucia, B. Krüger, O. A. Tretiakov, M. Kläui, *Multiscale model approach for magnetization dynamics simulations.* Phys. Rev. B **94**, 184415 (2016).

A. De Lucia, K. Litzius, B. Krüger, O. A. Tretiakov, M. Kläui, *Multiscale simulations of topological transformations in magnetic Skyrmions.* Phys. Rev. B In press, (2017)

Sworn declaration

With the present sworn declaration I affirm that I have written this thesis autonomously and without the help of others, without having employed any means or sources other than the mentioned ones. Neither this work, nor parts or similar forms of it, have been submitted as a doctoral thesis to any institution before.

Mainz, 27 March 2017

Hiermit erkläre ich an Eides statt, dass ich meine Dissertation selbständig und ohne fremde Hilfe verfasst und keine anderen als die von mir angegebenen Quellen und Hilfsmittel zur Erstellung meiner Dissertation verwendet habe. Die Arbeit ist in vorliegender oder ähnlicher Form bei keiner anderen Prüfungsbehörde zur Erlangung eines Doktorgrades eingereicht worden.

Mainz, den 27. März 2017 Andrea De Lucia